ALFRED-WEGENER-INSTITUT
HELMHOLTZ-ZENTRUM FÜR POLAR- UND MEERESFORSCHUNG

715
2018

Berichte
zur Polar- und Meeresforschung

Reports on Polar and Marine Research

The Expedition PS109 of the Research Vessel POLARSTERN to the Nordic Seas in 2017

Edited by
Torsten Kanzow
with contributions of the participants

HELMHOLTZ GEMEINSCHAFT

Die Berichte zur Polar- und Meeresforschung werden vom Alfred-Wegener-Institut, Helmholtz-Zentrum für Polar- und Meeresforschung (AWI) in Bremerhaven, Deutschland, in Fortsetzung der vormaligen Berichte zur Polarforschung herausgegeben. Sie erscheinen in unregelmäßiger Abfolge.

Die Berichte zur Polar- und Meeresforschung enthalten Darstellungen und Ergebnisse der vom AWI selbst oder mit seiner Unterstützung durchgeführten Forschungsarbeiten in den Polargebieten und in den Meeren.

Die Publikationen umfassen Expeditionsberichte der vom AWI betriebenen Schiffe, Flugzeuge und Stationen, Forschungsergebnisse (inkl. Dissertationen) des Instituts und des Archivs für deutsche Polarforschung, sowie Abstracts und Proceedings von nationalen und internationalen Tagungen und Workshops des AWI.

Die Beiträge geben nicht notwendigerweise die Auffassung des AWI wider.

Herausgeber
Dr. Horst Bornemann

Redaktionelle Bearbeitung und Layout
Birgit Reimann

Alfred-Wegener-Institut
Helmholtz-Zentrum für Polar- und Meeresforschung
Am Handeshafen 12
27570 Bremerhaven
Germany

www.awi.de
www.reports.awi.de

The Reports on Polar and Marine Research are issued by the Alfred Wegener Institute, Helmholtz Centre for Polar and Marine Research (AWI) in Bremerhaven, Germany, succeeding the former Reports on Polar Research. They are published at irregular intervals.

The Reports on Polar and Marine Research contain presentations and results of research activities in polar regions and in the seas either carried out by the AWI or with its support.

Publications comprise expedition reports of the ships, aircrafts, and stations operated by the AWI, research results (incl. dissertations) of the Institute and the Archiv für deutsche Polarforschung, as well as abstracts and proceedings of national and international conferences and workshops of the AWI.

The papers contained in the Reports do not necessarily reflect the opinion of the AWI.

Editor
Dr. Horst Bornemann

Editorial editing and layout
Birgit Reimann

Alfred-Wegener-Institut
Helmholtz-Zentrum für Polar- und Meeresforschung
Am Handeshafen 12
27570 Bremerhaven
Germany

www.awi.de
www.reports.awi.de

Titel: Eisbär vor der kalbenden Front des 79° Nord Gletschers (Foto: C. Rohleder)

Cover: Polar bear in front of the calving front of the 79 North Glacier (Photo C. Rohleder)

The Expedition PS109 of the Research Vessel POLARSTERN to the Nordic Seas in 2017

Edited by
Torsten Kanzow
with contributions of the participants

Please cite or link this publication using the identifiers
hdl:10013/epic.27a7a460-bc30-4b9f-be99-10589b49b0ae and
https://doi.org/10.2312/BzPM_0715_2018

ISSN 1866-3192

PS109

16.09.2017 – 14.10.2017

Tromsø - Bremerhaven

Chief scientist
Torsten Kanzow

Coordinator
Rainer Knust

Contents

1. ÜBERBLICK UND FAHRTVERLAUF

Torsten Kanzow AWI

Am Nachmittag des 12. September verließ der Forschungseisbrecher *Polarstern* den Hafen von Tromsø. Mit an Bord waren Wissenschaftlerinnen und Wissenschaftler aus sieben Nationen, die das Spektrum von Physikalischer Ozeanographie, Geochemie, Glaziologie, Geodäsie, Geologie, Geophysik, Atmosphärenphysik- und Chemie sowie Biologie und Biogeochemie abdecken. Auf der Expedition “Greenland ice sheet/ocean interaction” (GRISO) sollten die komplexen physikalischen Wechselwirkungen zwischen dem Ozean und dem Eisschild in Nordostgrönland sowie deren Auswirkungen auf das marine Ökosystem erforscht werden (siehe Abbildung 1.1 für die Fahrtroute).

Zunächst jedoch stand zu Beginn der Reise ein seismologisches Experiment an einem langgezogenen untermeerischen Gebirge - dem Knipovich Rücken – im Mittelpunkt. Um besser zu verstehen, wie neuer Ozeanboden an diesem ultralangsamen Rücken entsteht, sollten kleinste Erdbeben aufgezeichnet werden, die diesen Prozess begleiten. Bei unruhiger See und starkem Wind wurden in dieser Woche 4 Ozeanbodenseismometer nahe der Rückenachse ausgebracht. Aus den Tiefen der Erdbebenherde können wir dann auf die Mächtigkeit der jungen Ozeanlithosphäre schließen und ihre Temperatur bestimmen. Die Erdbebenverteilung wird uns aktive Störungen anzeigen und Bereiche, in denen die neue Lithosphäre sich ganz ohne Erdbeben bewegen kann.

Nach Abschluss der seismologischen Arbeiten führte uns der Weg in die Framstraße – der Meeresenge zwischen dem Europäischen Nordmeer und dem Nordpolarmeer. Entlang des Greenwich-Meridians gelangten wir in die Eisrandzone hinein bis 80°50’N nach Norden – dem nördlichsten Punkt, den diese Expedition insgesamt ansteuerte. Entlang der Fahrtroute wurden Messungen der Hydrographie und der Zirkulation vorgenommen und Wasserproben genommen.

In der östlichen Framstraße führt der Westspitzbergenstrom als Verlängerung des Systems Golfstrom – Nordatlantikstrom warmes, salzhaltiges Wasser gen Norden. Während ein Teil des Wassers seinen Weg ins Nordpolarmeer fortsetzt, verlässt ein erheblicher Teil den Westspitzbergenstrom im Bereich der Framstraße nach Westen, um dann auf der Westseite dieser Meeresenge seine Rückreise gen Süden anzutreten. Diese Querzirkulation ist bislang wenig erforscht, spielt aber eine zentrale Rolle für die Forschungsfragen unserer Expedition. Die Stärke der Querzirkulation entscheidet letztlich darüber, welche Menge an ozeanischer Wärme auf den Schelf von Nordostgrönland einströmen kann, um dort zum Abschmelzen der marinen Auslassgletscher beizutragen.

Am Abend des 16. Septembers überquerten wir den eisfreien Ostgrönlandstrom und befanden uns auf dem Schelf von Nordostgrönland (Abbildung 1.2a). Hier kündigte uns die Sicht auf erste Eisberge die Nähe der grönländischen Küste an. Zu Beginn konzentrierten sich unsere Arbeiten noch auf den Bereich der Schelfkante am Eingang zum Westwind Trog - einer sich zum inneren Schelf fortsetzenden, kanalartigen Vertiefung. In diesem Trog befindet sich am Boden das verhältnismäßig warme Atlantikwasser. Neben hydrographischen Messungen

standen hier geologische Sedimentarbeiten mit dem Schwerelot im Mittelpunkt. Letztere sollen einen Aufschluss darüber erlauben, wie weit sich der grönländische Eisschild auf den Kontinentalschelf während der letzten Eiszeit erstreckte, und in welcher Abfolge er sich wieder zurückzog. Ebenso konnten wir in diesem Gebiet gezielt Sedimente vom Meeresboden beproben, anhand derer untersucht werden soll, wie der Schmelzwassereintrag durch die grönländischen Gletscher die benthisch-biogeochemischen Prozesse beeinflussen. Das Team der Meereisbiologen an Bord beabsichtigte, Polardorschlarven nahe des Grönlandschelfs zu fischen. Zwei mal kam in diesem Bereich das Bongonetz zum Einsatz. Das Ziel ist es, genetische Unterschiede zwischen verschiedenen arktischen Polardorschpopulationen zu erfassen und mehr über die Diversität und Anpassungsfähigkeit des Polardorschs zu erfahren.

Vorbei an einer Vielzahl von Eisbergen folgte *Polarstern* hiernach dem Verlauf des Westwind Trogs nach Westen, in dem die geologischen und benthischen Arbeiten fortgesetzt wurden. Dichtes Meereis war nun für die nachfolgenden beiden Wochen unser ständiger Begleiter. Wir setzen den Weg an die grönländische Küste bis zum Eingang des Djimphna Sundes fort, den wir am 20. September erreichten. Sehr dichtes Eis ließ uns dabei nur langsam vorankommen. Der Djimphna Sund führt - umrahmt von steilen, verschneiten Felsen - zur verhältnismäßig kleinen, nördlichen Kalbungsfront des 79N Gletschers. Am Eingang des Sundes konnten wir eine ozeanographische Verankerung bergen, die seit August 2016 kontinuierlich das Ausströmen des gletscherbeeinflussten Ozeanwassers vermessen hatte. Angesichts der Präsenz von tiefreichenden Eisbergen waren wir sehr glücklich, dass uns diese Bergung gelungen ist.

Hiernach gelangten wir an der grönländischen Küste ca. 30 Meilen südwärts, um am 21. September in die felsenumrahmte, verschneite und atemberaubend schöne Bucht vor der Hauptkalbungsfront des 79N Gletschers zu gelangen (Abbildung 1.2b) – einem sehr wichtigen Ziel unserer Expedition. Dieser Gletscher weist eine zwischen Felsen eingekeilte schwimmende Eiszunge auf, die auf einer Länge von 80 km eine mit Meerwasser gefüllte, mehrere Hundert Meter tiefe Kaverne aufweist. Es konnten alle vier im letzten Jahr direkt vor der Gletscherfront ausgelegten ozeanographischen Verankerungen geborgen. Dabei handelt es sich um die ersten Zeitserienmessungen in diesem Bereich überhaupt. Ferner wurde ein schiffsbasiertes Messprogramm der Atlantik- und Schmelzwasserzirkulation und eine intensive chemische Wasserprobennahme durchgeführt. Auch weitere benthische und geologische Untersuchungen im Zusammenhang mit dem 79N Gletscher standen Vordergrund. Zudem können wir von einem erfolgreichen Einsatz des autonomen Tauchboot PAUL entlang des komplexen Einstrompfades des Atlantikwassers zum 79N Gletscher berichten. Die Arbeiten liefen dabei bei Außentemperaturen bis zu -15°C und rasch voranschreitender Neueisbildung ab. Dem unermüdlichen Einsatz und der enormen Erfahrung des Brücken- und Deckspersonals von *Polarstern* war es zu verdanken, dass wir komplexe Messsysteme wie die CTD Rosette, die benthischen Lander oder auch das Tauchboot bei diesen Bedingungen erfolgreich betreiben konnten.

Aufgrund der großen Einsatzbereitschaft des Helikopterteams und der zuverlässigen Vorhersagen der Bordwetterwarte zeigten die flugbasierten Arbeiten trotz der recht unvorteilhaften, variablen und winterlichen Bedingungen einige Erfolge. Die Geodäten installierten erfolgreich zwei GPS Messstationen auf dem grönländischen Festland. Es handelte sich dabei im Orte, an denen durch Widerholungsmessungen in unterschiedlichen Jahren langzeitliche Landhebungsprozesse untersucht werden. Die Seismologen bauten Seismometer auf dem felsigen Untergrund nahe der Aufsetzlinie des 79N Gletschers auf, um kontinuierlich kleine, durch Gletscherbewegungen hervorgerufene Beben aufzuzeichnen. Die Glaziologen wiederum konnten eine Reihe von Dickenmessungen der Gletschereiszunge mit einem phasensensitiven Radar durchführen. Aus dem Vergleich mit ebensolchen Messungen während der iGRIFF Kampagne auf dem 79N Gletscher im Frühsommer dieses Jahres sollen dann hieraus basale Schmelzraten an der Unterkante der Eiszunge abgeleitet werden.

Am 25. September ließen wir den 79N Gletscher hinter uns. Drei Verankerungen, die sich am nördlichen Ausgang der Bucht befinden, um die Zirkulation am Übergang vom Norske Trog im Süden und dem Westwind Trog im Norden zu erfassen, konnten auf Grund des dichten Eises nicht geborgen werden. Wir setzen daher an diesem Tag unsere Reise nach Süden fort. Unser Trost ist, dass die Verankerungen auch in einem oder zwei Jahren noch sicher zu bergen sein werden und auch weiterhin Messdaten aufzeichnen werden.

Wir verbrachten hiernach die nächsten Tage in Nahdistanz zu einer direkt der grönländischen Küste vorgelagerten Inselkette zwischen Norske Oer im Norden und Ile-de-France im Süden. Wenn sich der Nebel lichtete, bekamen wir die winterliche Felsenlandschaft und auch den einen oder anderen Eisbären zu sehen. Auf 4 unterschiedlichen Schnitten führten wir erfolgreich hydrographische Messungen unter teilweise schwierigen Eisbedingungen durch. Die wissenschaftliche Zielsetzung der Ozeanographen war die Erforschung der Zirkulationspfade des Atlantikwassers sowohl entlang der Achse des Norske Trogs als auch zwischen dem Norske Trog und der westlich der Inselkette liegenden Jøkelbugten (Abb. 1.2c). In letzterer Bucht mündet der Zachariae Isstrøm, ein Gletscher, der wie der unmittelbar nördlich davon liegende 79N Gletscher vom nordostgrönländischen Eisstrom gespeist wird.

Die Meerestiefen um die Inselkette herum sind bis dato weitestgehend unbekannt. Es gelang uns unter Führung der Geologen, die Meerestiefen am Eingang der beiden größten Meeresengen zwischen den Inseln mit dem schiffseigenen Fächerecholot zu kartieren – inmitten von beeindruckend langgesteckten und großen Eisbergen. Auf der Basis der Kartierungen konnten die Ozeanographen dann an gezielten Positionen hydrographische Vermessungen durchführen. Die Daten werden es uns erlauben zu verstehen, in welcher Form der Zachariae Isstrøm dem Einstrom von Atlantikwasser ausgesetzt ist. Begleitet wurde das Programm von überaus erfolgreichen Arbeiten der Geologen mit dem Schwerelot.

Die benthischen Biologen brachten den Multicorer an drei ausgewählten Orten zum Einsatz und konnten zudem eine Landerauslegung verbuchen – gefolgt von der Bergung zwei Tage später. Erfolgreich kamen auch die Arbeiten mit einem autonomen Fluggerät voran, das dafür ausgelegt ist, in bis zu 1000 m Höhe Proben der Methanverteilung in der Atmosphäre zu sammeln.
Derweil erschwerten die schlechten Sichtbedingungen auf Grund von niedriger Bewölkung, Nebel und teilweise auch gefrierendendem Regen die Helikopter gebundenen Arbeiten leider erheblich. Flüge über größere Distanzen waren damit aus Sicherheitgründen in dieser Woche ausgeschlossen. Trotz der Widrigkeiten gelang es den Helipiloten, kürzere Wetterfenster zu nutzen, so dass die Geodäten zumindest eine GPS Messstation auf einer nahegelegenen Insel ausbringen und später in der Woche auch wieder sicher bergen konnten. Den Geologen gelang es dort dann auch, die ersehnten kosmogenen Gesteinsproben zu sammeln. Ferner konnten die Ozeanographen mit mobilen Geräten vom Meereis aus eine Tiefenlotung und eine hydrographische Messung in der Jøkelbugten vornehmen, die vom Schiff aus auf Grund des Festeises und der Eisberge nicht befahrbar ist. Andere wichtige fluggestützte Ziele jedoch, wie die Installation einer Eisboje vor dem Zachariae Isstrøm, weitere glaziologische Messungen auf dem 79N Gletscher oder eine biologische Eisstation konnten nicht realisiert werden.

Im Gegensatz zu vier Tagen zuvor verliefen die Verankerungsarbeiten am 29. September indes sehr erfreulich. Es gelang uns, alle vier auf dem Ile-de-France Schnitt quer über den Norske Trog vor einem Jahr ausgelegten Verankerungen binnen eines Tages zu bergen. Die Daten werden uns weitere wichtige Aufschlüsse über die Stärke und die zeitlichen Schwankungen der Atlantikwasserzirkulation liefern. In diese Woche fiel zudem auch unser Bergfest, das wir nahe der Südspitze der Insel Norske Oer mit einem Grillabend am 30. September begingen.

Am Abend des 1. Oktober hieß es Abschied nehmen von der grönländischen Küste. Wir ließen die Eisberge und das Meereis hinter uns und gelangten in südöstlicher Richtung entlang der

Achse des Norske Trogs in den Bereich des mittleren Schelfs, in dem sowohl eine Schwelle im Trog vorhanden als auch der nördliche Hang hin zur flachen Belgica Bank besonders steil ausgeprägt ist. An dieser Stelle erwarteten wir, dass der Zustrom von Atlantikwasser gen Küste besonders fokussiert als Randstrom auftreten würde. Hier kam das autonome Tauchboot PAUL erneut zum Einsatz, um den Randstrom gezielt zu vermessen. Begleitende schiffsbasierte Messungen (CTD, Mikrostruktur und LADCP sowie benthische Sedimentproben) bestätigten die Gegenwart des Randstroms.

Am 3. Oktober begaben wir uns auf einen nördlich des Norske Trog ostwärts verlaufenden Kurs zum äußeren Schelf hin, um bei 10°O nach Süden in den Bereich des Trogs zurückzukehren. Entlang der Route kamen hydrographische Messungen zum Einsatz, ergänzt durch biologische Probennahmen mit dem Bongonet, dessen Einsatz nun außerhalb des Eises wieder möglich wurde. Wir konnten zeigen, dass auch in dieser relativ flachen Region des Schelfs warmes Atlantikwasser in Bodennähe vorhanden ist. Insgesamt legten wir 3 Verankerungen auf dem Weg aus, die 2018 wieder geborgen werden sollen. Nachfolgende Analysen sollen dann zeigen, ob von dieser Region aus Atlantikwasser in den Trog eingespeist wird, um so zur Küste Grönlands zu gelangen.

Am 4. Oktober setzten wir unsere Fahrt entlang der Trogachse in Richtung Schelfkante fort. Hier bargen wir eine im letzten Jahr ausgelegte ozeanographische Verankerung, nahmen Sedimentproben für biogeochemische Arbeiten und legten an derselben Position einen Lander aus. In der Folge absolvierten wir entlang des Schnitts über die Schelfkante auf den Kontinentalabhang hinaus ein Programm aus hydrographischen Messungen, Schwereloteinsätzen, biologischen Netzfängen sowie Sedimentprobennahmen.

Hier machten uns am 5. Oktober und in der folgenden Nacht stürmische Winde zu schaffen. Eine geplante Landerauslegung wurde abgesagt, und stundenlang war gar kein Geräteeinsatz möglich. Am nächsten Morgen legten wir bei deutlich ruhigeren Bedingungen eine ozeanographische Verankerung zur Erfassung des Atlantikwassers im Ostgrönlandstrom aus, um den Bezug zwischen der Zirkulation im Norske Trog und dem großräumigen Strömungssystem in der Framstraße herzustellen. Wir konnten hiernach den zwei Tage zuvor ausgelegten Lander bergen und in der folgenden Nacht das entsprechend gekürzte, am Vortag begonnene Messprogramm auf dem Kontinentalabhang beenden.

Im Verlauf des 7. Oktobers verließen wir den Kontinentalabhang nach Südosten in Richtung Grönlandsee. Hier standen zwecks Gerätekalibrierung zwei Tiefsee-CTD Stationen an, die regional an eine vom AWI vor etlichen Jahren begonnene Zeitserienstation anschlossen. Unsere aktuellen CTD Messungen legen nahe, dass die langzeitliche Erhöhung der Bodenwassertemperaturen in der Grönlandsee sich weiter fortgesetzt hat, vermutlich bedingt durch das Ausbleiben tief reichender, winterlicher Konvektion in dieser Region. Hiernach traten wir in der folgenden Nacht den langen Transit nach Bremerhaven an, wo wir am Abend des 13. Oktober eintrafen.

Vor dem Hintergrund des globalen Meeresspiegelanstiegs und des Rückzugs des grönländischen Eisschildes diente die Expedition PS109 der Erforschung der Wechselwirkung zwischen dem Ozean und den Gletschern Nordostgrönlands sowie der Auswirkung dieser Wechselwirkung auf das regionale Ökosystem. Insbesondere während der Arbeiten vor der Küste Grönlands in der zweiten und dritten Woche konnten wir mit Sicht auf den 79N Gletscher inmitten von dichtem Meereis bei winterlichen Bedingen und umgeben von Eisbergen einen starken visuellen Bezug zwischen unserem Messprogramm und der rauen Natur Nordostgrönlands herstellen. Wir kehren mit vielen wertvollen Datensätzen und Proben, Erinnerungen an atemberaubende Ausblicke und voller Dank an den Kapitän und die Besatzung von *Polarstern* nach Hause zurück.

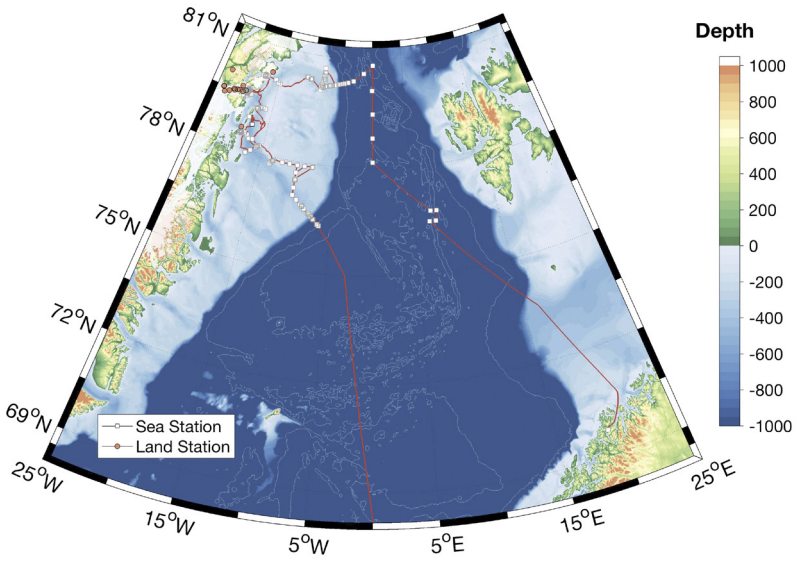

Abb. 1.1: Fahrverlauf (rote Linien), Schiffsstationen (weiße Punkte) und Landstationen (rote Punkte) der Expedition PS109. Siehe https://doi.pangaea.de/10.1594/PANGAEA.883343 für eine Darstellung des master tracks in Verbindung mit der Stationsliste.

Fig. 1.1: Cruise track (red lines), vessel stations (white dots) and land stations during of the expedition PS109. See https://doi.pangaea.de/10.1594/PANGAEA.883343 to display the master track in conjunction with the list of stations.

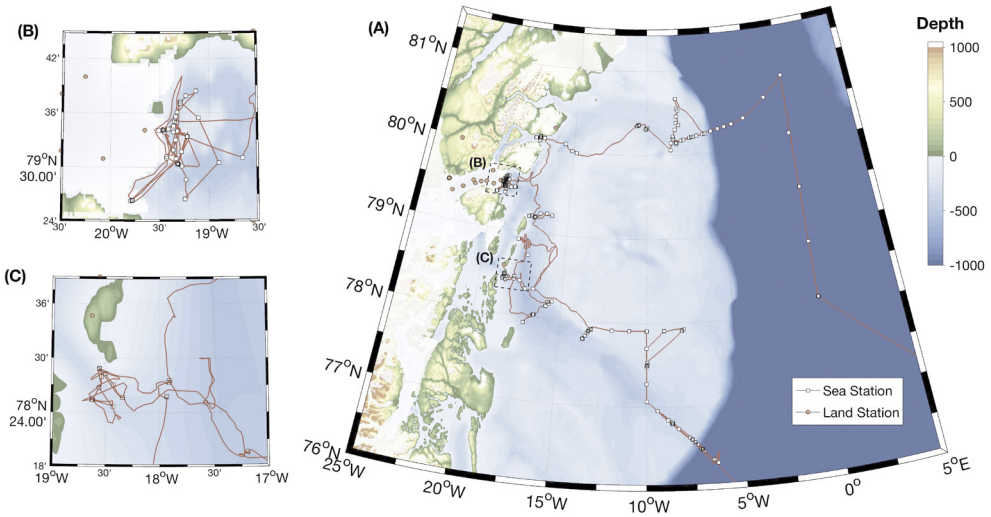

Abb. 1.2: Fahrverlauf (rote Linien), Schiffsstationen (weiße Punkte) und Landstationen (rote Punkte) der Expedition PS109. Das Bild A zeigt die Route und Stationen auf dem grönländischen Schelf, wohingegen die Bilder B und C detailliert die Arbeiten vor der Kalbungsfront des 79N Gletscher bzw. am Übergang vom Norske Trog zur Jøkelbugten darstellen.

Fig. 1.2: Cruise track (red lines), vessel stations (white dots) and land stations (red dots) during of the expedition PS109. Panel A shows the route of Polarstern and the stations on the shelf of Greenland, whereas panels B and C display in detail the work accomplished at the calving front of the 79N Glacier and at the transition from Norske Trough to Jøkelbugten, respectively.

SUMMARY AND ITINERARY

In the evening of 12 September the research icebreaker *Polarstern* left the port of Tromsø (Norway). On board there were scientists from seven nations covering the range from physical oceanography, geochemistry, glaciology, geodesy, geology, geophysics, atmospheric physics and chemistry as well as marine biology and biogeochemistry. The aim of the “Greenland ice sheet/ocean interaction” (GRISO) expedition is to unravel the complex physical interactions between the ocean and the ice sheet of Northeast Greenland, as well as their implications for the marine ecosystem (see Fig. 1.1 for cruise track).

The first focus of the expedition, however, was a submarine mountain range – the Knipovich Ridge. To better understand how new ocean floor is created at these so-called ultraslow spreading ridges, we intended to record the small earthquakes that accompany this process. In rough seas four ocean bottom seismometers were deployed at the ridge axis. The depths of the earthquake foci would allow us to estimate the thickness of the young ocean lithosphere and to determine its temperature. The earthquake distribution would tell us where active deformation takes place and will delineate areas that deform without any earthquakes.

Having accomplished the seismological work we steamed toward Fram Strait – marking the transition between the Nordic Seas and the Arctic Ocean. Going along the prime meridian we reached the marginal ice zone before arriving at 80°50’N – the northernmost location of this expedition. Along the transect, observations of the hydrography and the circulation were acquired and water samples were taken.

In eastern Fram Strait, the West Spitsbergen Current - representing the extension of the Gulf Stream – North Atlantic Current System - carries warm, saline waters to the north. While a part of this water subsequently continues its voyage to the Arctic Ocean, a sizable fraction of it leaves the boundary current and moves to the west within Fram Strait - only to flow back southward along its western side. This recirculation so far has received little scientific attention, yet it supposedly plays a central role for the research questions of our expedition. Ultimately, the strength of the recirculation determines the amount of oceanic heat that can be transported onto the shelf of Northeast Greenland, where it contributes to the melting of the marine outlet glaciers.

In the evening of September 16 we crossed the ice-free East Greenland Current and found ourselves on the shelf of Northeast Greenland (Fig. 1.2a). Here the first sightings of icebergs reminded us of the proximity of the Greenlandic coast. At the beginning our work was concentrated on the area of the shelf break of at the mouth of Westwind Trough, the latter representing a depression leading toward the inner shelf. In the trough relatively warm Atlantic Water can be found near the sea floor. Besides hydrographic measurements, geological sediment investigations using the gravity corer were a major focus. By means of this, we tried to establish the area over which the Greenland ice sheet extended during the time of the last ice age, and in which succession it subsequently retreated. Also, we were able to collect sea floor samples using corer and lander systems based on which the impact of the glacial meltwater input into the ocean on benthic-biogeochemical processes shall be investigated. The Sea Ice Biology Team aimed to sampling polar cod larvae on the Northeast Greenland shelf. In this

area two initial net trawls were accomplished. The team aimed at investigating the genetic connectivity of Greenland populations with other Arctic populations in order to understand the polar cod's spatial and temporal dynamics, population diversity and adaptive divergence.

Passing a number of icebergs, *Polarstern* followed toward the west along the axis of the trough, in which geological and benthic work were pursued. For the following two weeks we found ourselves with the sea ice. We continued our way towards the coast of Greenland into Djimphna Sound that we reached on 20 September. Dense ice fields allowed us only to move ahead rather slowly. Wedged between steep mountain ranges, Djimphna Sound leads toward the relatively small, northern calving front of the 79N Glacier. We succeeded to recover an oceanographic mooring at the mouth of the sound, that had been measuring the outflow of the glacier-influenced ocean waters since August 2016. Given the presence of deep-reaching icebergs, we are very pleased about the save recovery of the instrumentation.

Subsequently, *Polarstern* sailed approximately 30 miles toward the south, and on 21 September then entered the breathtakingly beautiful bay in front of the main calving front of the 79N glacier, framed by snow-covered mountain ranges (Fig. 1.2b). This area represents a very important target of our expedition. The glacier exhibits a floating ice tongue, below which an 80 kilometers long cavity filled with sea water can be found. We succeeded to recover all four oceanographic moorings deployed last year in close vicinity of the calving front. Thus, the first-ever time series measurements from the ocean-glacier interface of the 79N Glacier have become available. Apart from that a vessel-based measurement programme of the Atlantic Water and meltwater circulations in the bay and a chemical water sampling programme were carried out. In addition successful biogeochemical benthic sampling as well as geological coring efforts related to the ocean-glacier interaction were executed. We can further report a successful dive of the autonomous underwater vehicle PAUL along the complex circulation pathway of the Atlantic Water toward the 79N glacier. The work programme was accompanied by outside temperatures of up to -15°C and rapidly progressing new-ice formation. It is a result to the tireless efforts and the enormous experience of both the bridge and deck crews of *Polarstern* that we were able to operate complex measurement systems like the CTD rosette, the benthic landers or the underwater vehicle successfully.

Owing to the persistent readiness of the helicopter team and the reliable predictions of the weather service on board, also the flight-based operations showed some successes despite the unfavourable variable and winterly conditions. The geodesists were able to install two GPS measurement systems on the mainland of Greenland. By repetition of these measurement in different years, long-term land elevation changes are studies in this area. The seismologists put up seismometers in rocky ground near the grounding line of the 79N glacier to be able to monitor small quakes associated with the movement of the glacier. Finally, the glaciologists succeeded in performing a series of thickness measurements of the floating ice tongue of the 79N Glacier using a phase-sensitive radar. By comparison with the same type of measurements conducted on the 79N glacier during the iGRIFF campaign earlier this summer, estimates of basal melt rates at the underside of the ice tongue should be obtained.

On 25 September we left the 79N Glacier behind us. As a result of very dense sea ice coverage we were unable to recover 3 moorings deployed near the northern edge of the embayment of the 79N Glacier, in order to observe the circulation at the transition from Norske Trough in the South to Westwind Trough in the North. We therefore continued our voyage toward the south on the same day. It is a consolation to know that these moorings may be safely recoverable in one or two years from now and will also continue to record measurements.

We subsequently spent one week at a close distance from a chain of islands located directly in front of the coast of Greenland between Norske Oer in the North and Ile-de-France in the South. At times when the fog receded we could catch sight of winterly, rocky coastlines and one or the

other polar bear. In partly difficult sea ice conditions we successfully carried out hydrographic measurements along four different sections. The scientific goal of the oceanographers were to study the circulation pathways of the Atlantic Water both along the axis of Norske Trough and between the trough and Jøkelbugten (Fig. 1.2c), an embayment located to the west of the aforementioned island chain. It is in this bay, that another major glacier - Zachariae Isstrøm - discharges the ice masses supplied by the Northeast Greenland Ice Stream – the same ice stream drained from by the neighboring 79N Glacier.

The waterdepths around the island chain are still largely unknown today. The geologists conducted a survey of the bathymetry using the vessel mounted swath echosounder – among impressingly wide and huge icebergs. After the surveys, the oceanographers conducted hydrographic measurements at positions based on the freshly produced depth charts. The data will allow us to understand, in which way the Zachariae Isstrøm is exposed to the inflow of Atlantic Water. This work in turn was accompanied by a highly successful geology programme relying on gravity coring. In addition, the benthic biologists operated the multicorer at 3 selected sites and further can look back on a deployment of their lander system and its subsequent recovery two days later. Fine progress can also be reported from the sea ice biology team. Their quadrocopter – designed to collect air samples to establish the distribution of methane in the air column – accomplished a flight up to a height of 1,000 m.

Meanwhile the poor visibility caused by clouds, fog and also icy rain restricted the helicopter based work substantially. Flights over larger distances could not be conducted at all due to security reasons. Despite of the adverse conditions, the helicopter pilots managed to make use of short weather windows, such that the geodesists were able to both install a GPS measurement station on an island near-by and subsequently recover it later in the week. At the same location the geologists succeeded in collecting cosmogenic rock samples. Further the oceanographers succeeded in conducting a depth sounding and hydrographic measurements from an ice floe using mobile instrumentation in Jøkelbugten, which is out of reach of *Polarstern* due to the melange of fast ice and icebergs found in the bay. Other important aims depending on helicopter flights, however, like the installation of an ice buoy right next to the Zachariae Isstrøm, additional glaciological measurements or a biological ice station had to be cancelled, unfortunately.

In contrast to 4 day earlier, the subsequent mooring on 29 September went absolutely smoothly. Within just one day we were able to recover all four moorings on the Ile-de-France section across Norske Trough that had been deployed one year ago. The data will provide us with important information on the strength and fluctuations of the Atlantic Water circulation in Norske Trough. We also celebrated our mid-cruise barbecue party in this week close the southern tip of Norske Oer on 30 September.

In the evening of 1 October we left the coast of Greenland. Leaving icebergs and sea ice behind us, we steamed in a southeasterly direction along the axis of Norske Trough toward the mid-shelf, where both a sill can be found in the trough and the northern slope toward the shallow Belgica Bank is particularly steep. In this location we expected to find the inflow of the Atlantic Water to be particularly focussed as a boundary current. Here the autonomous underwater vehicle Paul was launched one more time in order to observe the detailed structure of the boundary current. This was accompanied by vessel-based measurements (CTD, microstructure, LADCP, benthic sediment samples) which confirmed the presence of the boundary current.

On 3 October upon completion of the task, we headed eastward along a course located to the north of Norske Trough toward the outer shelf, only to return southward along 10°E to the area of Norske Trough. Along the passage we operated hydrographic measurements, complemented by biological sampling based on the bongo net. We were able to show that even

in this relatively shallow area of the shelf, warm Atlantic Water was present near the sea floor. Three moorings in total were deployed, that shall be recovered again in 2018. Subsequent analyses shall show whether Atlantic Water from this region is injected into the trough, such that it is transported to coast of Greenland.

On 4 October we continued our way toward the shelf edge along the axis of Norske Trough. Here we were able to recover an oceanographic mooring, took sediment samples for biogeochemical studies and subsequently deployed a lander at the same site. We then pursued a programme along a section across the shelf edge onto the continental slope, composed of hydrographic measurements, gravity corer operations, biological net catches and sediment sampling.

Here, stormy winds challenged our progress during 5 October and the following night. A lander deployment had to be cancelled and for many hours any deployment of scientific gear became impossible. In significantly calmer conditions on the next morning we deployed an oceanographic mooring in the East Greenland Current, in order to be able to connect the circulation in Norske Trough with the large-scale current system in Fram Strait. We then successfully recovered the lander we had deployed two days earlier and in the following night we completed the somewhat shortened measurement programme on the continental slope that we had started on the previous day.

Over the course of 7 October we left the continental slope in a southeasterly direction toward Greenland Sea. Here two deep-sea CTD casts were performed for instrument calibration purposes in a region in which AWI had started a time series station many years back. Compared to the historical observations our measurements suggest, that the long-term increase of the bottom water temperatures in Greenland Sea has steadily progressed further – most likely as a result of the shift from deep to shallower winter-time convection in this area. In the following night we started the transit to Bremerhaven, where we arrived in the evening of 13 October.

In the context of global sea level rise and the widespread retreat of the Greenland ice sheet, the expedition PS109 served the study of both the interaction between the ocean and glaciers in Northeast Greenland and the impact of this interaction on the regional marine ecosystem. It was especially during the second and third week of the expedition, when we conducted our field programme in the vicinity of the coast – in sight of the 79N Glacier within dense sea ice in winterly conditions, surrounded by icebergs – that we were able to make a strong visual connection between our measurement programme and the rough nature of Northeast Greenland. We returned home with many valuable data sets and samples, memories of spectacular sights and full of thanks to the captain and the crew of *Polarstern*.

2. WEATHER CONDITIONS DURING PS109

Max Miller, Juliane Hempelt, Christian Rohleder — DWD

Tuesday afternoon, September 12 2017, 15:15 pm, *Polarstern* left Tromsø for the campaign PS109. Light and variable winds, 15° C and mostly cloudy skies were observed.

A low over southern Norway and North Sea moved slowly east and a high over Laptev Sea spread towards Svalbard. Therefore strong easterly winds could be expected north of Norway. After leaving the fjords winds veered east and increased rapidly. On Wednesday (Sep. 13) and Thursday easterly winds peaked at Bft 8 forcing a sea state of 4.5 m. Near Svalbard we approached the high and on Thursday evening south-easterly winds abated Bft 3 to 4.

At the same time a trough formed off the east coast of Greenland and moved slowly east. After only light southerly winds on Friday (Sep. 15) they freshened up to Bft 6 to 7 during the night to Saturday, combined with rain and snow. Saturday afternoon we crossed the centre area of the trough and reached its west side. Therefore fresh winds veered north. At the north-eastern end of Greenland a new low formed and headed northeast. Until Monday (Sep. 18) it caused rapid changes of wind direction from north to south and vice versa with peaks at Bft 6.

From Tuesday (Sep. 19) on a high became the dominant feature and winds remained light and variable for several days. Close to Greenland's coast wind direction was influenced by topography, too. Above coastal waters or ice low stratus and fog were often present, while sunshine could be observed over Greenland.

On Friday (Sep. 22) a low formed near Jan Mayen and headed towards Svalbard. Therefore, winds veered north to northeast but freshened only temporarily up to Bft 5. Furthermore, coastal mountains near the 79°- glacier caused a lee effect. During the following days a trough over Fram Strait remained preserved with only light and variable winds. Cold air flowing down forced a local wind circulation in front of the glacier. Low clouds along the coast still hampered the flight operations.

On Wednesday (Sep. 27) a strong high over Scandinavia expanded towards Fram Strait. Winds veered south and freshened but *Polarstern* operated temporarily inside the lee of some islands off Greenland's coast. From Thursday on warmer air masses flowing over the ice caused fog. On Friday (Sep. 29) a low south of Iceland built a trough towards Fram Strait. Winds abated but now rain and sleet obstructed helicopter flights. On Saturday (Sep. 30) conditions improved temporarily because offshore winds dried up the ground layer. But already during the night to Sunday winds veered northeast and renewed the misty situation. On Monday (Oct. 02) small secondary lows formed inside the trough over Fram Strait. *Polarstern* left the ice. Northerly winds remained light to moderate, visibility improved only temporarily and freezing drizzle war observed.

On Tuesday (Oct. 03) a low moved towards Norway via Iceland. *Polarstern* got at its northwest side with freshening northerly winds and precipitation changed into snow. On Thursday (Oct. 05) a small secondary low formed southwest of Svalbard. It moved rapidly south and caused northerly winds at Bft 8 and a sea state of 4 m in the evening. Already during the night to Friday

winds started to abate again. Afterwards the high over Greenland expanded east. On Saturday (Oct. 07) and Sunday light and variable winds were prevailing. Saturday evening the return journey to Bremerhaven started.

A low near Cape Farvel reached Iceland on Monday (Oct. 09) and became stationary. At first *Polarstern* steamed at its east and later at its south side. From Monday afternoon until noon on Wednesday south-easterly to southerly winds were often blowing at Bft 7 to 8 with isolated peaks up to Bft 9 forcing a sea state of up to 4 m. On Wednesday afternoon winds veered west to northwest and abated, but peaked once more up to Bft 8 on Thursday (Oct. 12). Inside North Sea we approached a high over Central Europe. On Friday winds veered southwest and abated gradually.

On Friday evening, October 13 2017, *Polarstern* reached Bremerhaven at fresh south-westerly winds.

For further statistics see attached files (Fig. 2.1 – Fig. 2.6).

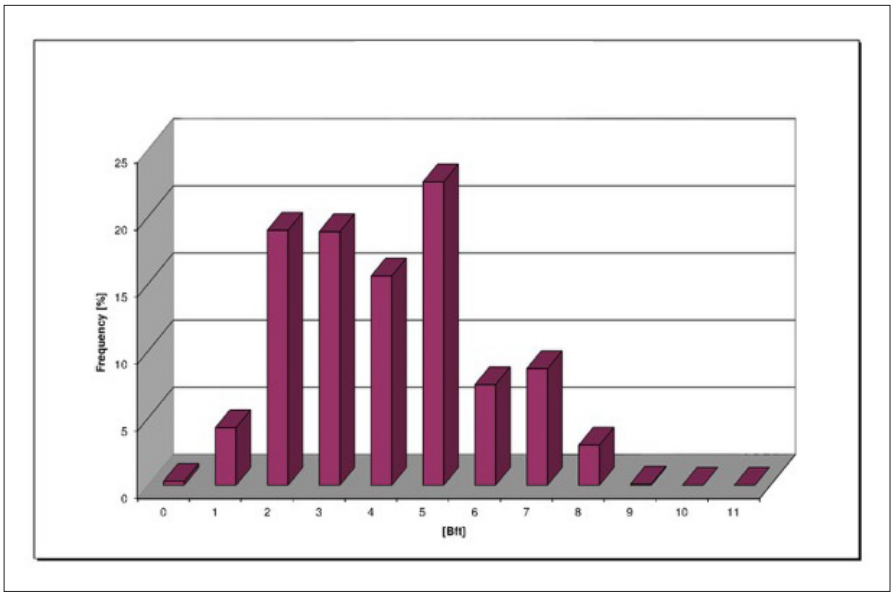

Fig. 2.1: Distribution of wind force during PS109

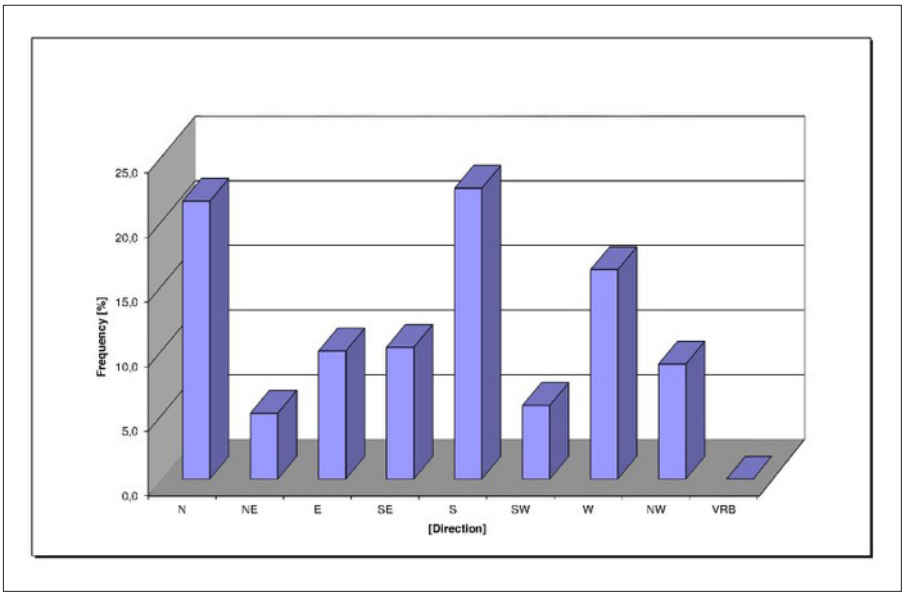

Fig. 2.2: Distribution of wind direction during PS109

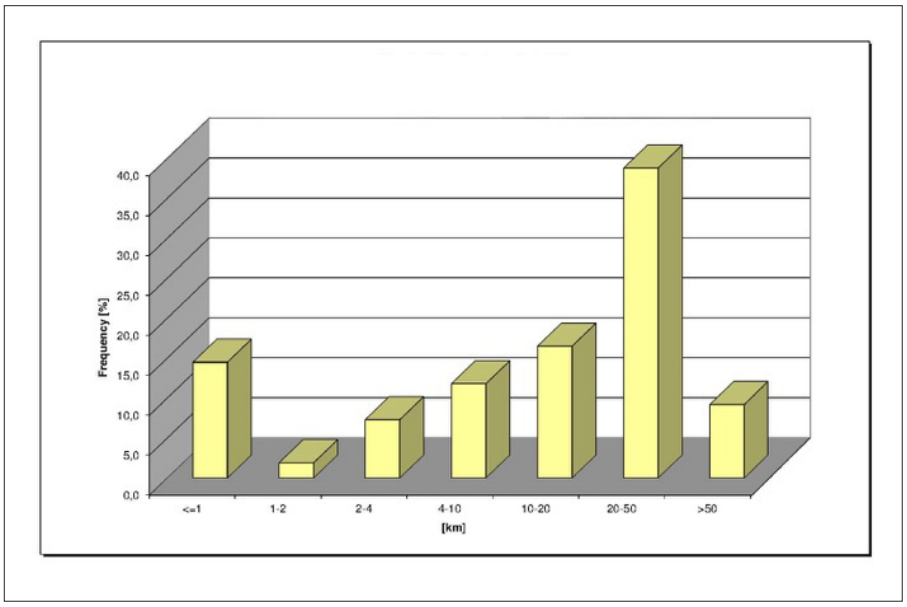

Fig. 2.3: Distribution of visibility during PS109

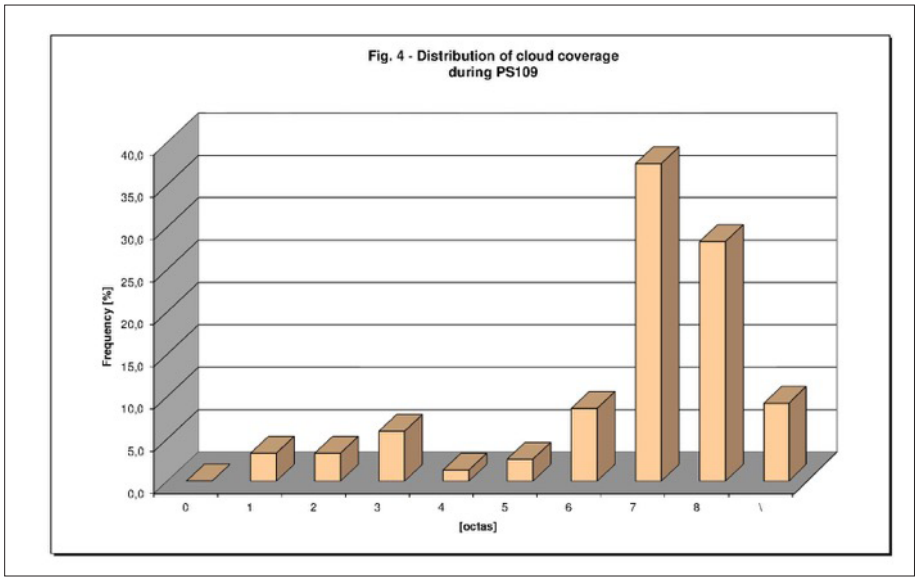

Fig. 2.4: Distribution of cloud coverage during PS109

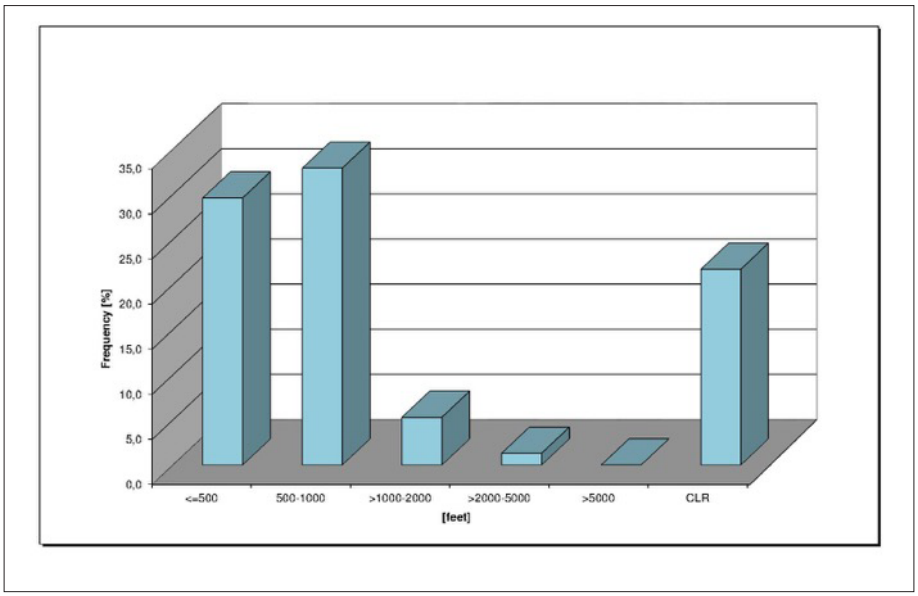

Fig. 2.5: Distribution of ceiling during PS109

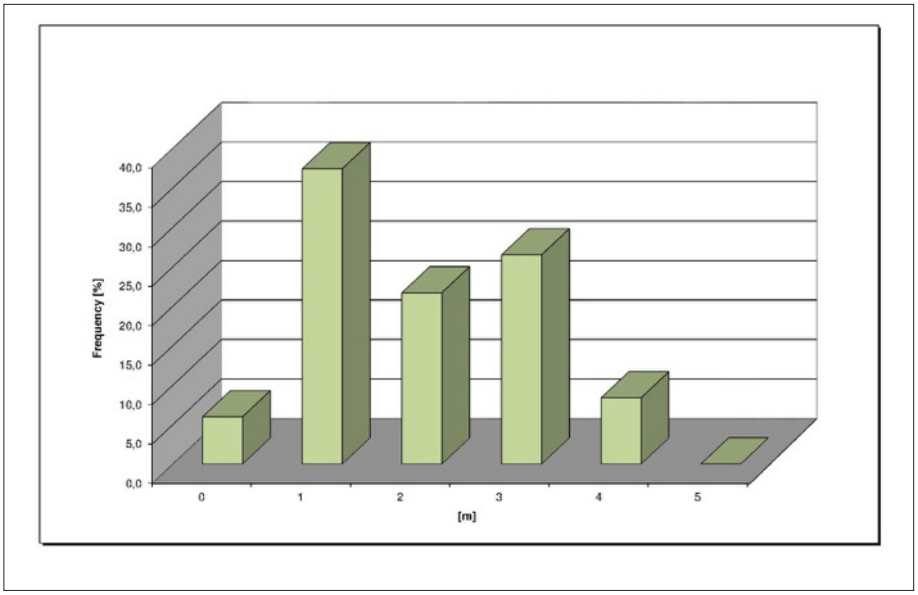

Fig. 2.6: Distribution of sea state during PS109

3. PHYSICAL OCEANOGRAPHY

Janin Schaffer[1], Torsten Kanzow[1], Carina Engicht[1], Rainer Graupner[1], Nils Hutter[1], Andreas Münchow[2], Peter Washam[2], Nicolas Beaird[3], Zerlina Hofmann[4], Mia Sophie Specht[4], Luisa von Albedyll[5]
not on board: Fiammetta Straneo (SCRIPPS), Malene Simon (Greenland Institute of Natural Resources)

[1]AWI
[2]UDEL
[3]WHOI
[4]GEOMAR
[5]UHB

Grant No. AWI_PS109_03

Background and objectives

Mass loss from the Greenland Ice Sheet presently accounts for a third to a quarter of sea-level rise (Milne et al., 2009) and the rate of mass loss is increasing (Velicogna, 2009). The dominant mechanism is increased mass discharge along the marine margins where numerous major outlet glaciers have undergone a nearly simultaneous retreat, acceleration and thinning (Rignot and Kanagaratnam, 2006; Howat et al., 2008; Stearns and Hamilton, 2007; Dietrich et al., 2007). Both data and models indicate that this acceleration was triggered by a change at the tidewater margins of these glaciers (Thomas 2004; Nick et al., 2009; Pritchard et al., 2009), suggesting that the ocean plays a key role in modulating the ice sheet's mass balance (Vieli and Nick, 2011; Straneo et al., 2012).

The proposed oceanic trigger is supported by recent studies showing that warm Atlantic waters are present and circulating in Greenland's glacial fjords (Holland et al., 2008; Straneo et al., 2010; Murray et al., 2010; Straneo et al., 2011) and by the observation that these waters were warming and accumulating in the subpolar North Atlantic at the same time as the glaciers started to retreat (e.g., Bersch et al., 2007).

Greenland's glacier acceleration has concentrated along the southeastern and western margins terminating in the subpolar North Atlantic. Only recently, Helm et al. (2014) observed a general reduction in ice sheet elevation near the margins in the northeast of Greenland. Here, mainly two glaciers Nioghalvfjerdsfjorden glacier (also referred to as 79 North Glacier) and Zachariæ Isstrøm drain the Northeast Greenland Ice Stream (NEGIS) whose drainage basin contains more than 15 % of the Greenland Ice Sheet area (Rignot and Kanagaratnam, 2006). Zachariæ Isstrøm lost about 5 Gt/yr of its mass since 2003 and was observed to retreat at an accelerated rate since fall 2012, whereas no mass loss but an increased bottom melting was found at the 79 North Glacier (Mouginot et al., 2015). Khan et al. (2014) observed an acceleration of the ice flow of 79 North Glacier and a sustained dynamic thinning of NEGIS, which they linked to a regional warming. The fact that a warming and thickening of the Atlantic layer has recently been observed in the Nordic Seas (e.g. in Fram Strait; Beszczynska-Möller et al., 2012) raises the question of whether the ocean changes may have triggered the fast retreat of Zachariæ Isstrøm (as suggested by Mouginot et al., 2015) and will trigger unstable behaviour of the 79 North Glacier.

Warm Atlantic water is carried to the North by the North Atlantic Current - Norwegian Atlantic Current - West Spitsbergen Current system. In Fram Strait a sizable fraction of the Atlantic water recirculates to the south on the East Greenland continental slope. Studies on the eastern Greenland shelf in the 1980s and 1990s found this recirculating Atlantic water (RAW) to penetrate through seabed troughs onto the Northeast Greenland continental shelf (e.g., Bourke et al., 1987) below the fresh and cold polar waters (PW).

The Atlantic water mass found on the shelf was described by Bourke et al. (1987) as Atlantic Intermediate Water (AIW) with temperatures ranging between 0°C and 3°C and salinities between 34.5 and 34.9. Budéus et al. (1997) found two distinct types of Atlantic waters in the trough system. They found 1°C warm Atlantic waters with salinities of 34.9 to be present throughout the southern Norske Trough, which cooled and freshened toward the 79 North Glacier, and 0.5°C warm Atlantic waters with salinities of 34.8 in the northern Westwind Trough. An anticyclonic surface circulation on the continental shelf following the trough axis was found based on hydrographic observations (Bourke et al., 1987, Schneider and Budéus, 1995), moored (Topp and Johnson 1997) and ship-based (Johnson and Niebauer ,1995) velocity measurements. In addition, Topp and Johnson (1997) proposed an anticyclonic subsurface circulation from moored measurements in Westwind Trough, in contrast to Budéus et al. (1997), who proposed that there is no one-directional flushing of the trough system. In the trough area east of the outlet glaciers, i.e., between Westwind and Norske Trough, Budéus and Schneider (1995) suggested a sill depth of 250 m causing the differences in water properties. This part of the shelf has rarely been studied due to a perennially fast sea ice cover (e.g., Schneider and Budéus, 1995; Schneider and Budéus, 1997), but is of strong interest when studying warm water pathways towards the outlet glaciers.

A survey of the 79 North Glacier in the mid-1990s led to very high estimates of submarine melt rates (about 40 m/yr locally, with a mean basal melt rate of 8 m/yr), which account for the bulk of the ice shelf mass loss (Mayer et al., 2000). The melting was attributed to the presence of AIW in the 600 m to 800 m deep subglacial cavity as observed in several conductivity, temperature and depth (CTD) profiles collected at the glacier's margins (Thomsen et al., 1997; Mayer et al., 2000). A more recent survey conducted in the summer of 2009 (Straneo et al., 2012) confirmed that the AIW found under the floating ice tongue still contains large amounts of heat to drive melting. Based on three CTD sections taken north of the main glacier front, Wilson and Straneo (2015) discussed that warm AIW cannot enter the cavity through Dijmphna Sund due to a sill of 170 m depth but needs to pass the eastern pinned glacier front. They proposed that the exchange of warm Atlantic waters between the continental shelf and the cavity through Norske Trough occurs on timescales of less than a year.

Nonetheless these implications are not based on observations towards the east/southeast of the 79 North Glacier. Based on historic and recent hydrographic and bathymetric measurements Schaffer et al., 2017 proposed a direct pathway of warm AIW from the shelf break, through Norske Trough toward the 79 North Glacier. First direct measurements of the heat transport into the cavity have been accomplished during *Polarstern* cruise PS100 in summer 2016. Those revealed a very complex bathymetry, steering the flow of AIW into the subglacial cavity.

Work at sea

Moorings

In summer 2016 moorings were deployed by the Alfred Wegener Institute and the University of Delaware on the Northeast Greenland continental shelf (PS100). The majority of the 14 moorings were recovered successfully on PS109 (Table 3.1). Three moorings were attempted to recover but could not be reached due to a thick sea ice cover. The data return of the recovered

instruments was good with most time series of the planned duration and instrument problems detected so far.

Furthermore, five moorings were deployed belonging to the physical oceanography section of AWI: four at the shelf break off Northeast Greenland and a fifth at the calving front of the 79 North Glacier (Table 3.1, Fig. 3.1). The settings of the data recording instruments deployed on PS109 is documented in Tables 3.5 to 3.11.

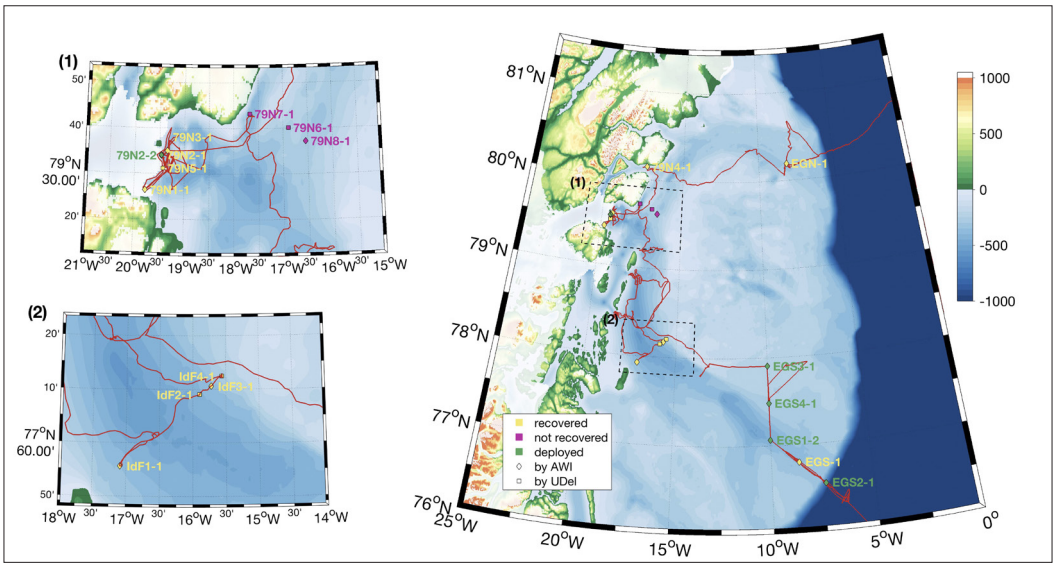

Fig. 3.1: Map of recovered and deployed moorings during PS109

Tab. 3.1: Overview of the mooring actions on PS109 with the latitude, longitude, water depth in meters, station number, and mooring number as well as the action taken

Latitude	Longitude	Depth [m]	Station	Mooring	Status
80° 11.49’ N	8° 08.96’ W	308	PS109/0020-1	EGN-1	recovered
76° 48.09’ N	8° 36.93’ W	353	PS109/0139-1	EGS-1	recovered
77° 55.62’ N	17° 05.22’ W	365	PS109/0114-1	IdF1-1	recovered
78° 09.02’ N	15° 54.00’ W	416	PS109/0113-1	IdF2-1	recovered
78° 10.59’ N	15° 43.26’ W	351	PS109/0112-1	IdF3-1	recovered
78° 12.45’ N	15° 33.68’ W	266	PS109/0111-1	IdF4-1	recovered
79° 26.40’ N	19° 46.64’ W	326	PS109/0052-1	79N1-1	recovered
79° 34.13’ N	19° 27.58’ W	474	PS109/0051-1	79N2-1	recovered
79° 35.06’ N	19° 20.56’ W	359	PS109/0050-1	79N3-1	recovered
80° 08.92’ N	17° 24.56’ W	172	PS109/0044-1	79N4-1	recovered
79° 31.17’ N	19° 25.83’ W	297	PS109/0070-1	79N5-1	recovered
79° 40.15’ N	16° 53.36’ W	257		79N6-1	under ice
79° 43.23’ N	17° 40.40’ W	404		79N7-1	under ice
79° 37.15’ N	16° 32.61’ W	287		79N8-1	under ice
77° 03.97’ N	10° 00.10’ W	425	PS109/0138-2	EGS1-2	deployed

Latitude	Longitude	Depth [m]	Station	Mooring	Status
76° 32.76' N	7° 22.58' W	763	PS109/0148-1	EGS2-1	deployed
77° 54.40' N	9° 59.79' W	233	PS109/0132-2	EGS3-1	deployed
77° 28.98' N	10° 00.15' W	262	PS109/0133-1	EGS4-1	deployed
79° 34.01' N	19° 27.83' W	476	PS109/0071-1	79N2-2	deployed

Tab. 3.2: Overview of the instruments recovered from moorings on PS109. The type is identified in Table 3.4. Also given are the serial numbers of the instruments and their depths in meters from the surface according to the mooring drawings.

Mooring	Type	SN	Depth [m] (drawing)
79N1-1	SBE37	10937	206
	SBE37	2386	322
	SBE56	6384	236
	SBE56	6385	266
	SBE56	6386	296
	QMADCP	24053	320
79N2-1	SBE37	10934	204
	SBE37	2382	467
	SBE56	6387	240
	SBE56	6388	264
	SBE56	6390	294
	SBE56	6391	324
	SBE56	6392	354
	SBE56	6393	384
	SBE56	6404	414
	SBE56	6405	434
	AQD	12665 / 7655	464
	LRADCP	23613	454
79N3-1	SBE37	3813	186
	SBE37	2385	227
	SBE37	10950	360
	SBE56	6406	272
	SBE56	6407	317
	600ADCP	19316	187
	300ADCP	1368	359
79N4-1	300ADCP	951	168
	SBE37	236	170
EGN-1	SBE37	1237	120
	SBE37	437	309
	SBE56	6222	140
	SBE56	6257	170
	SBE56	6295	200
	SBE56	6300	230

Mooring	Type	SN	Depth [m] (drawing)
	SBE56	6335	260
	QMADCP	24070	300
IdF1-1	AuralM2	00251LF	192
	SBE37	2396	192
	SBE37	439	334
	SBE56	6374	214
	SBE56	6375	244
	SBE56	6376	274
	SBE56	6377	304
	SBE56	6378	360
	QMADCP	24068	354
	SBE26	227	365
IdF3-1	AuralM2	00252LF	178
	SBE37	2392	178
	SBE37	447	320
	SBE56	6379	200
	SBE56	6380	230
	SBE56	6381	260
	SBE56	6382	290
	SBE56	6383	346
	QMADCP	24052	340
	SBE53	439	351
EGS-1	AuralM2	00179LF	130
	SBE37	2100	130
	SBE37	2393	220
	SBE37	438	345
	SBE56	6358	160
	SBE56	6359	190
	SBE56	6360	240
	SBE56	6361	260
	SBE56	6362	290
	SBE56	6373	320
	RCM8	11890	320
	LRADCP	24013	320
IdF2-1	LRADCP	3194	409
	SBE37	2932	416
79N5-1	LRADCP	3656	293
	SBE37	2917	293
IdF4-1	LRADCP	3655	258
	SBE37	2925	265

Tab. 3.3: Overview of the instruments deployed on moorings on PS109. The type is identified in Table 3.4. Also given are the serial numbers of the instruments and their depths in meters from the surface according to the mooring drawings.

Mooring	Type	SN	Depth [m] (drawing)
EGS1-2	AuralM2	000722CF	138
	SBE37 ODO	14004	110
	SBE37 ODO	13487	210
	SBE37	225	342
	SBE56	7061	135
	SBE56	7062	160
	SBE56	7063	185
	SBE56	7064	235
	SBE56	7065	260
	SBE56	7066	300
	SBE56	7083	417
	QMADCP	22388	340
	SBE26	227	425
EGS2-1	AQD	11328	80
	AQD	11333	200
	AQD	12699	300
	SBE37 ODO	13491	80
	SBE37	224	420
	SBE56	7076	110
	SBE56	7068	140
	SBE56	7069	170
	SBE56	7070	200
	SBE56	7071	250
	SBE56	7072	300
	SBE56	7073	360
EGS3-1	AuralM2	273	106
	AQD	11330	130
	AQD	11348	203
	SBE37 ODO	13490	103
	SBE37	230	228
	SBE56	7074	128
	SBE56	7075	153
	SBE56	7076	178
	SBE56	7077	203
	SBE53	439	233
79N2-2	SBE37 IMP	15723	84
	SBE39plus IM	8419	120
	SBE39plus IM	8416	155

Mooring	Type	SN	Depth [m] (drawing)
	SBE39plus IM	8420	191
	SBE39plus IM	8418	226
	SBE37 ODO	13489	235
	SBE37 ODO	13488	375
	SBE37	229	393
	SBE56	7078	270
	SBE56	7079	305
	SBE56	7080	340
	SBE56	7081	436
	SBE56	7082	456
	1200ADCP	22753	385
	LRADCP	23977	456
	DataLogger	12084	228
EGS4-1	SBE37 ODO	13983	108
	SBE37	226	257
	SBE56	7084	132
	SBE56	7086	157
	SBE56	7087	182
	SBE56	7088	207
	SBE56	7089	232
	QMADCP	14087	253

Tab. 3.4: Abbreviations of the instrument types used in Table 3.2 and Table 3.3 along with the long names and the parameters measured by those instruments

300ADCP	RDI 300 kHz ADCP	velocity profiles, temperature, pressure
600ADCP	RDI 600 kHz ADCP	velocity profiles, temperature, pressure
1200ADCP	RDI 1200 kHz ADCP	velocity profiles, temperature, pressure
LRADCP	RDI 75 kHz ADCP	velocity profiles, temperature, pressure
QMADCP	RDI 150 kHz ADCP	velocity profiles, temperature, pressure
AQD	NORTEK Aquadopp deep water	point velocity, temperature
AuralM2	ASL Aural sound recorder	sound
RCM8	Aanderaa mechanical current meter	point velocity, temperature, pressure

SBE37 ODO	SeaBird SBE37 CTD with oxygen sensor	temperature, conductivity, pressure, oxygen
SBE37	SeaBird SBE37 CTD	temperature, conductivity, pressure
SBE37 IMP	SeaBird SBE37 for inductive mooring	temperature, conductivity, pressure
SBE39 IM	SeaBird SBE39 plus for inductive mooring	temperature
SBE56	SeaBird SBE56 temperature recorder	temperature
SBE26	SeaBird SBE26 bottom pressure recorder	pressure, temperature
SBE53	SeaBird SBE53 bottom pressure recorder	pressure, temperature

Tab. 3.5: Example command file for 75kHz ADCPs

```
>TS 17/09/21,16:16:31
>CR1
>CQ255
>CF11101
>EA0
>EB0
>ED4540
>ES35
>EX00111
>EZ1111101
>WA50
>WB1
>WD111100000
>WF704
>WN70
>WP1
>WS800
>WV175
>TE00:00:07.00
>TP00:07.00
>TC20
>TB01:00:00.00
>TF17/09/21 18:30:00
>CK
>CS
```

Tab. 3.6: Example command file for 150kHz ADCPs

```
>TS 17/09/26,18:09:24
>CR1
>CF11101
>EA0
>EB0
>ED0
```

```
>ES35
>EX00111
>EZ1111101
>WA50
>WB1
>WD111100000
>WF352
>WN70
>WP1
>WS400
>WV175
>RN22388
>TE00:00:04.00
>TP00:04.00
>TB01:00:00.00
>TC50
>TF17/09/26 18:12:00
>CK
>CS
```

Tab. 3.7: Command file for 1200 kHz ADCP used to measure turbulence parameters.

```
>TS 17/09/21,16:38:22
>CR1
>CF11101
>EA0
>EB0
>ED3900
>ES35
>EX00111
>EZ1111101
>WA50
>WB0
>WD111100000
>WF44
>WN19
>WP2
>WS20
>WV175
>RN22753
>TE00:00:02.00
>TP00:00.50
>TB01:30:00.00
>TC300
>TF17/09/21 18:30:00
>CK
>CS
```

Tab. 3.8: Example summary of programmed settings for Aquadopps

```
============================================================
Deployment   : EGS2-1
Current time : 28.09.2017 08:36:21
Start at     : 28.09.2017 09:00:00
Comment:

------------------------------------------------------------
Measurement interval  (s) : 1200
Average interval      (s) : 60
Blanking distance     (m) : 0.50
Measurement load      (%) : 22
Power level               : HIGH
Diagnostics interval(min) : 720:00
Diagnostics samples       : 20
Compass upd. rate     (s) : 600
Coordinate System         : BEAM
Speed of sound      (m/s) : MEASURED
Salinity            (ppt) : 35
Analog input 1            : NONE
Analog input 2            : NONE
Analog input power out    : DISABLED
Raw magnetometer out      : OFF
File wrapping             : OFF
TellTale                  : OFF
AcousticModem             : ON
Serial output             : ON
Baud rate                 : 9600
------------------------------------------------------------
Assumed duration   (days) : 400.0
Battery utilization   (%) : 57.0
Battery level         (V) : 11.2
Recorder size        (MB) : 9
Recorder free space  (MB) : 8.973
Memory required      (MB) : 1.8
Vertical vel. prec (cm/s) : 0.6
Horizon. vel. prec (cm/s) : 0.4
------------------------------------------------------------
Instrument ID             : AQD11328
Head ID                   : A6L 6257
Firmware version          : 3.37
------------------------------------------------------------
Aquadopp Deep Water Version 1.40.14
```

Tab. 3.9: Example start protocol of microcats with oxygen sensor.

```
ds
SBE37SMP-ODO-RS232 v2.3.1  SERIAL NO. 13491  21 Sep 2017 10:28:14
vMain = 13.32, vLith =  3.11
samplenumber = 3488, free = 395969
```

not logging, stop command
sample interval = 10 seconds
data format = converted engineering
output temperature, Celsius
output conductivity, S/m
output pressure, Decibar
output oxygen, ml/L
transmit real time data = no
sync mode = no
minimum conductivity frequency = 3320.0
adaptive pump control enabled
<Executed/>
DateTime=09212017102850
<Executed/>
Adaptivepumpcontrol=1
<Executed/>
Outputformat=1
<Executed/>
TXxrealtime=0
<Executed/>
Sampleinterval=3600
<Executed/>
Samplenumber=0
memory pointers will be modified
repeat command to confirm:
Samplenumber=0
<Executed/>
StartDAteTime=100120102017090000
<start dateTime = 01 Oct 2017 09:00:00/>
<Executed/>
startlater
<!--start logging at = 01 Oct 2017 09:00:00, sample interval = 3600 seconds-->
<Executed/>
ds
SBE37SMP-ODO-RS232 v2.3.1 SERIAL NO. 13491 21 Sep 2017 10:30:41
vMain = 13.30, vLith = 3.11
samplenumber = 0, free = 399457
not logging, start at 01 Oct 2017 09:00:00
sample interval = 3600 seconds
data format = converted engineering
output temperature, Celsius
output conductivity, S/m
output pressure, Decibar

output oxygen, ml/L
transmit real time data = no
sync mode = no
minimum conductivity frequency = 3320.0

Tab. 3.10: Example start protocol of microcats without oxygen sensor.

ds
SBE37-SM V 1.6 SERIAL NO. 0224   21 Sep 2017 09:19:40
not logging: received stop command
sample interval = 10 seconds
samplenumber = 3009, free = 112134
do not transmit real-time data
store time with each sample
A/D cycles to average = 4
reference pressure = 0.0 db
serial sync mode disabled
wait time after serial sync sampling = 120 seconds
temperature = 18.82 deg C
S>DDMMYY=21092017
S>HHMMSS=092100
S>FORMAT=1
S>STORETIME=Y
S>TXREALTIME=N
S>INTERVAL=900
S>SAMPLENUM=0
S>STARTDDMMYY=011017
S>STARTHHMMSS=090000
start time = 01 Oct 2017 09:00:00
S>start STARTLATER
start time = 01 Oct 2017 09:00:00
S   SBE 37-SM
S>
S>ds
SBE37-SM V 1.6 SERIAL NO. 0224   21 Sep 2017 09:23:15
not logging: waiting to start at 01 Oct 2017 09:00:00
sample interval = 900 seconds
samplenumber = 0, free = 115143
do not transmit real-time data
store time with each sample
A/D cycles to average = 4
reference pressure = 0.0 db

serial sync mode disabled
wait time after serial sync sampling = 120 seconds
temperature = 18.86 deg C

Tab. 3.11: Example start protocol of SBE53 bottom pressure recorders.

logging will start in 10 seconds
SBE 53 BPR
S>ds
SBE 53 BPR V 1.1e SN 439 03 Oct 2017 09:58:35
user info=
quartz pressure sensor: serial number = 134957, range = 10000 psia
internal temperature sensor
conductivity = NO
iop = 7.7 ma vmain = 20.3 V vlith = 9.1 V
last sample: p = -99.0000, t = -99.0000

tide measurement: interval = 15 minutes, duration = 3 minutes, power pressure sensor continuously
measure reference frequency every 672 tide samples
logging start time = 28 Jul 2016 15:00:00
logging stop time = do not use stop time

tide samples/day = 96.000
memory endurance = 20560.3 days
nominal battery endurance = 504 days alkaline, 1469 days lithium
total recorded tide measurements = 0
total recorded reference frequency measurements = 0
tide measurements since last start = 0
transmit real-time tide data = NO

status = logging started
logging = YES

CTD and salinometer

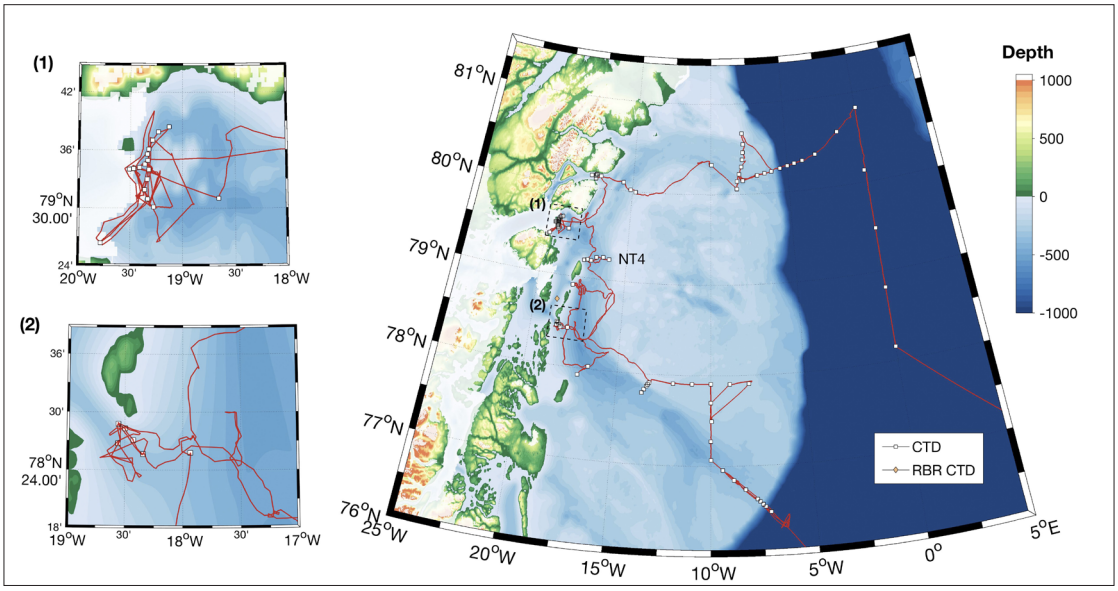

Fig. 3.2: Map of CTD stations and a single RBR CTD station accomplished during PS109

Hydrographic measurements during the PS109 cruise were conducted by a CTD system. The CTD's sensors, main unit and rosette were provided by the physical oceanography group from AWI (OZE rosette). During the entire cruise Niskin bottles from the *Polarstern* rosette were used because most bottles of the OZE rosette could not be opened properly. Altogether 90 CTD profiles were conducted. Water samplings were mainly used for chemical tracer measurements.

The CTD sonde was mounted in a rosette with 24 bottles (12 liter each) for water sampling (bottles #1-24 were mounted). The CTD contained dual sensors for temperature and conductivity, one sensor for pressure and one for oxygen. A fluorometer for chlorophyll and fluorescence, a beam transmissiometer, and a downward looking altimeter were also attached to the frame and connected to the coaxial cable. Details of the sensors can be found in Tables 3.12 and 3.13. Upward and downward looking LADCP was in serve as well. There were few events to notice. The oxygen sensor showed suspicious values for the first couple of stations on the Northeast Greenland continental shelf. In the upper about 50 m they showed a large difference between downcast and upcast. After flushing the initial oxygen sensor a couple of times, it showed good values again. However, a second additional oxygen sensor was added after station 036_01 to control the values of the initial sensor. Afterwards sensor configuration 2 was used. Adding the second oxygen sensor to the Seabird Software was not working properly though. Therefore, the A/D voltage of the second oxygen sensor was changed after station 043_01. Sensor configuration 3 was used afterwards. Changing the A/D voltage did not solve the problem. Nevertheless, the second oxygen sensor stayed attached for the time being.

Tab. 3.12: CTD configuration 1. Used for station 005_01 to 036_01

	Type	SN and calibration date
CTD	SBE911plus	
CTD-Sensors	SBE3 T0 (primary)	5101, cal.date 13-Dec-2016
	SBE4 C0 (primary)	3290, cal.date 13-Dec-2016
	SBE9plus pressure	0937, 20-Nov-2012
	SBE3 T1 (Secondary)	5112, cal.date 13-Dec-2016
	SBE4 C1 (secondary)	3570, cal.date 13-Dec-2016
Oxygen	SBE43 (primary)	2292, cal.date 07-Oct-2012
Altimeter	Benthas PSA916	47768, cal.date 23-Mar-2009
Transmissometer	WETLabs C-Star	1220, cal.date 02-Apr-2009
Fluorometer	WETLabs ECO-AFL/FL	1853, cal.date 26-May-2010
Rosette	SBE Carousel	24 bottles á 12L
Winch	EL 32	

Tab. 3.13: CTD configurations 2 and 3. Configuration 2 used for station 041_01 to 043_01. Configuration 3 used for station 044_02 to 157_01ww

	Type	SN and calibration date
CTD	SBE911plus	
CTD-Sensors	SBE3 T0 (primary)	5101, cal.date 13-Dec-2016
	SBE4 C0 (primary)	3290, cal.date 13-Dec-2016
	SBE9plus pressure	0937, 20-Nov-2012
	SBE3 T1 (Secondary)	5112, cal.date 13-Dec-2016
	SBE4 C1 (secondary)	3570, cal.date 13-Dec-2016
Oxygen	SBE43 (primary)	2292, cal.date 07-Oct-2012
	SBE43	1834, cal.date 12-Jul-2016
Altimeter	Benthas PSA916	47768, cal.date 23-Mar-2009
Transmissometer	WETLabs C-Star	1220, cal.date 02-Apr-2009
Fluorometer	WETLabs ECO-AFL/FL	1853, cal.date 26-May-2010
Rosette	SBE Carousel	24 bottles á 12L
Winch	EL 32	

Stations 044_02 and 045_01 were initially conducted with a different station number. The names were changed in all files afterwards. They could not be changed in the header files. Table 3.14 shows all stations, that had to be renamed. At station 057_01 the pump did not start working. After waiting a while the CTD was brought up back on deck. The sensors were frozen. After flushing the sensors with warm water the problem was solved and the CTD station could be conducted. At station 063_01 the altimeter detected the bottom at around 100 m depth even though the hydrosweep showed water depth of about 300 m. The cast was stopped once the altimeter showed 10 m readings above ground. After station 080_01 bottles 9, 14, and 16 were replaced as bottle number 14 did not close properly anymore, number 9 was leaking repeatedly and in number 16 the spring broke while preparing the CTD for the next cast. The bottles used for the replacement were taken from the *Polarstern* rosette. As on the former cruise PS107 all bottles from the *Polarstern* rosette and the OZE rosette were swopped, bottles 9, 14 and 16 are now back again on their initial rosette. Station 144_01 was aborted by the captain due to severe weather conditions during the downcast.

Tab. 3.14: List of stations that had to be renamed

Initial station number	Changed station number	Station number after processing	Station number in station book
045_02	044_02	044_02	044_02
046_01	045_01	045_01	045_01
086_01	086_02	086_02	087_01
120_01	120_01	120_01	119_03

Behaviours of temperature and salinity sensors were monitored by taking differences between values of primary and secondary sensors (secondary minus primary). In general, the sensors performed well and no drift has been detected (Fig. 3.3). The difference between the records of the temperature sensors at depth is in a range of ± 0.01°C for most stations. The difference of conductivity sensors is ± 0.01 mS/cm for most stations. The difference in salinity derived from both conductivity cells is less than 0.004 PSU. All sensors show notable events at several stations (station numbers 126_01, 144_01, and 151_01) where they differ from the range given above. Additionally, the conductivity sensors show a large offset at stations 128_01 (Δcond = 0.018) and 153_01 (Δcond = 0.022) close to deepest depths.

In order to define offset and drift of conductivity sensors, 59 salt samples were taken at 23 stations. Conductivities were measured under temperature and pressure controlled environment using the Optimare Precision Salinometer on-board *Polarstern* (SN. 006) and standard seawater from Ocean Scientific International. The salinity measurements with the salinometer were conducted following a guideline of Operational manual of Precision salinometer System issued on 1 May 2011. Preliminary results suggest that the primary and secondary conductivity sensors may have an offset of 0.0012 ± 0.0021 [psu] and +0.003 ± 0.0028 [psu], respectively (Fig. 3.4). Precise calibration on the conductivity sensors will be carried out later on. Likewise, we collected 35 oxygen samples from 6 casts using a titration method for later calibration of the oxygen sensor.

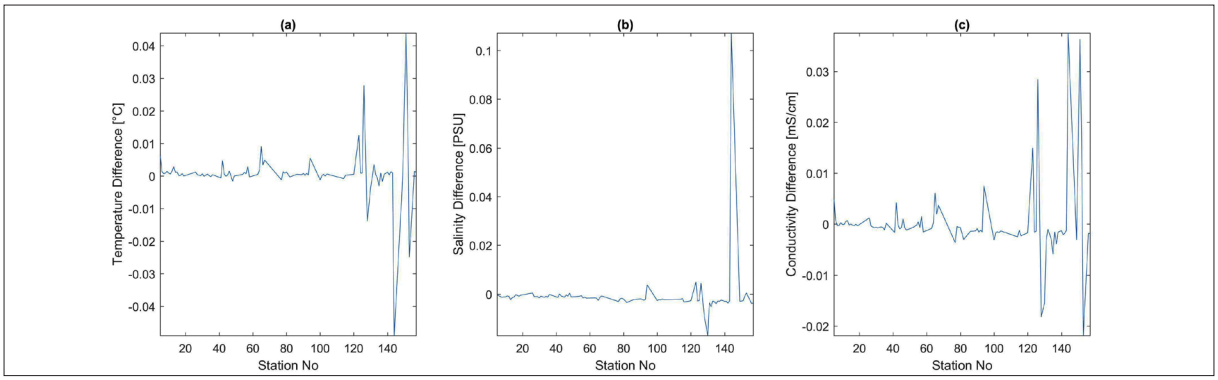

Fig. 3.3: (a) Difference in temperature sensors (secondary - primary). (b) Difference in salinity values (secondary - primary). (c) Difference in conductivity sensors (secondary - primary).

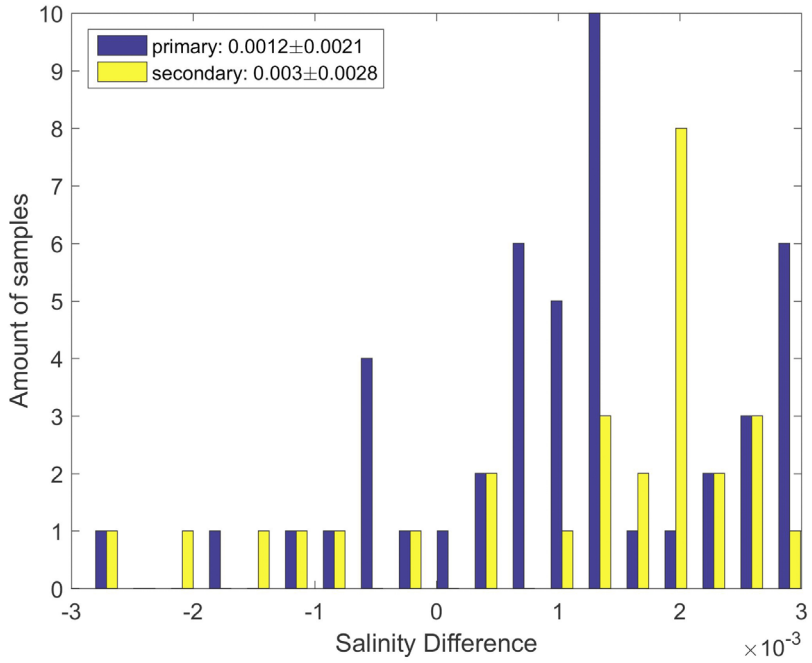

Fig. 3.4: Difference in salinity measurement as histogram. Salinity derived from primary (secondary) sensors in blue (yellow).

Tab. 3.15: CTD salinometer results

Date	Station	Cast	Depth	OSA	Standardization	Remarks
18.09	5	01	1013	34.9108	2017-09-18 09:31	
18.09	5	01	911	34.9059		
18.09	5	01	809	34.9171		
18.09	5	01	711	34.9111		
18.09	6	01	1015	34.9148		
18.09	8	01	709	34.8825		
18.09	11	01	3228	34.9293		
18.09	11	01	3054	34.9284		
18.09	11	01	2849	34.9216		
18.09	11	01	2644	34.924		
19.09	6	01	911	34.9159	2017-09-19 14:27	
19.09	6	01	810	34.9187		
19.09	7	01	2819	34.927		
19.09	7	01	2749	34.9246		
19.09	7	01	2542	34.9222		
19.09	7	01	2032	34.9193		
19.09	7	01	1776	34.9162		
19.09	8	01	1014	34.9006		
19.09	8	01	810	34.8889		
19.09	11	01	2440	34.9198		
19.09	11	01	2235	34.9211		
19.09	11	01	2235	34.9209		
19.09	14	01	1534	34.9168		
19.09	14	01	350	34.8954	2017-09-30 12:33	
30.09	8	01	911	34.8948		
30.09	43	01	430	34.8471		
30.09	65	01	459	34.8332		
30.09	67	01	463	34.8254		
30.09	67	01	405	34.7534		
30.09	86	01	485	34.9187		
30.09	86	01	405	34.9135		
30.09	90	01	384	34.9225		
30.09	90	01	354	34.9205		
30.09	103	01	429	34.9236		
30.09	103	01	405	34.9232		
02.10	6	01	708	34.929	2017-10-02 09:52	
02.10	43	01	405	34.8467		
02.10	65	01	404	34.7503		
02.10	115	01	504	34.9273		
02.10	115	01	405	34.9252		

Date	Station	Cast	Depth	OSA	Standardization	Remarks
09.10	93	01	385	34.9249	2017-10-09	
09.10	93	01	324	34.9160	09:22	
09.10	116	01	664	34.9376		
09.10	120	01	470	34.9159		
09.10	120	01	455	34.9141		
09.10	120	01	352	34.8958		
09.10	126	01	396	34.9305		
09.10	126	01	303	34.9666		
09.10	137	01	345	34.9401		
09.10	142	02	1168	34.9108		
09.10	142	02	1012	34.9033		
09.10	143	01	771	34.8915		
09.10	153	01	496	34.9297		
09.10	156	01	3388	34.9159		
09.10	156	01	3052	34.9173		
09.10	156	01	1013	34.9165		
09.10	157	01	3687	34.9169		
09.10	157	01	3567	34.9168		
09.10	157	01	1013	34.9162		

RBRconcerto CTD and Echosounder

The RBR*concerto* CTD system (serial number 060470) and the Echosounder (Fish-finder S2009) were used for a helicopter borne deployment east of Zachariæ Isstrøm (Fig. 3.2). The RBR*concerto* conductivity, temperature, pressure logger was set to record at 12 Hz to the internal memory. The time of the sensor was set to UTC via the time setting of the used laptop. The RBR*concerto* was attached to an 800 m fishing line together with an electronic high seas fishing pole in order to achieve a system with maximum flexibility and light weight handling requirements. Above the CTD a buoyancy element (- 2.5 kg) was attached to the line. Below the CTD a 10 m long line with a lead weight of 2 kg was attached. Both upcast and downcast speeds were roughly 0.5 - 1 m/s. The fishing pole's electrical motor was powered by rechargeable batteries located in a water-tight box.

The instrument was started using its twist mode, i.e., using its WLAN module. However, operating the RBR CTD with the WLAN module uses a lot of power (~ 0.4 V/30 min) and should better be avoided in the future. The data was read out back on board of *Polarstern* because the limited helicopter time did not allow a second cast anyways. The data agrees well with CTD measurements conducted with the regular CTD system. Significant differences were detected between the wire out readings of the fishing pole and the depth calculated from the pressure sensor. The wire out reading was up to 10 % smaller than the depth calculated from the pressure sensor. The time when the weights had reached the bottom could be clearly detected as the tension on the fishing line vanished. The maximum water depth was confirmed from the echosounder readings carried out beforehand.

With this set- up, one station in the ice-covered area in front of Zachariæ Isstrøm was occupied which could not be reached by *Polarstern*. From the helicopter a half-meter wide crack between two large ice floes (fast ice) was selected. The helicopter was landed on one of the ice floes. Upon landing of the helicopter, the position of the helicopter's GPS was recorded manually. The operators were connected to the helicopter by a rope and then walked to the side of the ice floe. The new ice (slush) filling the crack between the ice floes was broken with a metal pole. Then the Echosounder was deployed and lowered by about 18 m into the water (with its 20 m long cable connected to the deckunit). After about 5 min the echosounder received a depth signal of 442 m. Based on these depth records it was decided to carry out a RBR CTD cast at the same site. The RBR CTD was deployed with the fishing line from the side of the floe. During the upcast water drops froze to the fishing rod. In addition, the water in the crack between the ice floes started to refreeze and thus needed to be broken with a metal pole from time to time. If the deployment through the slushed ice damaged the fishing line remained unknown. The cast was completed successfully. The station time between landing of the helicopter and subsequent take off was about 1 hour 15 minutes. The maximum depth reached by the RBR CTD was 454 m.

At another time the RBR CTD was planned to be used over the side of *Polarstern*. However, when deploying the RBR CTD into the water, the fishing line broke and the instrument got lost. If this was caused by too strong tension put on the fishing line or a potentially damaged fishing line (due to the former deployment through ice slush) remained open. In the future one should better lower the buoyancy element first into the water before deploying the CTD/ weight to reduce the tension on the fishing line while deployment and avoid operations with temperatures well below the freezing point.

Lowered ADCP

Set-up

Two 300kHz RDI Workhorse ADCPs were mounted on the rosette to act as lowered ADCPs. The LADCP consists of the two 300kHz ADCPs and a battery container. Communication was established to a computer in the winch room via two cables (for master and slave) that were attached before and after each cast to the ADCPs. The ADCPs were operated using the GUI of the LADCP tool V1.7 from GEOMAR. The LADCP computer time was synchronized with the ships NTP server directly.

Data collection

LADCP measurements were conducted at all CTD stations. The data was downloaded after each cast with a download rate of about 5.7 kb/sec resulting in download times of approximately 20 min for deep casts of 3,000 m and 5 min for shallow casts of 300 m and saved as binary files. The Master (downward looking device) and slave (upward looking device) data file names consist of the station number (three digits), an abbreviation indicating the viewing direction (UP for upward and DN for downward) and a running number with three digits beginning with 000, representing the file number, in case there are multiple files. For example at station 5, data is saved in the files "005DN000.000" and "005UP000.000". These files are stored in a folder named like the station number. In these folders log files documenting all actions conducted as starting (with configurations), stopping and downloading are kept as well.

When starting a new cast, the ADCP software automatically counts upwards to define the new station number. If the next station number differs from that, it is possible to set the counter of the software to any other number.

At station numbers 5, 6, 41, 44, 45, 52, and 54 the casts were originally recorded with a different station number. To facilitate processing together with the CTD data and to avoid confusion, the names of the files were changed afterwards to the station names of the corresponding CTD stations. A backup copy of the files with their original names was kept and a text file describing the renaming was added to the folder of the respective stations. So far, no problems occurred during the processing of the renamed files.

At station 27, 47, and 92 the data files of the Master were damaged. A first indicator of this particular problem was an unrealistic high end voltage (e.g., 179 824 for station 27) at the end of the download routine. Second, when checking the data in WinADCP, the total cast was far longer than in reality, a warning of “Extra Data in file” was displayed and an average ensemble time significantly larger 1:30 sec was found. Opening the binary files showed that after a certain ping number the file contained additional lines with numbers without any reference to the cast. As these additional lines were added to the recording after the ADCP was on deck, all information collected beforehand seemed to be useful. Therefore, the files were split with WinADCP in subsets and stored in a folder called subset within the original station folder. For example, the files 047DN000.000, 047DN001.00, 047DN002.000, 047DN003.000, 047D004.000, and 047DN005.000 contain the pings 1-1335 of the original file 047DN000.000. Pings > 1336 were not included in the subset to avoid copying the damaged part.

After cast 34 it was impossible to reconnect to the ADCP, neither via the LADCP tool nor BBtalk. First, we assumed that the batteries were dead, but even with an external power supply, connecting was not successful. However, the ADCPs continued (or possibly restarted) pinging. After station 35 (followed shortly after station 34), communication to the ADCPs was established via the software again. Download was successful, but the two casts were recorded in many files. It seems like the ADCPs stopped working properly at the upcast of station 34, creating multiple files containing a few or even no pings. A file 034UP010.000 was on the ADCP, but could not be downloaded. As it had a size of 0 bite, the file was erased. A backup was created from all files downloaded after the cast 35. The files 034DN000 to 034DN006 looked good and were used in the processing Matlab routine. The files 034DN007, 034DN008, 034DN009 were empty and therefore deleted. 034DN010 and 034DN011 contain some information and are part of the upcast of station 34. 034DN012 has stored all data for station 35 and was renamed to 035DN000 and stored in a new folder 035. Station 34 is recorded in the files 034UP000 to 034DN009. Files 034UP011 and 034UP111 appear identical and contain data for station 35, i.e., 034UP011 was renamed to 035UP000 and moved to folder 035.

Even though the LADCP seemed to work normally during a check after station 35, no connection could be established to the instrument after station 36 again. This time, a very low battery voltage of 29 V was measured (instead of regular 46 V). After exchanging the batteries, the LADCP worked again without any problems.

At cast 79 the master was not started properly. The log file of the start shows an incomplete transmission of the configurations. Consequently, no downward looking data was recorded.

Because station 92 had an unrealistic high end voltage coming along with “Extra data in file”, the batteries were exchanged a second time to prevent a second failure of the instruments as occurring at station 34 to 36. Later, detailed analysis showed that the high voltage is not necessarily followed by a failure of the instrument (e.g., station 47).

At station 153 the ADCP was not turned off and running for about 10 hours resulting in a very large data file. The ADCP could be restarted after downloading all files and continued to function as normal.

Configurations

The settings documented in Tables 3.16 and 3.17 were used during the entire cruise. Specifically, we used a bin size of 10 m, a maximum range of 200 m, beam coordinates, no blanking after transmission, narrow band processing, and a timing of the master and slave such that the acoustic energy of the master is separated by 0.55 seconds from the acoustic energy of the slave. These configurations were tested on PS103 and found to produce satisfying results.

Data processing

On board data processing was carried out with the GEOMAR LADCP software Version 10.21 April 2016 that is executed in Matlab. The software combines, if available, data from the LADCP, CTD, navigational data, and a vessel mounted ADCP to conduct the velocity inversion method.

The CTD data was prepared using a data conversion programme called prladcp that opens seabird and initiates the steps datcnv, celltm, binavg, and trans. The resulting file has 1-second resolution. Furthermore a CTD data file is needed which has a resolution of 1 dbar that was provided through the programme Manage CTD ran on the CTD computer. Navigational information were obtained from the CTD data as the programme Seasave, used for ctd data recording, saves the NMEA navigational data string during the cast.

Data was repeatedly reprocessed when additional information were available (e.g., reprocessed LADCP data). The software package produces a lot of diagnostic output. The written one is stored in a log file in the log folder and 16 figures are created and saved in the folder plots. The output not only displays the calculated velocities in West to East (u) and South to North (v) direction, but also additional figures that help to identify error sources and problems of the acquisition process.

Overall, the obtained information resembled the scientific assumptions and agreed well with SADCP data. The error of the velocities was most of the time in the order of 5 cm/s.

Table 3.18 summarizes which casts suffered from one or more of the most common warnings that include compass issues, a time lag between both ADCPs, weak beam performance and a small range of good data, as well as a large offset between SADCP and LADCP data. Reprocessing the data with corrected SADCP data or with a different setting may change these problems.

Common warnings were:

- Large **compass differences** (> 15°) occur due to the high latitude of the study area.
- The routine does not only the **velocity inversion**, but calculates a solution based on the **shear method** as well. If both disagree substantially, the error estimate is larger.
- **Beam performance** is targeted in different plots. If there are issues with a beam, the beam performance is reduced, as well as the range of good data significantly below 100 (Fig. 2). A third indicator for weak beams of one instrument is Fig. 3 (center column). Horizontal banding indicates consistency between the data from the two instruments. Reduced beam performance often occurred on casts following each other but came back to the former higher level later on without any changes made.
- Comparing **SADCP** data and LADCP data, various issues were detected. In a lot of cases, both data sets agreed well, but on others the SADCP data was far outside of the error range of the LADCP data. In some cases no overlapping finite SADCP data was

found for the time period of the LADCP cast; an issue that is often caused by rough weather or the use of the thruster. For a few casts, all SADCP values were removed due to low weight during the inversion.

- Another group of warnings deals with the **time of master and slave**. In all processed casts, there was the warning “data at beginning of downlooker is missing” indicating that uplooking and downlooking instruments differ in their timing. Also, the ping rate seems to vary in the downward looking instrument. The processing routine finds the best lag between both instruments by matching the vertical velocity. The lag is found via two routines and if both routines disagree, there is another warning saying “Different lag results!!! Check new routine”. As set in the configuration on purpose, the slave pings 0.55 secs after the master. This provokes a difference in timing between both instruments. However, it remains unclear so far whether this difference leads to all the warnings above. So far, one could not identify that any problems arise from the time lag.

In the context of the lost connection to the instrument at station 34, the battery changes, and the unrealistic high voltage at casts 27, 47, and 92, the voltage transmission was examined in Fig. 2 of the processing routine. The output of station 34 shows an uneven transmission quickly changing from 50 to 0 Volt and back. After exchanging the batteries (after station 36 and 92) the mean transmission increased, however the transmission does not decrease continuously between these changes. Also, no clear indications were observed in the output of the stations that could predict a failure of the battery.

The data of station 47 and 92 could only be processed without CTD data (disagreement between the two data sets due to splitting of 47 and 92). Station 79 (missing master file) could not be processed so far.

Tab. 3.16: Configuration file of the Master LADCP (if other than default)

CR1	;Set to factory defaults
WM15	;LADCP water ping mode 15
WV250	;Ambiguity velocity 250
WN20	;20 bins
WS1000	;10 m bins
WF0	;No blank after transmit
WB1	;Narrow band
EZ0111101	;Fixed speed of sound
EX00111	;Beam coordinates, use pitch/roll, 3 beam solution, bin mapping
WP1	;Single ping data
TP 00:00.90	;Ping length of 0.9 seconds
TE 00:00:01.20	;Ensemble length of 1.2 seconds
SM1	;Master, SM2 for Slave
SI0	;Sync pulse on every ping, n/a for Slave, but needs ST0300
SA011	;Sync pulse before every ensemble
SW5500	;Wait 0.55 seconds which is 550.0 milliseconds, n/a for Slave
RN 005DN	;cast specific name of the file ;here station 005
CK	;Keep parameters as user default
CS	;Start pinging

Tab. 3.17: Configuration file of the Slave LADCP (if other than default)

CR1	;Set to factory defaults
WM15	;LADCP water ping mode 15
WV250	;Ambiguity velocity 250
WN20	;20 bins
WS1000	;10 m bins
WF0	;No blank after transmit
WB1	;Narrow band
EZ0111101	;Fixed speed of sound
EX00111	;Beam coordinates, use pitch/roll, 3 beam solution, bin mapping
WP1	;Single ping data
TP 00:00.90	;Ping length of 0.9 seconds
TE 00:00:01.20	;Ensemble length of 1.2 seconds
SM2	;Master, SM2 for Slave
SA011	;Sync pulse before every ensemble
ST200	;wait time before starting pinging without sync pulse 200 sec
CQ255	;power output
RN 005UP	;cast specific name of the file;here station 005
CK	;Keep parameters as user default
CS	;Start pinging

Tab. 3.18: List of common problems with corresponding station numbers.

Station	Large Compass difference (> 15°)	elevated shear-inverse difference	beam per-formance	SADCP outside of error range LADCP	Large error of velocity	No overlapping finite SADCP data found	Large time diff./ different lag results
5	x						
6							
7		x					
8							
9							
10		x					
11					x		
12		x					
13							
14		x					
15				x		x	
16				x			
17				x			
18				x			
19			x				
26			x		x		
27		x	x	x			

Station	Large Compass difference (> 15°)	elevated shear-inverse difference	beam per-formance	SADCP outside of error range LADCP	Large error of velocity	No overlapping finite SADCP data found	Large time diff./ different lag results
29				x			
30				x			x
31			x	x			
33			x	x			
34			x	x			
35				x			
36	x			x			
41	x			x	x		
42				x			
43				x			
44							
45							
46							
47	Cannot process data together with CTD data (only possible without CTD)						
48			x		x		
49					x		
52					x	x	
54						x	
55						x	
56						x	
57						x	
58						x	
63			x			x	
64							
65							
66							
67							
77							
78				x			
79	Cannot process because only slave						
80							
82							
86	x						
89			x	x			
90				x			
91	x		x				

Station	Large Compass difference (> 15°)	elevated shear-inverse difference	beam per-formance	SADCP outside of error range LADCP	Large error of velocity	No overlapping finite SADCP data found	Large time diff./ different lag results
92	Cannot process						
93	x		x	x			
94			x	x			
100							
101							
102							
103							
104							
114				x			
116	x						
120				x			
123	x		x				x
124			x	x			
125	x			x			
126				x			
128	x						x
130							x
131							x
132							X
133			x				
134	x		x				x
135	x		x	x			
136	x		x				
137			x	x			
138							
140					*SADCP removed: low weight		
141	x			x			x
142							x
143				x			
144	Cast aborted due to high waves						
149	x						
151	x						
152							
153			x				
156		x					
157		x					

Vessel mounted ADCP

Polarstern contains a vessel-mounted acoustic Doppler current profiler (VmADCP) that sends and receives sound near 153 kHz (Firmware 23.16) from which to estimate vertical profiles of horizontal ocean velocity. Data are collected in beam co-ordinates with convex orientation nominally 30 degrees from vertical. Velocity vectors are measured relative to the moving ship whose velocity vector must be removed in order to measure water currents. Two independent methods are available to estimate the ship's velocity over ground. The first uses GPS while the second uses a bottom tracking pulse. The latter is always more accurate, but limited to water depths less that about 700 m. Hence, we profiled the water column below the ship's hull during PS109 in two configurations that are listed in Table 3.19.

The deep-water setting was used during transit to and from the continental shelf off North-east Greenland where we used the shallow-water settings. Table 3.20 lists the files along with their start and end times and locations.

Tab. 3.19: Configurations of the VmADCP used during PS109.

Configuration Parameter	Shallow-water	Deep-water
NN (# of vertical bins)	50	80
NP (pings per ensemble)	1	1
NS (bin length in meters)	8	4
NT (transmit length in meters)	8	4
NF (blanking after transmit in meters)	8	4
BP (bottom-tracking pings per ensemble)	1	0
BX (bottom-tracking range in meters)	800	n/a

Tab. 3.20: List of all VmADCP data files.

File	Start time (UTC) and location (Lon E and Lat N)	End time (UTC) and location (Lon E and Lat N)
00*	2017 09-12 13:12 19.074657 69.697835	2017 09-14 18:47 4.965955 77.160165
01*	2017 09-14 18:47 4.964045 77.160573	2017 09-16 10:35 -0.628025 80.717565
02*	2017 09-16 10:35 -0.630015 80.717455	2017 09-16 22:25 -4.539117 80.308265
03*	2017 09-16 22:31 -4.537772 80.307923	2017 09-16 22:34 -4.551795 80.308867
04	2017 09-16 22:38 -4.600520 80.305220	2017 09-17 22:50 -6.754148 80.211185
05	2017 09-17 22:50 -6.754088 80.211173	2017 09-19 08:16 -10.083518 80.366405
06	2017 09-19 08:16 -10.083823 80.366390	2017 09-19 22:21 -13.331477 80.002717
07	2017 09-19 22:21 -13.332167 80.002697	2017 09-21 00:24 -17.414392 80.103355
08	2017 09-21 00:25 -17.413472 80.103405	2017 09-21 18:35 -19.784070 79.438995
09	2017 09-21 18:35 -19.783912 79.438982	2017 09-22 21: 4 -19.298838 79.567292
10	2017 09-22 21: 4 -19.298800 79.567295	2017 09-24 14:14 -19.324410 79.571410
11	2017 09-24 14:14 -19.323925 79.570828	2017 09-25 13:54 -17.506778 79.551395
12	2017 09-25 13:55 -17.504712 79.551532	2017 09-26 16:52 -17.099092 79.124760
13	2017 09-26 16:53 -17.099492 79.124488	2017 09-27 18:37 -18.469050 78.379480
14	2017 09-27 18:37 -18.469825 78.379702	2017 09-28 10:53 -18.340190 78.428115
15	2017 09-28 10:54 -18.340163 78.428128	2017 09-29 22:14 -16.567277 78.031557

File	Start time (UTC) and location (Lon E and Lat N)	End time (UTC) and location (Lon E and Lat N)
16	2017 09-29 22:14 -16.567120 78.031567	2017 10-01 10:39 -17.963633 78.907040
17	2017 10-01 10:40 -17.963680 78.907055	2017 10-02 09:19 -15.695562 78.244990
18	2017 10-02 09:19 -15.693392 78.244940	2017 10-03 10:11 -13.158120 77.939490
19	2017 10-03 10:12 -13.158060 77.939592	2017 10-04 11:29 -10.029763 77.277670
20	2017 10-04 11:29 -10.029888 77.277658	2017 10-04 15:25 -9.666655 77.003270
21	2017 10-04 15:25 -9.662773 77.002535	2017 10-05 15:12 -6.370263 76.312987
22	2017 10-05 15:13 -6.369758 76.313108	2017 10-07 09:16 -6.002793 76.181992
23*	2017 10-07 09:21 -5.958898 76.168457	2017 10-08 12:50 -1.783817 72.574452
24*	2017 10-08 12:50 -1.783427 72.573718	2017 10-09 12:39 0.037162 68.228260

(*) Deep-water configuration

The shallow water setting uses an 8-m long pulse that maximize water-tracking range beyond 350-m in a good scattering environment such as the continental shelf. In water less than 800-m deep we always use a separate bottom tracking pulse that generally found the bottom up to 720 m depths. The long pulse emphasizes depth penetration over surface layer resolution, that is, we do not obtain any velocity estimates within about 12-m below the 11-m deep hull of *Polarstern*, that is, the first velocity bin below the surface represents an average between 23 and 31 m below the sea surface. The deep-water setting used *Polarstern* default settings that were left untouched.

Processing

We calibrated the VmADCP using well-established methodology initially devised by Joyce (1989) that relates the beam co-ordinate system of the ADCP to one that is fixed to the earth. It includes finding the physical misalignment of the transducers (nominally 45 degrees on *Polarstern*) as well as a scaling constant that relates to beam forming characteristics, speed of sound uncertainties, etc. We here use all bottom track data that satisfied all the following criteria for each individual bottom tracking ping:

1. Bottom-tracking Error Velocity < 0.2 m/s;

2. Bottom-tracking 4-beam solutions only;

3. Bottom-tracking correlations > 245 counts;

4. Ship-Speed from GPS less than 7 m/s and more than 2 m/s.

All data passing this screening within a 2-min window were sorted with the largest and smallest 10 % of values removed to reduce outliers due to ice or bubbles or other material interfering with the acoustic signal transmission and receptions. Formally, this procedure forces the probability density distribution of velocity estimates within an ensemble towards a Gaussian or normal distribution. More details and an application to the VmADCP aboard USCGC Healy can be found in the appendix of Muenchow et al.,. (2007).

The above processing resulted in 5,635 ensembles of 2-minute ship velocity components to find misalignment and scaling factors which were

alpha = -44.046 and beta = 1.03675

Fig. 3.5 shows the scatter of the 5,635 estimates of alpha and beta as a function of ship speed.

Similarly processed values for PS85 in 2014 from only 529 ensembles collected in the same study area were $alpha_{2014}$ = -44.352 and $beta_{2014}$ = 1.033604 which are comparable to the more robust 2017 calibrations.

Hence the correct heading angle "hh" applied to ADCP beam co-ordinates from the ship's measured heading "Head" is hh = Head – alpha while the scaling is (u,v) = $(vx,vy)_e$ * beta where (u,v) are corrected and calibrated ship velocity components determined from the earth-referenced horizontal velocity vector $(vx,vy)_e$ which results after all rotational matrices for heading, pitch, and roll are applied. In the absence of bottom tracking, the misalignment angle and scaling constant must be applied to velocity profile data before the GPS-derived ship velocity vector is removed to result in absolute earth-referenced water velocity vectors.

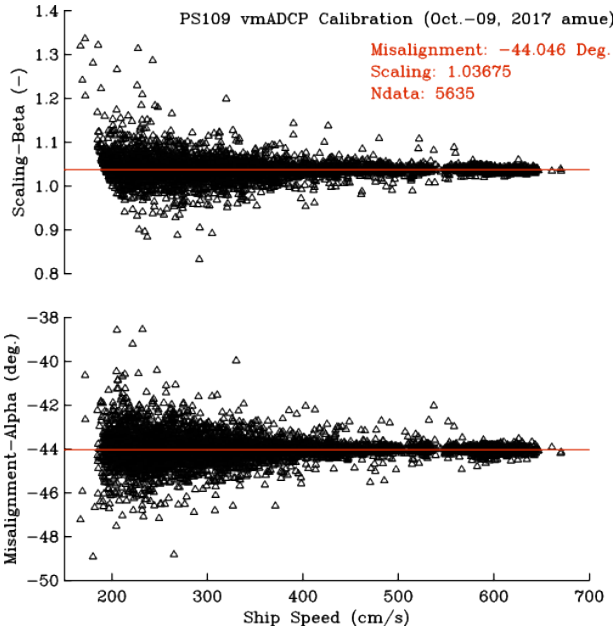

Fig. 3.5: PS109 VmADCP calibration

Performance

While the direct comparison of bottom-tracking (BT) and GPS-derived velocity components appear pleasing (not shown), a histogram of the actual velocity differences BT-GPS for both east and north components provides more quantitative evaluation of the instrument's performance. Note that these errors translate directly into water tracking errors. Fig. 3.6 shows the histogram, which estimate the probability density function (pdf) of velocity errors. The top panel shows this pdf in cumulative form.

The distribution peaks near zero velocity difference, however, substantial variance resides in the broad shoulders. More specifically, a 1 in 10 chance exists that the velocity error exceeds ± 6.5 cm/s. This is a conservative estimate of a 90 % confidence limit for VmADCP velocity measurements during PS109. Assuming a random GPS position error of about 2 m, say, we find a GPS velocity error of about 3.4 cm/s for 2 minute samples. Such a (GPS) error will disappear, if the ship's velocity is determined from a bottom tracking pulse. The errors will also be reduced via longer ensemble averaging periods.

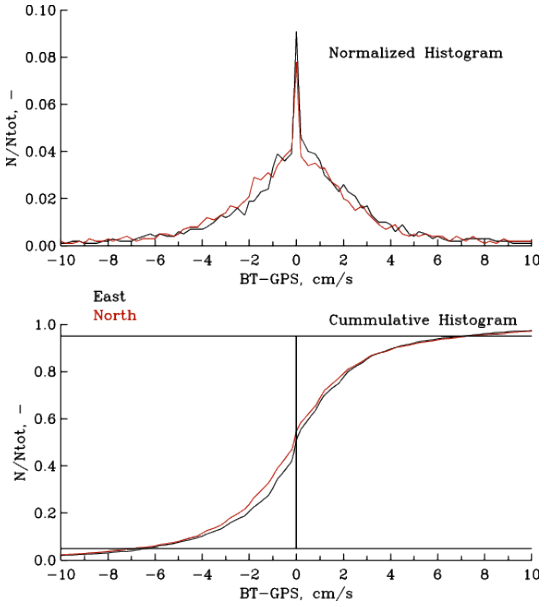

Fig. 3.6: Probability density function (pdf) of velocity errors. The top panel shows the pdf in cumulative form

Microstructure profiler

Microstructure measurements were carried out to estimate the strength of turbulent motion and the associated energy dissipation rates in the water column, which in turn can be interpreted as an indicator for the mixing strength. The key question is to quantify the turbulent exchange of properties between the warm and salty layer of Atlantic water at depth and the cold and fresh polar water layer sitting on top.

In total, 19 profiles were measured at 6 different locations on the Northeast Greenland continental shelf. The first station 071_02 is situated in front of the 79 North Glacier. Stations 096_01 and 111_01 are located in the northern part of Norske Trough, with the former close to the chain of islands east of the Zachariæ Isstrøm, and the latter on the Isle de France section. The last three stations (123_02, 125_04, 127_01) are located in the mid-part of Norske Trough.

The microstructure winch system was mounted onto *Polarstern's* stern railing, as measurements over the side of the ship were not possible due to the broken stern thruster. During the measurements, the ship slowly moved forward (~ 0.3 knots) to prevent the probe from moving under the ship. The ship track allowed for generally ice-free conditions during lowering and hoisting of the probe. The sinking depth of the probe after winch stop highly varied from station to station so that the target depth was usually corrected after the first cast. On few occasions the probe was falling 10-20 m above the ground and hoisting was started before the probe was at depth.

The used microstructure probe is of the type MSS90D (SN MSS075) and was equipped with a standard CTD sensor set (pressure, temperature and conductivity, SN 30707) as well as a Chlorophyll A sensor (SN 210 4588). Furthermore, the microstructure is resolved by two fast temperature sensors, i.e., NTC and NTCHP (SN 192 and 8048, respectively), and two high resolution current shear sensors SHE1 and SHE2 (SN C6046 and C6161, respectively).

The first planned station could not be conducted at all, as one of the plugs of the connection cable between the probe and the winch was broken. After the ship's electrician fixed the plug, we aimed at testing the performance of the probe in the water at station 044_03. However, the probe did not sink because it was not balanced before the cruise. In order to adjust the sinking velocity buoyancy elements and/or weight rings need to be added to/removed from the

probe. Before the next station (071_02), one buoyancy element and three weight rings of the sizes small, medium and large were removed. At station 071_02 we aimed at determining the sinking velocity. However, after two test profiles (that reached down to roughly 50 m depth), the connection between the profiler and the USB-Interface (connected to the notebook) cut off and the station was aborted. It turned out that the microstructure probe had problems to operate in cold conditions (with air temperatures of about -17 to -5°C). After starting the probe the voltage to the probe should range between 70 and 80 mA. Instead, the voltage was 210 mA and the probe did not start measuring. While sometimes the voltage reduced to 73 mA after some minutes, at other times the voltage remained constant at 210 mA and the probe could not be operated. After mailing to the manufacturer resistors were added to increase the maximum voltage to get the probe started. More tests were run to increase the probe's voltage. Although most of the tests succeeded, the problems occurred again from time to time and no adequate solution could be found on board. Due to these problems no measurements could be obtained in our main area of interest, i.e., the region in front of the 79 North Glacier, but some stations were completed inside Norske Trough.

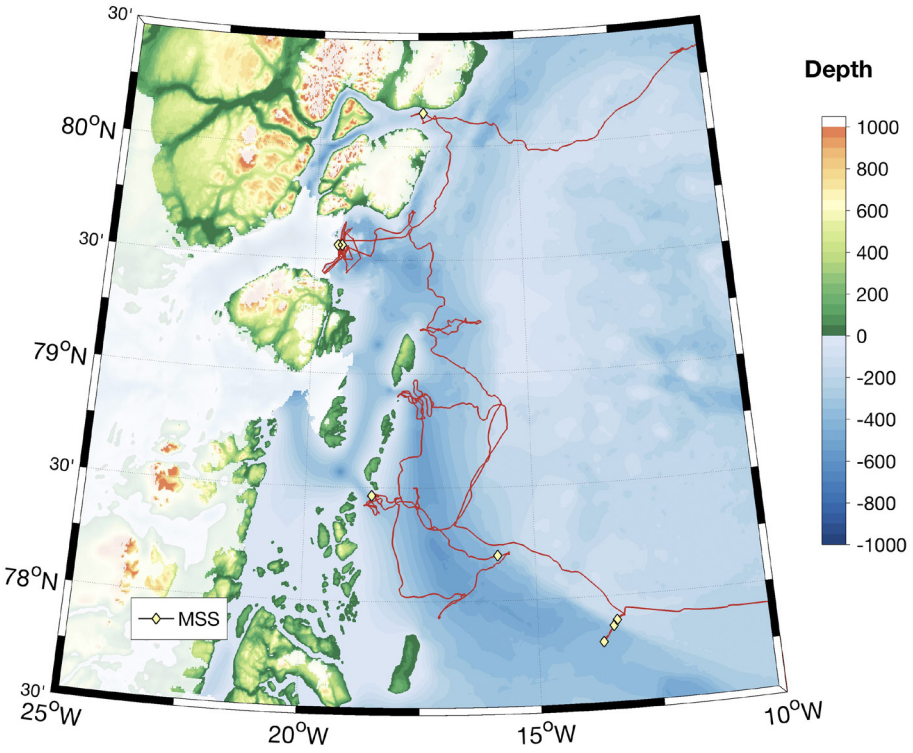

Fig. 3.7: Map of the microstructure sonde stations during PS109.

At stations 096_01, 111_01 and 123_02, the remaining weight rings were added stepwise to the probe (first the large one at station 096_01, then the small one at station 111_01 and lastly the medium one at station 123_02), as the sinking velocity generally appeared slightly too small in the processed data. We ended up with a sinking velocity of approximately 0.6-0.7 m s^{-1}.

Tab. 3.21: Microstructure profile overview

Cast #	Latitude	Longitude	Depth (HS) in m	Time: Start Winch	Depth (End Lower) in dbar	Comments
Station PS109_044_03				Sep 20, 2017		
1	80° 08.846‘ N	017° 23.411‘ W	164	16:19	/	MSS did not sink
Station PS109_071_02				Sep 23, 2017		Adjustment of the sinking velocity (one floating component & one of each weight rings (small, medium, large) has been removed
1	79° 33.861’ N	019° 27.167’ W	471	16:17	47	
2	79° 33.791’ N	019° 26.711’ W	273	16:53	50	
						Communication between MSS probe and USB interface failed
Station PS109_096_01				Sep 27, 2017		Large weight ring has been added
1	78° 27.924’ N	018° 32.306’ W	417	22:51	281	
2	78° 27.863’ N	018° 32.334’ W	402	23:07	380	
3	78° 27.773’ N	018° 32.385’ W	393	23:35	332	
Station PS109_111_01				Sep 29, 2017		Station 110_01 in the action log; cast 3 was skipped; small weight ring has been added
1	78° 11.926’ N	015° 48.211’ W	354	05:51	277	
2	78° 11.824’ N	015° 48.300’ W	355	05:58	309	
4	78° 11.725’ N	015° 48.353’ W	355	06:12	254	Recording was accidentally stopped at time of winch stop (i.e., before the probe fell down to maximum depth)
5	78° 11.725’ N	015° 48.353’ W	355	06:19	320	Recording from time of winch stop to time at depth
6	78° 11.602’ N	015° 48.446’ W	358	06:27	326	
Station PS109_123_02				Oct 02, 2017		Medium weight ring has been added
1	77° 53.511’ N	013° 20.102’ W	161	19:03	25	Was stopped due to problems with the cable
2	77° 53.546’ N	013° 19.994’ W	169	19:07	93	
3	77° 53.596’ N	013° 19.832’ W	158	19:13	129	

Cast #	Latitude	Longitude	Depth (HS) in m	Time: Start Winch	Depth (End Lower) in dbar	Comments
4	77° 53.666' N	013° 19.631' W	157	19:19	140	
5	77° 53.733' N	013° 19.418' W	152	19:26	140	
Station PS109_125_04				Oct 03, 2017		Station 125_05 in the action log
1	77° 47.892' N	013° 38.816' W	388	03:42	370	
2	77° 47.979' N	013° 39.078' W	388	03:57	348	Missing in the action log (position from previous action)
3	77° 48.044' N	013° 39.310' W	386	04:14	354	
Station PS109_127_01				Oct 03, 2017		
1	77° 52.063' N	013° 24.659' W	308	06:37	240	
2	77° 52.185' N	013° 24.751' W	286	06:48	236	
3	77° 52.301' N	013° 24.850' W	264	06:59	220	

Ice tethered profiler

The objective was to deploy an Ice-Tethered Profiler (ITP) in the embayment created by the recent disintegration of the floating ice tongue of Zachariæ Isstrøm (ZI). The ITP climbs its mooring wire every 8 hours, providing a high-resolution profile of temperature and salinity in the upper 550 m of the water column. These data would provide information on the oceanic forcing of ZI, the close neighbor of the 79 North Glacier.

Potential sites for deployment were determined using Sentinel and Landsat imagery, in conjunction with temperature and depth profiles made via helicopter during PS100. On September 23, an ice reconnaissance flight to the ZI region was made. The decision was made to deploy the ITP in fast sea ice near the remnant ice tongue that sits to the east of the calving front of ZI. Fog and bad weather followed for many days, prohibiting helicopter flights of the required length (6 hours) to deploy the ITP. On September 28 an attempt was made to begin the deployment, however the cloud ceiling came down to near sea level cancelling the operation before the first flight left.

Poor flying conditions persisted generally for the rest of the cruise. As the time drew close when *Polarstern* would have to leave flight range of ZI the decision was made to attempt an alternate deployment from the ship. Three potential sites were considered: the bay to the west of Franske Oer (accessible only by helicopter), the passage to the south of Norske Oer, or the sea ice over the deep part of Norske Trough. The western option was prohibited again by poor flying conditions. A short ice reconnaissance flight was made on September 30 to the Norske Oer passage and Norske Trough where the team landed and checked the ice thickness and water depth. The following day, October 1, *Polarstern* entered the passage south of Norske Oer and the ITP team searched for suitable locations. Thick fog and the large icebergs in the passage made for poor ITP deployment conditions.

Later on October 1 in the Norske Trough region the weather cleared and an acceptable ice flow was identified. Around 15:00 the ITP deployment commenced from the side of *Polarstern*. A 27 cm hole was drilled in the 3 m ice to deploy the ITP. All ITP deployment gear was staged, anchors were built and deployed below the ice. The ITP instrument was attached to the mooring, tested, and passed its deployment tests. However when the ITP was deployed through the hole, it became stuck. It is likely that the movement of ice below the flow blocked the hole during the ITP preparation. Considerable time was spend trying to free the instrument. Hot water was run from the ship onto the ice in an unsuccessful attempt to recover the instrument. The ITP team was concerned about damaging the instrument using too much force to free it. However a decision was made to risk using a boat hook to pull the ITP up. The team was able to free and recover the instrument with no apparent damage.

By the time the ITP was freed from the ice, the sun had begun to set, and the decision was made to abort the deployment. Roughly 45 minutes of work remained to break down and return the deployment gear to the ship. That night *Polarstern* was scheduled to leave the Greenland coast, and therefore the ITP was not deployed.

Persistent poor weather for flying was ultimately to blame for the failure of the proposed ITP deployment near ZI.

Preliminary (expected) results

During the cruise, the CTD and LADCP measurements were preliminarily analyzed. The CTD section along NT4 (Fig. 3.2) confirmed the expected distribution of water masses (Fig. 3.8). Warm salty modified Atlantic Water is present in Norske Trough not only on the outer but also on the inner shelf below the cold fresh Polar Surface Water. The velocity measurements indicate that the modified Atlantic Water is transported northward, i.e., toward the 79 North Glacier.

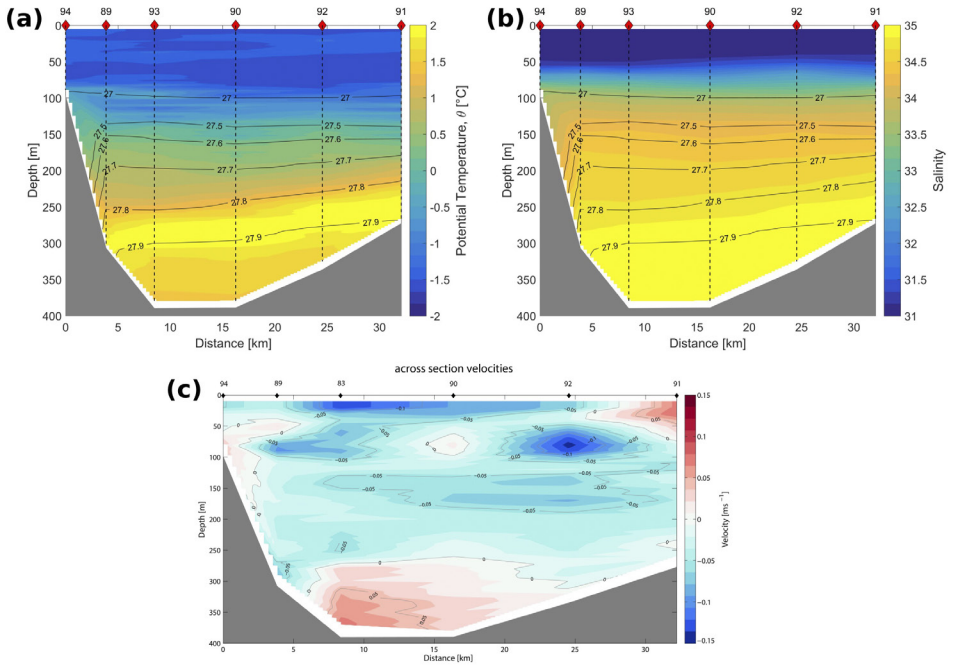

Fig. 3.8: Distribution of (a) potential temperature, (b) salinity, and (c) lowered ADCP velocities along the NT4 CTD section. The black squares at the top indicate the station locations.

Data management

The data recorded by the moored instruments recovered on PS109 will be processed after the cruise at AWI and submitted to the PANGAEA data publisher. The moorings deployed on PS109 will be recovered in 2018. The data recorded on those instruments will accordingly be processed after recovery and submitted to the PANGAEA data publisher at that time. The data collected during PS109 from the different CTDs, the VMADCP, the LADCP, and the microstructure profiler will be processed at AWI and afterwards submitted to the PANGAEA data publisher.

References

Bersch M, I Yashayaev, and K P Koltermann (2007) Recent changes of the ther- mohaline circulation in the subpolar North Atlantic, Ocean Dynamics, 57(3), 223–235, doi:10.1007/s10236-007-0104-7.

Beszczynska-Möller A, E Fahrbach, U Schauer, and E Hansen (2012) Variability in Atlantic water temperature and transport at the entrance to the Arctic Ocean, 1997-2010, ICES Journal of Marine Science: Journal du Conseil, 69(5), 852–863, doi: 10.1093/icesjms/fss056.

Bourke R H, J L Newton, R G Paquette, and M D Tunnicliffe (1987) Circulation and water masses of the east Greenland shelf, Journal of Geophysical Research: Oceans, 92(C7), 6729–6740, doi:10.1029/JC092iC07p06729.

Budéus G, and W Schneider (1995) On the hydrography of the Northeast Water Polynya, Journal of Geophysical Research: Oceans, 100 (C3), 4287–4299, doi:10.1029/94JC02024.

Budéus G, W Schneider, and G Kattner (1997) Distribution and exchange of water masses in the Northeast Water Polynya (Greenland Sea), Journal of Marine Systems, 10(14), 123 – 138, doi:10.1016/S0924-7963(96)00074-7.

Dietrich R, H-G Maas, M Baessler, A Rülke, A Richter, E Schwalbe, and P Westfeld (2007) Jakobshavn Isbræ, West Greenland: Flow velocities and tidal interaction of the front area from 2004 field observations, J Geophys. Res., 112(F03S21), doi: 10.1029/2006JF000601.

Helm V, A Humbert, and H Miller (2014) Elevation and elevation change of Greenland and Antarctica derived from Cryosat-2, The Cryosphere, 8 (4), 1539–1559, doi:10.5194/tc- 8-1539-2014.

Holland D M, R H Thomas, B de Young, M H Ribergaard, and B Lyberth (2008) Acceleration of Jakobshavn Isbræ triggered by warm subsurface ocean waters, Nature Geosci, 1(10), 659–664.

Howat, I M, I Joughin, M Fahnestock, B E Smith, and T A Scambos (2008) Synchronous retreat and acceleration of southeast Greenland outlet glaciers 2000-06: ice dynamics and coupling to climate, Journal of Glaciology, 54, 646–660, doi: 10.3189/002214308786570908.

Johnson, M, and H J Niebauer (1995) The 1992 summer circulation in the northeast water polynya from acoustic doppler current profiler measurements, Journal of Geophysical Research: Oceans, 100(C3), 4301–4307, doi:10.1029/94JC01981.

Khan S A, K H Kjær, M Bevis, J L Bamber, J Wahr, K K Kjeldsen, A A Bjørk, N J Korsgaard, L A Stearns, M R van den Broeke, L Liu, N K Larsen, and I S Muresan (2014) Sustained mass loss of the Northeast Greenland Ice Sheet triggered by regional warming, Nature Clim. Change, 4 (4), 292–299.

Joyce,T M (1989) On the in situ calibration of shipboard ADCP J Atmos. Ocean. Tech., 6, 169-172.

Mayer C, N Reeh, F Jung-Rothenhusler, P Huybrechts, and H Oerter (2000) The sub- glacial cavity and implied dynamics under Nioghalvfjerdsfjorden Glacier, NE-Greenland, Geophysical Research Letters, 27(15), 2289–2292, doi:10.1029/2000GL011514.

Milne, G A, W R Gehrels, C W Hughes, and M E Tamisiea (2009) Identifying the causes of sea-level change, Nature Geosci., 2 (7), 471–478.

Mouginot J, E Rignot, B Scheuchl, I Fenty, A Khazendar, M Morlighem, A Buzzi, and J Paden (2015) Fast retreat of Zachariæ Isstrøm, Northeast Greenland, Science, doi:10.1126/science.aac7111.

Muenchow A, K K Falkner, and H Melling (2007) Spatial continuity of measured seawater and tracer flux through Nares Strait, a dynamically wide channel bordering the Canadian Archipelago, J Mar. Res., 65, 759-788.

Murray T, K Scharrer, T D James, S R Dye, E Hanna, A D Booth, N Selmes, A Luckman, A L C Hughes, S Cook, and P Huybrechts (2010) Ocean regulation hypothesis for glacier dynamics in Southeast Greenland and implications for ice sheet mass changes, Journal of Geophysical Research: Earth Surface, 115 (F3), doi: 10.1029/2009JF001522, f03026.

Nick F M, A Vieli, I M Howat, and I Joughin (2009) Large-scale changes in Greenland outlet glacier dynamics triggered at the terminus, Nature Geosci, 2 (2), 110–114.

Pritchard H D, R J Arthern, D G Vaughan, and L A Edwards (2009) Extensive dynamic thinning on the margins of the Greenland and Antarctic ice sheets, Nature, 461(7266), 971–975.

Rignot E, and P Kanagaratnam (2006) Changes in the velocity structure of the Greenland ice sheet, Science, 311 (5763), 986–990, doi:10.1126/science.1121381.

Schaffer J, W-J von Appen, P A Dodd, C Hofstede, C Mayer, L de Steur, and T Kanzow (2017) Warm water pathways toward Nioghalvfjerdsfjorden Glacier, Northeast Greenland, J Geophys. Res. Oceans, 122, 4004-4020, doi:10.1002/2016JC012462.

Schneider, W, and G Budéus (1997) A note on Norske Ø Ice Barrier (Northeast Green- land), viewed by Landsat 5, Journal of Marine Systems, 10(14), 99 – 106, doi:10.1016/S0924-7963(96)00076-0.

Schneider W, and G Budéus (1995) On the generation of the Northeast Water Polynya, Journal of Geophysical Research: Oceans, 100 (C3), 4269–4286, doi:10.1029/94JC02349.

Stearns L A, and G S Hamilton (2007) Rapid volume loss from two east Greenland outlet glaciers quantified using repeat stereo satellite imagery, Geophysical Research Letters, 34(5), doi:10.1029/2006GL028982, l05503.

Straneo F, G S Hamilton, D A Sutherland, L A Stearns, F Davidson, M O Hammill, G B Stenson, and A Rosing-Asvid (2010) Rapid circulation of warm subtropical waters in a major glacial fjord in East Greenland, Nature Geosci, 3(3), 182–186.

Straneo, F, R G Curry, D A Sutherland, G S Hamilton, C Cenedese, K Vage, and L A Stearns (2011) Impact of fjord dynamics and glacial runoff on the circulation near Helheim glacier, Nature Geosci, 4 (5), 322–327.

Straneo F, D A Sutherland, D Holland, C Gladish, G S Hamilton, H L Johnson, E Rignot, Y Xu, and M Koppes (2012) Characteristics of ocean waters reaching Greenland's glaciers, Annals of Glaciology, 53(60), 202–210, doi:10.3189/2012AoG60A059.

Thomas H R (2004) Force-perturbation analysis of recent thinning and acceleration of Jakobshavn Isbræ, Greenland, Journal of Glaciology, 50, 57–66, doi:10.3189/172756504781830321.

Thomsen H H, N Reeh, O B Olesen, C E Bøggild, W Starzer, A Weidick, and A K Higgins (1997) The Nioghalvfjerdsfjorden glacier project, north-east Greenland: a study of ice sheet response to climatic change, Geology of Greenland Survey Bulletin, 176, 95–103.

Topp R, and M Johnson (1997) Winter intensification and water mass evolution from yearlong current meters in the Northeast Water Polynya, Journal of Marine Systems, 10(14), 157 – 173, doi:10.1016/S0924-7963(96)00083-8.

Velicogna I (2009) Increasing rates of ice mass loss from the Greenland and Antarctic ice sheets revealed by GRACE, Geophysical Research Letters, 36(19), doi:10.1029/2009GL040222, l19503.

Vieli A, and F M Nick (2011) Understanding and modelling rapid dynamic changes of tidewater outlet glaciers: Issues and implications, Surveys in Geophysics, 32(4), 437– 458, doi:10.1007/s10712-011-9132-4.

Wilson N J, and F Straneo (2015) Water exchange between the continental shelf and the cavity beneath Nioghalvfjerdsbræ (79 North Glacier), Geophysical Research Letters, 42(18), 76

4. INVESTIGATING PHYSICAL AND ECOLOGICAL PROCESSES IN THE OUTFLOW AREA OF THE 79° NORTH GLACIER USING AN AUTONOMOUS UNDERWATER VEHICLE AND UNMANNED AERIAL VEHICLES

Thorben Wulff[1], Sandra Tippenhauer[1], Sascha Lehmenhecker[1], Michael Busack[1], Jonas Hagemann[1] (not on board)

[1]AWI

Grant No: AWI_PS109_04

Objectives

The 79° North Glacier (79NG), located in northeast Greenland, is one of three outlet glaciers of the North East Greenland Ice Stream (NEGIS) draining ice into the Fram Strait. As one of the last glaciers in Greenland, the 79NG still has a stable floating tongue, which reaches about 60 km from the grounding line towards its southern outflow and its northern outflow in the Djimphna Sound respectively (Fig. 4.1). The Hovgaard Island separates the two floating tongues and associated outflow areas.

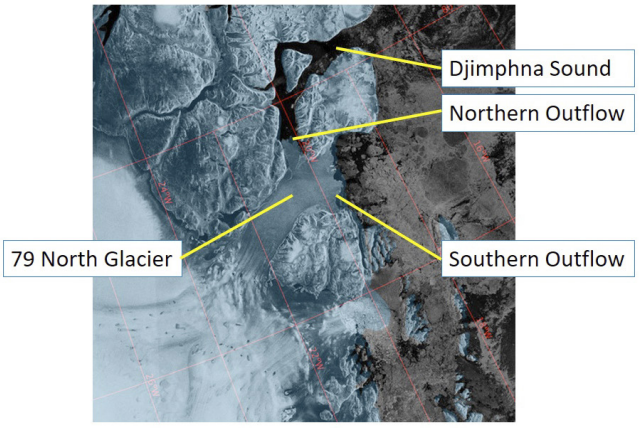

Fig. 4.1: Satellite image of the 79° North Glacier and its two outflows. Image by Polar View Sea Ice Monitoring Service

In the southern outflow, the glacier´s front is pinned by small islands. In summer 2016, *Polarstern* mapped the bathymetry in front of the southern outflow for the first time (PS 100), revealing a 15 km long meridional canyon and a single deep depression of 450 m water depth leading underneath the glacier (Fig. 4.2). Hydrographic studies during PS100 indicated the inflow of warm Atlantic Water via the depression, which eventually causes basal melting at the glacier´s floating tongue. The meridional canyon is partly blocked by a southern and a northern sill with a minimum depth of about 250 m.

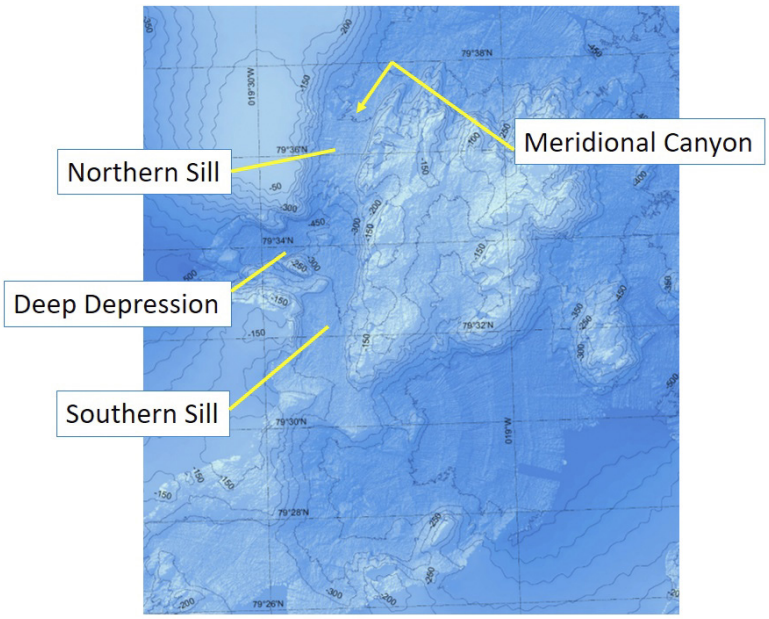

Fig. 4.2: Bathymetric Chart of the seafloor in front of the southern outflow of the 79NG. The glacier is to the west.

It was the main objective of the deployments of AWI´s autonomous underwater vehicle (AUV) "PAUL" to provide high-resolution hydrographic data from inside these canyons and to follow the path of the incoming Atlantic Water (Fig. 4.3). The advantage of AUV-deployments is that these vehicles can provide data in the horizontal plane whereas ship-lowered instruments rather cover vertical scales.

Fig. 4.3: AUV "PAUL" is being launched during PS 109. Image by Christian Rohleder (DWD).

Physical parameters were observed by the AUV with a set of sensors comprising a conductivity, temperature and depth probe (CTD), an acoustic Doppler current
profiler (ADCP), and a microstructure probe (MSP). Along with the physical sensors, biogeochemical sensors were deployed as well, yet parameters such as Chlorophyll a or Nitrate only were of minor relevance.

The scientific and technological objectives during PS 109 were:

- Conducting high-resolution water column studies in front of a glacier
- Measuring water currents using a vehicle mounted ADCP
- Measuring turbulences using vehicle mounted microstructure probes
- Operating an autonomous vehicle in the harsh conditions of the Arctic fall

Work at sea

During the expedition the AUV conducted two dives.

- Dive 1 (Dive ID: 039 / Sept. 22nd 2017)

The first dive was conducted close to the glacier to characterize the hydrographic structure of the inflow of Atlantic Water. For this reason, the AUV was deployed at 79.56927 °N / 19.29615 °W in the vicinity of the area where the deep depression separates from the meridional canyon and points towards the glacier (Fig. 4.4).

As the temperatures had dropped below 0 °C in the days before the dive, the entire area was completely covered with fresh ice of 5 – 10 cm thickness. As a consequence, *Polarstern* circumnavigated the deployment point several times to break the ice and create an area with open water. This open water area was supposed to serve both as the deployment and as the recovery position. Due to the risk which was involved in this dive (below solid ice cover, currents of up to 0.5 m/s pointing below the glacier), the dive was planned such that PAUL stayed within a distance of 2 – 2.5 km from the ship, which is within tracking range of the acoustic tracking system GAPS. In total, the dive had a length of about 8 km. For roughly 5 km, PAUL followed a "sawtooth" pattern through the water column with each "tooth" being about 100 m high. During both ascent and descent, the vehicle kept a pitch angle of ~30° and approached the seafloor by minimum 15 – 20 m. For the entire time of the dive (roughly 2 h), the vehicle operated below a solid ice cover.

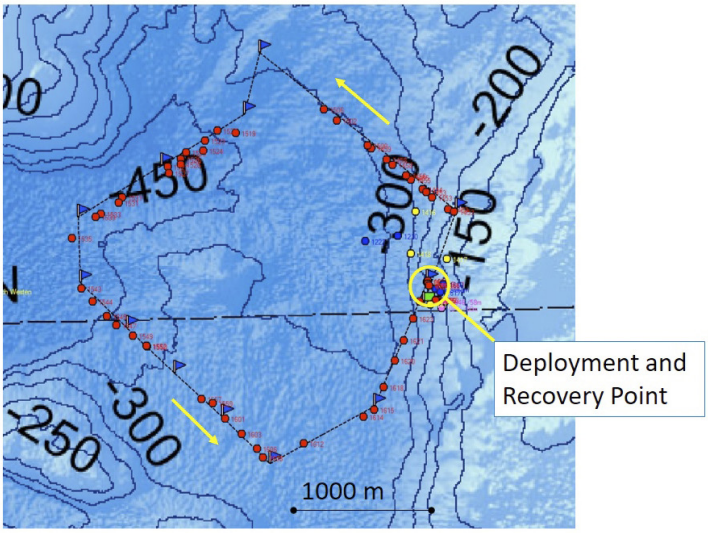

Fig. 4.4: Chart of Dive 1 with PAUL covering an 8 km long "loop" from the northern sill into the depression and up the southern sill.

After finishing the sawtooth-transect, PAUL transited towards its surface point in roughly 250 m water depth. As it reached the coordinates, it shut off its thruster and ascended vertically due to its residual buoyancy. Unfortunately, the open water area had almost closed at the time PAUL was about to surface and the vehicle got stuck below an ice floe. After some initial transmissions, the vehicle´s tracking signal was lost for over 2 h, which was likely caused by the noise of *Polarstern´s* thrusters covering the signals. Contact could be reestablished after a hydrophone was lowered from a Zodiac. Eventually, PAUL was located under the ice and the Zodiac´s crew was able to attach a rope to the main lifting point of the vehicle. During recovery, the vehicle suffered some minor damages to one of the temperature sensors of the MSP and its GPS antenna, yet repairs / replacements were completed within a day after the dive.

- Dive 2 (Dive ID: 040 / Oct. 02nd 2017)

For the second dive, the vehicle was deployed at 77.90030 °N / 13.35005 °W at a shallow site (150 m) above Belgica Bank. From here the vehicle was supposed to conduct a completely unattended mission southward into the Norske Trough. Following the terrain in 20 m altitude, it was planned that PAUL would reach its turning point in about 360 m water depth, ascends to 300 m water depth, approaches the trough´s northern slope in a northward transect and begins a last southward transect in 240 m water depth (Fig. 4.5).

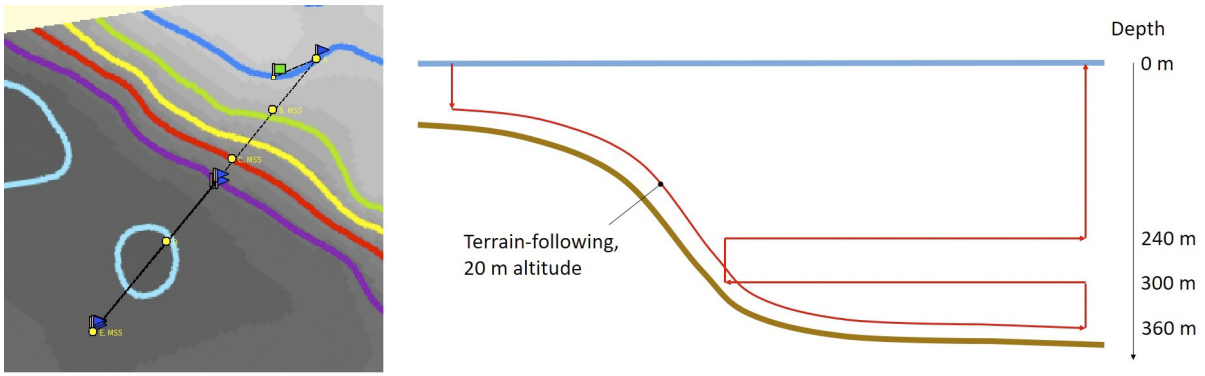

Fig. 4.5: Chart of dive 2 (left) and the planned mission profile (right)

Overall distance of the dive was calculated to be about 36 km with a dive time of 8 h, putting the recovery into night time. Scientifically, the dive aimed at resolving the fine structure of the flow of Atlantic Water, which stays close to the trough´s northern slope as it transits northward. *Polarstern* was supposed to conduct hydrographic measurements in parallel and conduct station work (CTD, microstructure casts) along the transect of the AUV.

Deployment of the vehicle was completed at a sea state of 2 m and slightly foggy conditions, with the forecast stating that fog might increase and the sea state would not change much. With *Polarstern* heading towards its first hydrographic station, underwater tracking was lost as expected shortly after the vehicle submerged. After 30 minutes, with *Polarstern* being on its first station, tracking could be reestablished and, again, was lost after PAUL had left the tracking range. No acoustic tracking signal was detected after that.

About 4 h into the dive, retrieving messages by the vehicle´s GPS / Iridium transceiver indicated that the vehicle was on the surface and loitered (actively stays in close range to a certain location) around its actual recovery point. This was further confirmed by ARGOS satellite tracking. At that time, *Polarstern* was in about 8 km distance to the vehicle. Station work was immediately aborted to recover the vehicle and close range approach was conducted using PAUL´s RDF signal and the visual signal of its flashing strobe.

Approaching the vehicle turned out to be difficult as no radio communication could be established and ship-bound acoustic communication failed as well. Thus, the vehicle stayed in its unpredictable loitering behavior. However, acoustic communication could be established from a Zodiac and the dive was aborted manually. The relatively high swell, fog and darkness made it difficult to recover the vehicle, yet finally it went smoothly.

Data analysis showed that the vehicle encountered a groundfault on one of its six major power lines. One of the connectors in the Battery negative line was identified to be the most likely cause for the groundfault (Fig. 4.6).

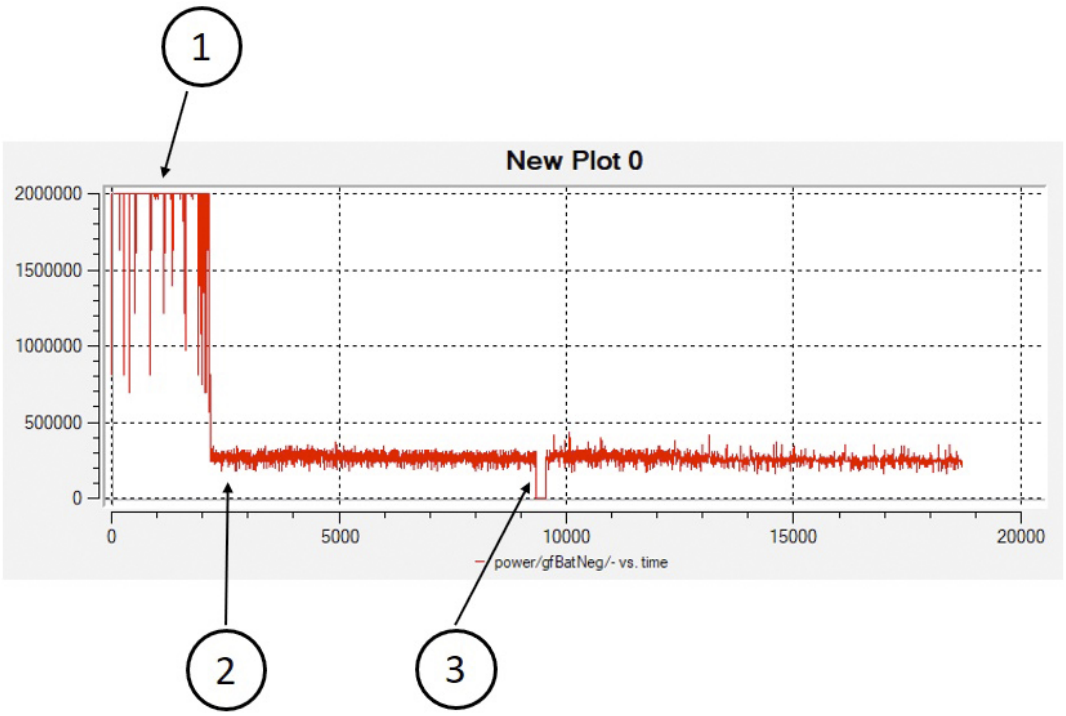

Fig. 4.6: Electrical Resistance on the Battery negative line during dive 2 in [Ω] vs. time after mission start in [s]

Shortly after the vehicle submerged, the electrical resistance on the Battery negative line started showing an irregular behavior as it dropped several times, yet recovered to its nominal value of 2,000 kΩ every time (1). As the vehicle dived deeper following the slope, pressure increased and the value dropped and remained at a critical level of 250 kΩ at a certain point (2). About 2.5 h after the vehicle submerged, in 390 m water depth, the electrical resistance dropped to 2 kΩ, which is a critical threshold for an abort (3). Consequently, PAUL stopped the mission, ascended to only 3 m water depth, and headed towards its recovery point, where it surfaced 53 minutes later.

Preliminary (expected) results

During the cruise, the AUV´s navigation data as well as most of the payload data were preliminarily processed. Data from the ADCP were processed using a routine that is currently under development. It is based on the ship´s ADCP processing routine from GEOMAR. The MSP data was processed with a routine similar to the one described in Tippenhauer et al. (2015). For ADCP and MSP processing the pre-processed AUV navigation data were used.

- Dive 1

  The main focus of dive 1 was to study the hydrography in front of the 79NG. Fig. 4.7 shows the potential temperature and salinity as observed from the AUV and from two close by lowered CTD stations. The AUV and CTD data are in good agreement. The AUV data illustrate nicely the warm Atlantic water to be concentrated in the deep depression. From the first analyses it seems as if the water was warmer at the northern sill compared to the southern sill. However, more precise analyses, which will especially consider the complex topography, will help to understand the circulation.

  Biological parameters have not yet been analyzed.

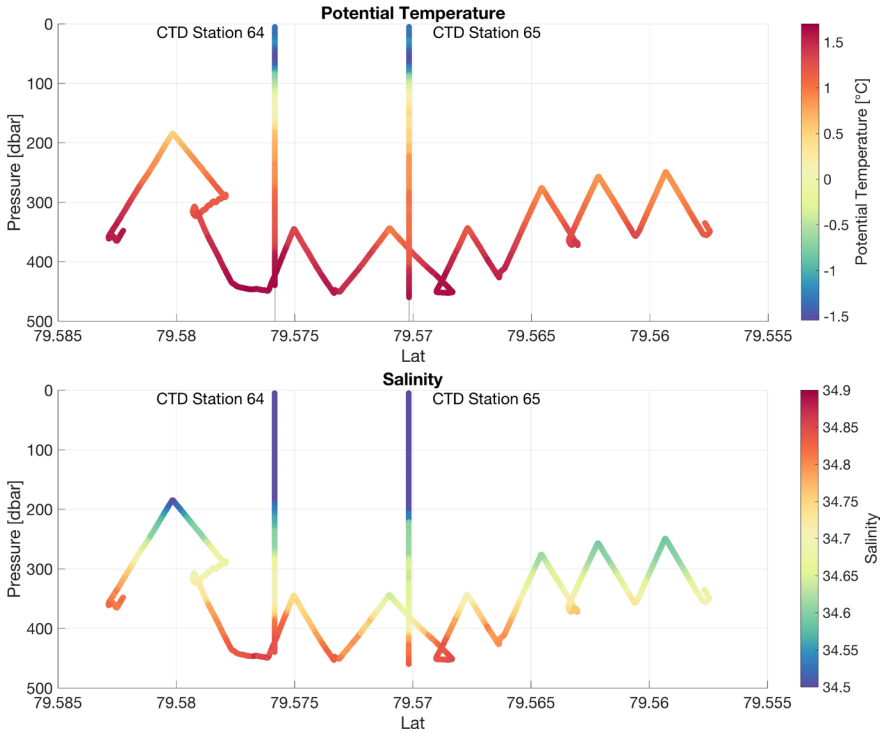

Fig. 4.7: Potential Temperature and Salinity observed from the AUV together with observations from two close by CTD stations in the trough system in front of the 79 North Glacier

- Dive 2

  The objective of dive 2 was to study the north-eastern flank of Norske Trough at about 77.8° N, 13.4° W. At this location, a boundary current of warm Atlantic Water was suspected to flow towards the 79NG. The AUV dive was planned such that the AUV would decent at the northern flank and then dive perpendicular to the channel axis towards the centre with 20 m altitude.

  The observed temperature and salinity were in good agreement with the observations from the lowered CTD. Below the polar waters at the surface, a warm water plume was observed at the northern trough flank (Fig. 4.8). Maximum temperature of more than 2.5 °C was detected at about 200-250 m depth.

The AUV based ADCP observations showed north-westward flow of about 0.3 m/s along the channel. The zonal and meridional velocity components where rotated to align with the channel axis. Additionally a 3 min (300 m) low pass filter was applied. The along-channel flow component is shown in Fig. 4.9. The velocity observed from the lowered ADCP system (LADCP) where in good agreement with the AUV based velocities. The LADCP data were also rotated to align with the channel axis and are shown together with the AUV data in Fig. 4.9.

Biological parameters have not yet been analyzed.

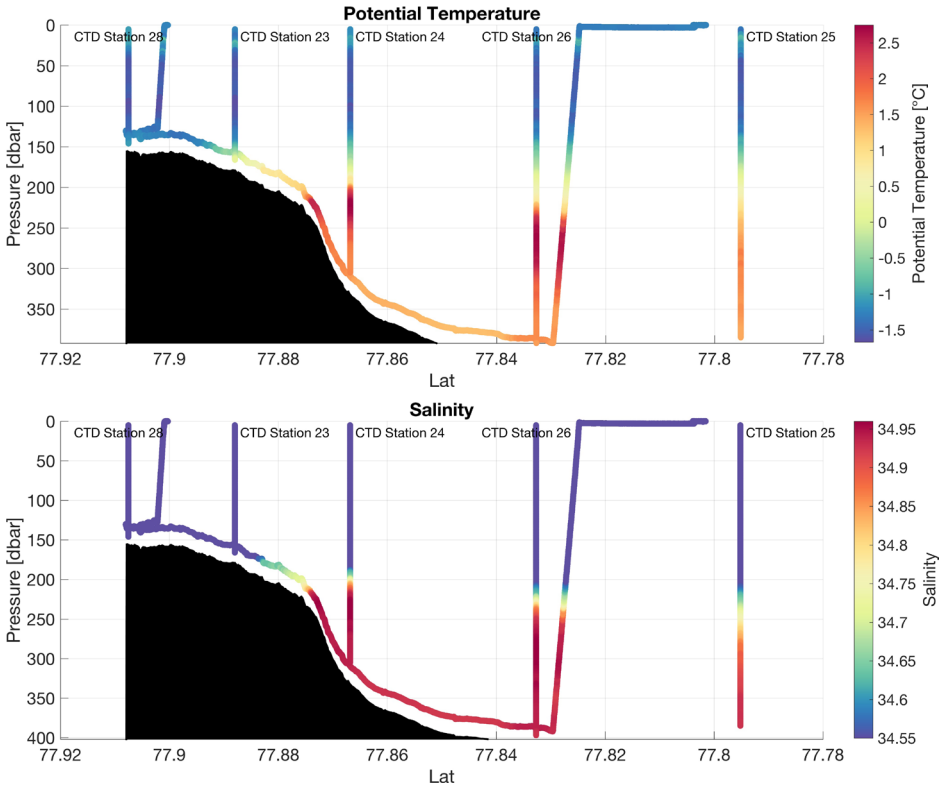

Fig. 4.8: Potential Temperature (upper) and Salinity (lower) observed from the AUV together with observations from lowered CTD section crossing the Norske Trough

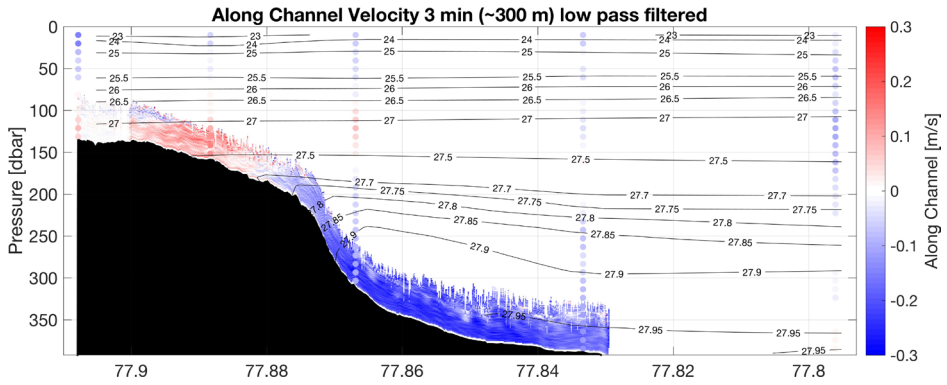

Fig. 4.9: Along channel velocity as observed from the AUV (3 min low pass filtered) and the LADCP. Contours indicate potential density observed from the lowered CTD.

Data management

Processing the data of the several types of instruments will be differently time-consuming. The time period from post processing to data provision will vary from three months for data such as fluorescence and dissolved oxygen to nine months for microstructure and ADCP data. Until then preliminary data will be available to the cruise participants and external users after request to the senior scientist. The finally processed data will be submitted to the PANGAEA data library. The unrestricted availability from PANGAEA will depend on the required time and effort for acquisition of individual datasets and its status of scientific publication.

References

Tippenhauer S, M Dengler, T Fischer and T Kanzow (2015) Turbulence and finestructure in a deep ocean channel with sill overflow on the mid-atlantic ridge, Deep Sea Research Part I: Oceanographic Research Papers, 99, 10–22, 2015.

5. STABLE NOBLE GAS ISOTOPES (^{3}HE, ^{4}HE, NE) AND ANTHROPOGENIC TRANSIENT TRACERS (CHLOROFLUOROCARBONS, CFC; SULFUR HEXAFLUORIDE, SF_6) TO INVESTIGATE BASAL GLACIAL MELTING AND WATER MASS CIRCULATION AT 79NG

Oliver Huhn[1], Tilia Breckenfelder[1], Jonas Brünjes[1], Monika Rhein[1] (not on board)

[1]UHB-IUP

Grant-No. AWI_PS109_05

Objectives

Greenland Ice Sheet (GrIS) basal melting is one of the major contributors to GrIS ice mass loss and thus sea level rise, and accelerating melt rates are caused by intrusions of warm Atlantic Water into the sub-glacial cavity. However, estimates of submarine melt rates are usually based on indirect methods (difference between total mass loss from remote sensing methods and surface mass balance or estimated from measurements of ice velocities and ice thickness changes) and are still uncertain. So far, there are no sufficient data available that might allow to trace and to quantify the glacial melt water (GMW) in the ocean.

The major aims of our (repeated and extended) stable noble gas isotope and transient tracer measurements in the vicinity of the 79° North Glacier (79NG, in northeast Greenland) are to investigate the interaction of the 79NG with the ambient water masses (warm Atlantic Water, AW, cold Polar Water, PW) and to quantify and trace the GMW formed at the 79NG in its near and far field. Together with data from *Polarstern* expedition PS100 (in 2016) and historic data we will assess the possible variability of GMW formation, its inventory and circulation.

We will use the transient tracer measurements to investigate the oceanic transport and storage of (anthropogenic) carbon in AW and PW on the northeast Greenland shelf.

Approach and methods

The oceanic measurement of the low-solubility and **stable noble gases** helium (^{3}He, ^{4}He) and neon (Ne) provide a useful tool to identify and to quantify (basal) GMW (e.g. Huhn et al., 2008). Atmospheric air with a constant composition of these noble gases is trapped in the ice matrix during formation of the meteoric ice. Due to the enhanced hydrostatic pressure at the base of the shelf ice, these gases are completely dissolved in the water, when the ice is melting from below. This leads to an excess of Δ^4He = 1280% and ΔNe = 890% in pure GMW (Loose & Jenkins, 2015; the Δ stands for the noble gas excess over the air-water solubility equilibrium). Frontal or surface melt water would equilibrate quickly and not lead to any noble gas excess in the ocean water. With an accuracy of <0.5% for He measurements performed at the IUP Bremen, basal GMW fractions of <0.05% are detectable. The ^{3}He/^{4}He isotope ratio provides complementary information. Primordial helium (mantle helium with a far higher ^{3}He/^{4}He ratio,

δ^3He ≈ 800%) enters the ocean from spreading regions of submarine ridge systems or other hydrothermal active sites like hydrothermal vents or submarine volcanoes.

The anthropogenic transient trace gases **chlorofluorocarbons** (CFC-11 and CFC-12) and sulfur hexafluoride (SF_6) allow to estimate the time scales of the renewal and ventilation of inner oceanic water mass transport (e.g. Huhn et al., 2013). They enter the ocean by gas exchange with the atmosphere. Since the evolution of these transient tracers in the ocean interior is determined on first order by their temporal increase in the atmosphere and subsequently by advection in the ocean interior, they allow to quantify the time scales of subsurface water mass transport and formation. In a higher order approach, using the so called Transit Time Distribution (TTD) method (or water mass age spectra), they allow to determine the integrated advection and mixing time scale of a water mass. These CFC and TTD method based time scales of ventilated water masses integrate residence, circulation, and transport on the shelf, slope, and deep basin and allow determining water mass ventilation and formation rates. Combined CFC based time scales with noble gas based melt water inventories allow to calculate basal glacial melting rates.

Additionally, the CFCs and TTD method can be used to estimate the anthropogenic carbon content in deep water masses as in AW or PW by applying the CFC based TTDs to the well known atmospheric anthropogenic carbon history. That method is very reliable particularly in deep water masses and it is fully independent of carbon measurements and back calculating methods, which require additional geochemical observations or linear regression methods.

Work at sea

In total we took 540 water samples for stable noble gas isotopes (^{3}He, ^{4}He, Ne) in copper tubes from 45 stations on the northeastern Greenland shelf and near 79NG (black circles in Fig. 5.1 and Fig. 5.2).

For the transient tracers CFC-12 and CFC-11 we took in total 410 samples on 39 stations (red dots in Fig. 5.1 and Fig. 5.2) and for CFC-12 and SF_6 we took 95 samples on 8 stations on the northeastern Greenland shelf and near the 79NG (magenta dots in Fig. 5.1 and Fig. 5.2).

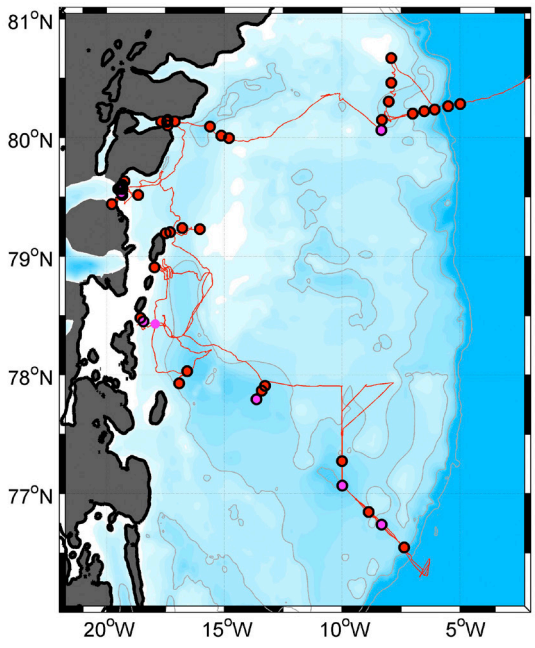

Fig. 5.1: Map of entire area of investigation indicating stations with noble gas and transient tracer samples during PS109. Black circles are stations with noble gas (He, Ne), red dots are stations with transient tracers (CFC-11, CFC1-12) and magenta dots with transient tracers (SF_6, CFC-12). The red line is the cruise track.

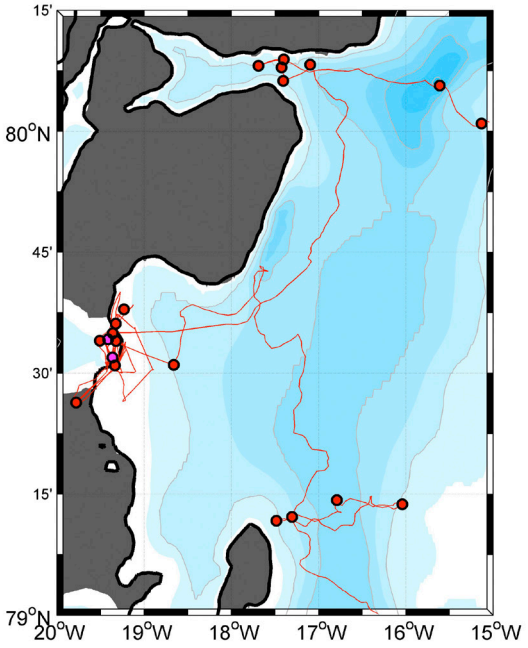

Fig. 5.2: Zoom into the nearer vicinity of the 79NG indicating stations with noble gas and transient tracer samples during PS109. Black circles are stations with noble gas (He, Ne), red dots are stations with transient tracers (CFC-11, CFC1-12) and magenta dots with transient tracers (SF_6, CFC-12). The red line is the cruise track.

The water samples for helium isotopes and neon were stored from the CTD/water bottle system into gas tight copper tubes, which are clamped of at both sides. The noble gas samples are analyzed later in the IUP Bremen noble gas mass spectrometry lab. The copper tube water samples are processed in a first step with an ultra high vacuum gas extraction system. Sample gases are transferred via water vapor into a glass ampoule kept at liquid nitrogen temperature. For analysis of the noble gas isotopes the glass ampoules are connected to a fully automated ultra high vacuum mass spectrometric system equipped with a two-stage cryogenic trap system. The system is regularly calibrated with atmospheric air standards (reproducibility better ±0.2%). Also measurement of blanks and linearity are done. For details see Sültenfuß et al., 2009.

For the transient tracers (CFC-11 and CFC-12) water samples from the CTD/water bottle system were collected into 100 ml glass ampoules (and 200 ml for SF_6 and CFC-12). They were flame sealed after a CFC free headspace of pure nitrogen had been applied. The CFC and SF_6 samples are later analyzed in the CFC-laboratory at the IUP Bremen. The determination of CFC and SF_6 concentrations will be accomplished by purge and trap sample pre-treatment followed by gas chromatographic separation on a capillary column and electron capture detection. The amount of CFC degassing into the headspace will be accounted for during the measurement procedure in the lab. The system will be calibrated by analyzing several different volumes of a known standard gas. Additionally the blank of the system will be analyzed regularly. For details see Bulsiewicz et al., 1998.

All samples will be shipped home after the expedition and will be analyzed in the UHB-IUP noble gas and CFC laboratories. The measurements are expected to be completed one year after arrival in our home lab in Bremen. A careful data quality check will be carried out then.

Expected results

As soon as the measured data are available, we will use the stable noble gas data (^{3}He, ^{4}He, Ne) to quantify the GMW inventories in the 79NG outflow region and its far field and to trace the GMW pathways near the glacier and on the shelf. We will compare our new noble gas data with those from *Polarstern* expedition PS100 (2016, in the same region) and with available historic noble gas data further downstream to assess possible temporal variability of the melt water discharge and inventory.

We will use the transient tracer (CFC, SF_6) data to determine the time scales of circulation and residence to assess the formation rates of GMW (basal melting rates) of the 79NG. We will use the transient tracer data to trace the pathways, circulation and recirculation and the related time scales of AW and PW. We will also use the CFC and SF_6 data to estimate the anthropogenic carbon content in PW and AW. We will combine our new transient tracer data set with those from *Polarstern* expedition PS100 (2016 in the same region) and with available historic transient tracer data to assess possible temporal variability of transit times and carbon content and water mass transfer on the northeastern Greenland Shelf.

Data management

All our data will be made public on the PANGAEA data base as soon as we have them available (approximately one year after the cruise), carefully quality controlled, and published in a peer reviewed journal. Our cooperation partners will receive the data as soon as the final data set is available.

Acknowledgment

We gratefully thank the master and crew of *Polarstern* for all support, maneuvering and running heavy gear, the oceanographic group of Torsten Kanzow et al. for providing water samples and hydrographic information, and AWI for the chance of participation.

References

Bulsiewicz K, Rose H, Klatt O, Putzka A, Roether W (1998) A capillary-column chromatographic system for efficient chlorofluorocarbon measurement in ocean waters. Journal of Geophysical Research 103, (C8), 15959-15970, doi: 10.1029/98JC00140

Huhn O, Hellmer HH, Rhein M, Rodehacke C, Roether W, Schodlok MP, Schröder M (2008) Evidence of deep- and bottom-water formation in the western Weddell Sea. Deep Sea Research Part II: Topical Studies in Oceanography 55, (8-9), 1098-1116, doi: 10.1016/j.dsr2.2007.12.015.

Huhn O, Rhein M, Hoppema M, van Heuven S (2013) Decline of deep and bottom water ventilation and slowing down of anthropogenic carbon storage in the Weddell Sea, 1984–2011. Deep Sea Research Part I: Oceanographic Research Papers 76, 66-84, doi: 10.1016/j.dsr.2013.01.005.

Loose B, Jenkins WJ (2014) The five stable noble gases are sensitive unambiguous tracers of glacial meltwater. Geophysical Research Letters 41, (8), 2835-2841, doi: 10.1002/2013GL058804

Sültenfuß J, Roether W, Rhein M (2009) The Bremen mass spectrometric facility for the measurement of helium isotopes, neon, and tritium in water. Isotopes in Environmental and Health Studies 45, (2), 83-95, doi: 10.1080/10256010902871929.

6. BASAL MELT RATES OF THE FLOATING PART OF 79°N GLACIER

Angelika Humbert[1,2], Daniel Steinhage[1], Ole Zeising[3] (all not on board), Christine Lüttig[1], Julia Eis[2]

[1]AWI
[2]UHB
[3]UHH

Grant-No. AWI_PS109_06

Objectives

The 79°N Glacier is one of three outlet glaciers of the only large ice stream in Greenland, the NEGIS (North-East Greenland Ice Stream). In contrast to other glaciers in Greenland, which are typically tidewater glaciers, the 79°N Glacier forms a floating tongue and is rather comparable to an ice shelf (Fig. 6.1). As the NEGIS drains about 8 % of the ice sheet, the question whether its contribution to sea level change is increasing is coming more into focus. The floating tongue is pinned by ice rises along the ice front, which keeps its lateral extent at the moment stable, however, the ice flow velocities at its grounding line are slightly increasing (Joughin, pers. comm.) and the upstream ice surface elevation has started to decrease in the past few years (Helm et al., 2014). Warm water masses were also already detected to drain underneath the floating tongue and hence the question arises if the warm water increases the basal melt of the floating tongue, causing grounding line retreat and weakening of the tongue itself.

Thus, we aim to measure the seasonal variation of basal melt rates of the 79°N Glacier at locations on its floating tongue. The melt rates at the ice-ocean transition are measured using a phase sensitive radar (pRES) (Corr et al., 2002; Jenkins et al., 2006), which measures the change of the distance between internal layers of the glacier. This method can separate the ice thickness change due to stretching of the glacier from the thickness change due to basal melt. As the basal melt over a short period of time is too small to be detected by the amplitude of the radar signal, the phase of the radar signal is used for this purpose. The radar is a multi-frequency radar that sends a burst of radar signals with defined repetition times and gives hence a change of the phase and hence the basal melt rate over time. With this method we can thus detect the penetration of warm water masses underneath the tongue that cause the change of the melt rates.

During the land-based iGRIFF campaign in June-July 2017 Daniel Steinhage installed autonomous pRES stations and also did a survey of about 50 locations which require then a revisit, retrieving a second dataset allowing to estimate the amount of melt during that period. During PS109 a first revisit of a subset of the 50 locations will be carried out, so that beside an annual mean melt rate also a melt rate over about three month time, late summer, can be estimated.

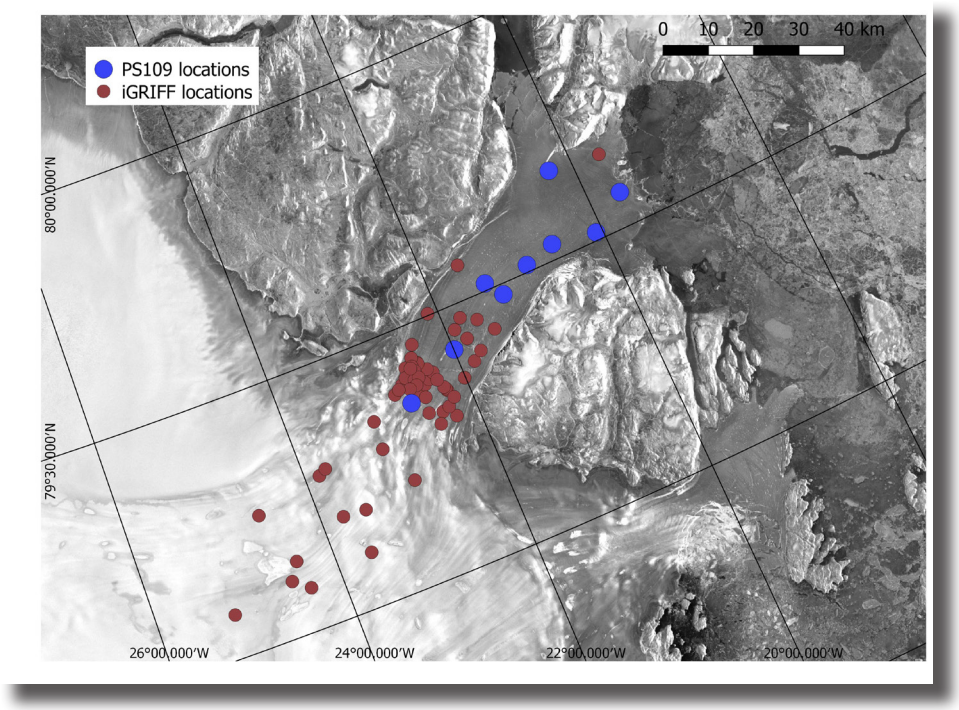

Fig. 6.1: Overview of the 79NG in the vicinity of the calving front showing pRES sites

Work at sea and on land

Using the helicopter a group of 2 scientists plus a polar bear watch was flown to the glacier to repeat the measurements of the phase sensitive radar. The first 8 measurements were taken on 23.09.2017 from 09:00 a.m. to 02:00 p.m. in the frontal part of the floating tongue. During a second flight in the afternoon of the same day another station in the area of the grounding line was visited. The coordinates of the stations are given in Table 6.1.

Tab. 6.1: Coordinates of visited pRES sites

Station name	Latitude	Longitude
g1_p02	79° 30.85' N	21° 24.47' W
g1_p03	79° 39.96' N	20° 15.76' W
g1_p05	79° 34.08' N	19° 39.19' W
g1_p06	79° 30.94' N	20° 04.44' W
g1_p07	79° 31.87' N	20° 33.78' W
g1_p08	79° 30.84' N	20° 54.49' W
g1_p09	79° 28.78' N	21° 16.18' W
g2_p15	79° 25.08' N	21° 59.70' W
GPS08	79° 21.11' N	22° 38.62' W

For all measurements the same parameter settings as during the field campaign in June-July 2017 were used. Because the stations were marked with bamboo flags it is guaranteed that the measurements are taken at exactly the same place and in the same orientations as in the iGRIFF campaign.

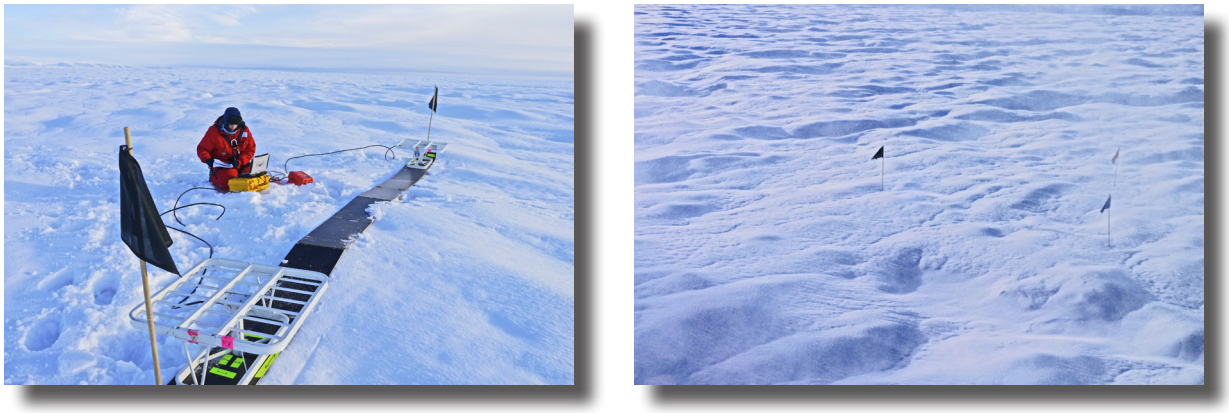

Fig. 6.2: Typical set-up of a pRES station. Left: setup during a measurement. Right: view of a pRES station from the helicopter.

Preliminary (expected) results

After processing of the raw data it is possible to create a plot which shows the amplitude over the range as shown for station g1_p02 in Fig. 6.3.

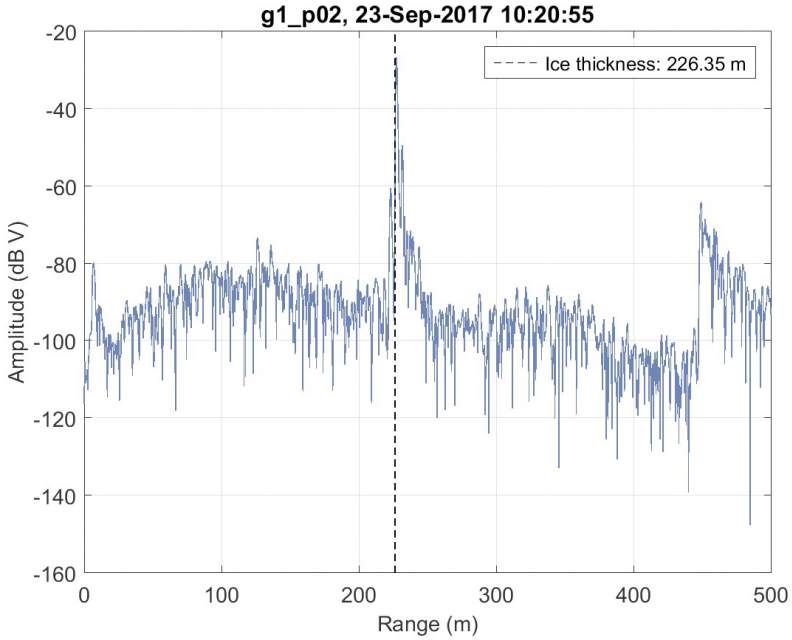

Fig. 6.3: Data derived at station g1_p02. The first peak shows the basal reflection and therefore gives the ice thickness.

The first steep ascent represents the basal reflection and the range of this point is the thickness of the ice at the measured location. By comparison of our measurements with those from the iGRIFF campaign the change in ice thickness over the period from July to September 2017 can be inferred. Further analysis steps are then required to derive basal melt rates. By compilation of the results from different measurement sites, the spatial distribution of late summer melt rates across the floating tongue shall be inferred.

Data management

Basal melt rate data will be uploaded in the PANGAEA database, if data check proves reasonable data quality and access to the data will be granted after about three years, pending analysis and publication.

References

Corr HFJ, Jenkins A, Nicholls KW, Doake CSM (2002) Precise measurement of changes in ice-shelf thickness by phase-sensitive radar to determine basal melt rates. Geophys. Res. Lett., 2, (8), p. 1232

Jenkins A, Corr HFJ, Nicholls KW, Stwart CL, Doake CSM (2006) Interactions between ice and ocean observed with phase-sensitive radar near an Antarctic ice-shelf grounding line. J. Glaciol., 52, (178),pp. 325–346

HelmV, A Humbert and H Miller (2014) Elevation and elevation change of Greenland and Antarctica derived from CryoSat-2. The Cryosphere, 8, 1539–1559, 2014, doi:10.5194/tc-8-1539-2014

7. NEGIS: RECONSTRUCTING THE HISTORY OF THE NORTHEAST GREENLAND ICE STREAM

Jerry M. Lloyd[1], Colm Ó Cofaigh[1], Richard S. Jones[1], Peter Codling[1], Katharina Streuff[1], Maria Kappelsberger[2], Nicole Syring[2], Michaela Meier[2], Flor Vermassen[3]

[1]DUR
[2]AWI
[3]GEUS

Grant-No. AWI_PS109_07

Background

The NEGIS project is supported through the Alfred Wegener Institute (Project N405) via the GRIFF I project and the *Polarstern* programme (cruises PS100 and PS109), as well as through funding from the UK Natural Environment Research Council (NERC Grant NE/N011228/1). The incursion of warm Atlantic Water (AW) over the last 15 years to many of Greenland's marine-terminating outlet glaciers, as well as increased air temperatures and sea-ice loss, have all been linked to Greenland Ice Sheet margin retreat and instability (Straneo et al., 2012; Mouginot et al., 2015; Wilson et al., 2015). However, despite an improved understanding of the forcing mechanisms that have driven recent glacier change in Greenland, the limited time-span of these observations provide only a short time series with which to understand the complex and non-linear response of ice streams to ocean and atmospheric forcing (Nick et al., 2010). This hinders our ability to understand and forecast how ice sheets will change over longer timescales (Seroussi et al., 2014). What we fundamentally lack is decadal to millennial scale input data with which to calibrate, validate and test the sensitivity of predictive numerical models. One solution to this problem is to identify patterns of former rapid ice margin change during past periods of warmer climate when the key forcing mechanisms that influence ice sheet stability can be simultaneously reconstructed and thus their relative importance can be determined.

The NEGIS project will investigate the dynamics of the Northeast Greenland Ice Stream (NEGIS); the main artery for ice discharge from the NE sector of the Greenland Ice Sheet (GrIS) to the North Atlantic. Unlike other sectors of the GrIS, NEGIS and the ice shelves that front it, have exhibited little response to increased atmospheric and oceanic warming over the last 20 years. However, very recent ice shelf loss and grounding line retreat (~ 4 km) post 2010 suggest that this sector of the GrIS, and NEGIS in particular, is starting to respond to recent atmospheric/oceanic change (Mouginot et al., 2015). Model projections suggest that ocean warming will double by 2100 (Yin et al., 2011) and air temperature will increase significantly in northeast Greenland (AMAP, 2011), so the future evolution of the NEGIS catchment is important not only for understanding the changing dynamics of this sector of the GrIS, but also for predicting sea-level rise. The NEGIS catchment as a whole holds a significant sea-level equivalent (SLE) of 1.1 to 1.4 m, but it is the marine-terminating part of the NEGIS system that is particularly vulnerable to marine ice sheet instability because it sits within a series of interconnected, over-deepened, subglacial troughs with a SLE of 0.12 - 0.35 m. A rapid retreat of this system would therefore have significant consequences for global sea-level rise.

A critical underlying component of this project is previous research that demonstrated that one of the NEGIS ice shelves (known as '79N') retreated 80 km during the mid-Holocene Thermal Maximum (HTM; 8.0 – 5.0 ka BP) (Bennike and Weidick, 2001). 79N is the only large-scale ice stream/shelf outlet system in Greenland that has a partially constrained Holocene retreat and re-advance history (Bennike and Weidick, 2001). The HTM was a period when radiative forcing and summer temperatures were up to 2°C higher than present, and analogous to those predicted for the next 100 years and beyond. Hence, increased air temperature could have played a role in ice stream fluctuation and ice shelf collapse, but we presently lack the data to assess the role of different forcing mechanisms (e.g. ocean warming) on ice stream fluctuation. This hinders our ability to predict the response of NEGIS to future climate change.

The overall aim of this project is to reconstruct the history of the NEGIS from the end of the last glacial maximum (LGM) through the Holocene. Working both onshore and offshore the project will generate a series of tie points to reconstruct ice sheet thickness, grounding line position, and ice shelf presence/absence. It will also generate a time series of forcing data on ocean and atmospheric temperatures. These datasets will be used to test and model the sensitivity of the ice stream to different forcing mechanisms at 100-1,000 year timescales.

Objectives

The NEGIS project has three key objectives:

- Objective 1: To constrain ice stream/ice shelf extent and thickness in order to determine rates of retreat and re-advance between 15 – 0 ka BP.
- Objective 2: To constrain oceanographic and atmospheric conditions and sea-level change adjacent to NEGIS between 15 – 0 ka BP.
- Objective 3: To apply the 3D BISCICLES numerical ice sheet model to test the sensitivity of NEGIS to atmospheric/oceanic /sea-level forcing and to explore feedbacks over 1,000 year timescales.

Work at sea and on land

The geological component of PS109 utilised five main tools for data collection along the cruise track (Fig. 7.1). First, bathymetric data was collected using the hull-mounted ATLAS Hydrosweep DS3 multibeam echo-sounding system. The instrument operated at a frequency between 13.6-16.4 kHz and was calibrated using sound velocity measurements of the water column collected from CTD stations. The data was processed and cleaned in CARIS Hips and Sips. The main aim of using the Hydrosweep system has been to establish the bathymetry and seafloor geomorphology of key areas and to characterise the geomorphological imprint and extent of the ice sheet on the NE Greenland shelf. Second, sub-bottom profiler data were collected using a hull-mounted Parasound DS III-P70 system operating at a pulse mode of between 4-20 kHz and a pulse length of 0.5 ms. The Parasound system has enabled us to acquire sub-seafloor acoustic stratigraphic data. This provides information on glacigenic and postglacial sediment thickness, architecture and distribution on the shelf and slope, and was used to identify sites for collecting sediment cores. Third, a gravity coring system with barrel length of 5 m was operated throughout the cruise. Recovery was variable depending on the nature of the target sediments. Our coring strategy was to: (i) sample different types of glacial, glacimarine and marine sedimentary environments on the shelf and slope to establish the nature of glacigenic sedimentation; (ii) recover the lithostratgraphic transition between subglacial sediments and overlying deglacial glacimarine sediments in order to constrain the timing of ice sheet retreat across the shelf. In total, we collected 24 gravity cores during the cruise (Table 1; Fig. 7.1). Fourth, a multi-corer was used to collect relatively undisturbed samples of the water-

sediment interface. The multi-corer collects relatively short sediment cores up to a maximum of 50 cm long. The rationale for using the multi-corer was to collect relatively undisturbed recent sediments to allow reconstruction of environmental conditions (particularly oceanographic conditions) covering the last few decades to centuries. Fifth, helicopter support was required for the onshore collection of rock samples for surface-exposure dating. This approach allows us to estimate the timing and rates of glacier thickness change through time. Five sites were targeted, but due to bad weather conditions we were unable to visit these locations. We did, however, successfully sample an alternative site on Franske Oer. The samples collected here (FO_17_01, 78.579 N, -18.627 E, 298 m asl; FO_17_02, 78.579 N, -18.626 E, 296 m asl), together with the adjacent sediment core data, will be used to reconstruct the retreat of Zachariae Isbrae onto the inner shelf.

During cruise PS109 the NEGIS project has concentrated on Objectives 1 and 2. The work during PS109 built on that completed in 2016 during cruise PS100 which collected geophysical data and sediment cores from Norske Trough, the area in front of the 79N ice shelf, Westwind Trough and Belgica Bank. However, during that cruise no cores were collected from Westwind Trough, hence this trough was a major target for our core operations in 2017. During PS109 data acquisition was focused first in Westwind Trough where we collected a series of sediment cores, initially from the outer shelf-shelf edge and then from the mid-trough region (Fig. 7.1). These cores were selected from Parasound data and they targeted ice-marginal features in the form of moraines and grounding-zone wedges which formed during ice sheet retreat. Data collection then moved to the area in front of 79N Glacier where we collected sediment cores and acquired further multibeam and sub-bottom profiler data to supplement that acquired during cruise PS100. The final area for data collection was Norske Trough. Here we acquired two blocks of multibeam data to determine seafloor morphology around the islands of Franske Oer and Norske Oer, supplemented by sediment cores, before moving to outer Norske Trough and the adjoining continental slope where we acquired additional gravity cores, multibeam and sub-bottom data.

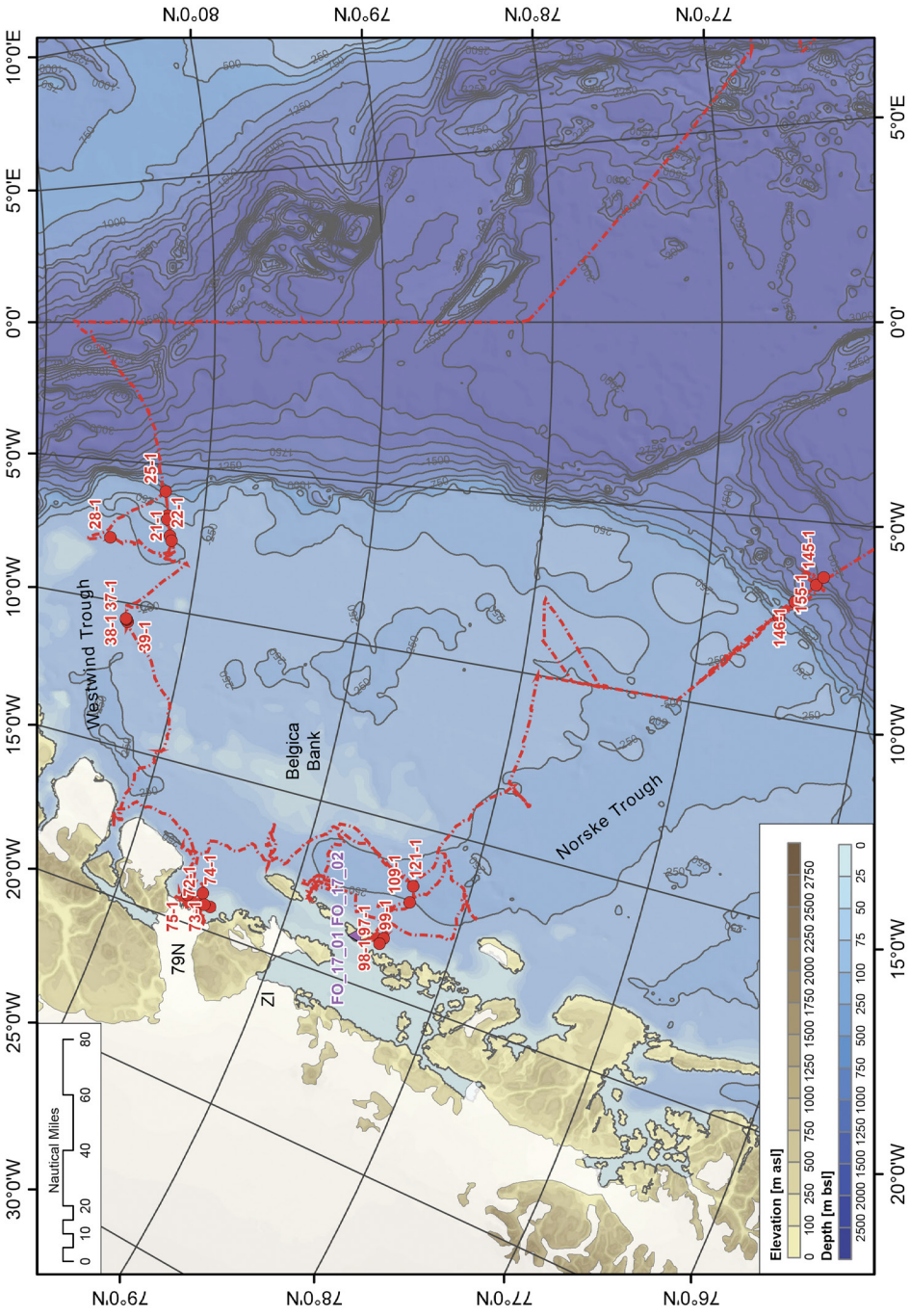

Fig. 7.1: An overview of the NE Greenland shelf showing the Norske Trough, Westwind Trough and Belgica Bank. Ship track and core locations from PS109 are shown by a red dashed line and red dots (with station number), respectively, while the surface-exposure samples on Franske Oer are shown by purple triangles. The offshore bathymetry and onshore topography is from IBCAO (version3).

Preliminary results

Westwind Trough

The Westwind Trough runs NE to E away from the coast towards the shelf break. It is generally shallower than the Norske Trough being less than 350 m deep for most of its length. The seafloor geomorphology of this trough shows spectacular streamlined subglacial bedforms in the form of mega-scale glacial lineations which can be traced to the outermost shelf (Fig. 7.2); iceberg scours are common in the trough particularly in water depth less than 200 m. Grounding-zone wedges are transverse glacigenic sedimentary landforms which form at the transition from the grounded ice sheet to an ice shelf. They were observed in the outer trough and at the shelf edge and were a key target for coring (Fig. 7.3). Preliminary on-board analysis of the cores from these features suggests the presence of subglacial sediments overlain by stratified glacimarine sediments. Parasound records from the mid-trough imaged a series of sharp-crested moraines and associated sedimentary wedges (Fig. 7.4). These were reported previously by Winklemann et al. (2010). Extensive thick sea ice precluded coring these features where they are best developed but we were able to take several cores directly to the south in the trough. In the inner trough, close to Dimphna Sund, deep, deglacial sedimentary basin fills are observed, similar to those observed in the inner parts of the Norske Trough and close to the 79N glacier.

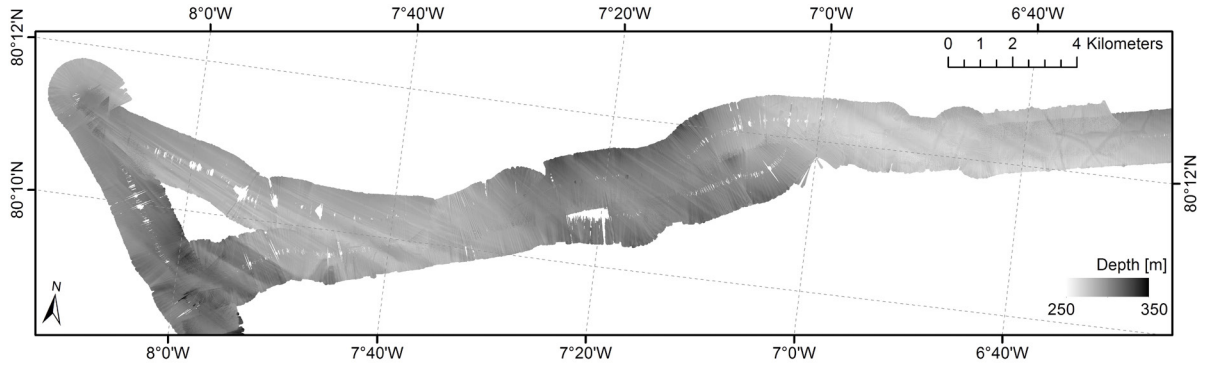

Fig. 7.2: Hydrosweep multibeam swath bathymetric record of mega-scale glacial lineations on the outer shelf of Westwind Trough. The lineations record flow of grounded ice along Westwind Trough to the shelf edge.

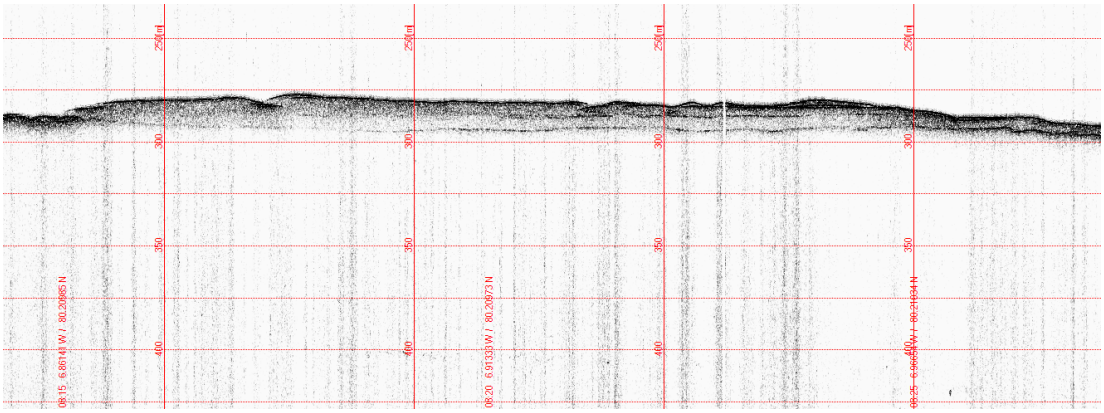

Fig. 7.3: Parasound image of a low amplitude grounding-zone wedge containing multiple internal sediment units in Westwind Trough. Note the strong basal reflector. Horizontal bars are 25 m apart.

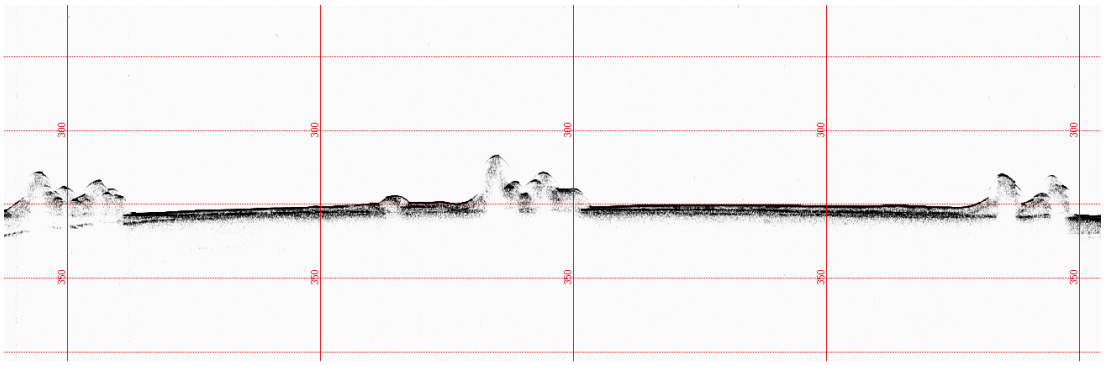

Fig. 7.4: Parasound image of moraines from mid-Westwind Trough. The moraines formed during ice sheet retreat in the trough, with the direction of ice retreat from left to right. See also Winkelmann et al. (2010). Horizontal bars are 25 m apart.

79N embayment

The inner trough and embayment in front of the 79N Glacier margin are characterised by distinctive stratified basins fills, in places over 75 m thick, separated by ice scoured bedrock highs that can be shallower than 100 m bsl (Fig. 7.5). We recovered four sediment cores from this region in order to ground-truth acoustic faces identified from Parasound records. Many of these cores were dominated by laminated-stratified, colour banded red and grey clays. These stratified muds probably represent deglacial and Holocene glacimarine sedimentation. On acoustic records stratified sequences are sometimes overlain by acoustically massive sediments, often lenticular in geometry, which are consistent with emplacement as debris flows probably fed from adjacent slopes and associated with high sedimentation rates in front of the ice shelf. On bedrock highs in the embayment stratified sediments often have a chaotic appearance and sediment cores from this ‘chaotic acoustic facies’ contained contorted and homogeneous red/grey muds. The final activity in this region was a short eastward extension to the multibeam survey collected in front of 79N Glacier during PS100.

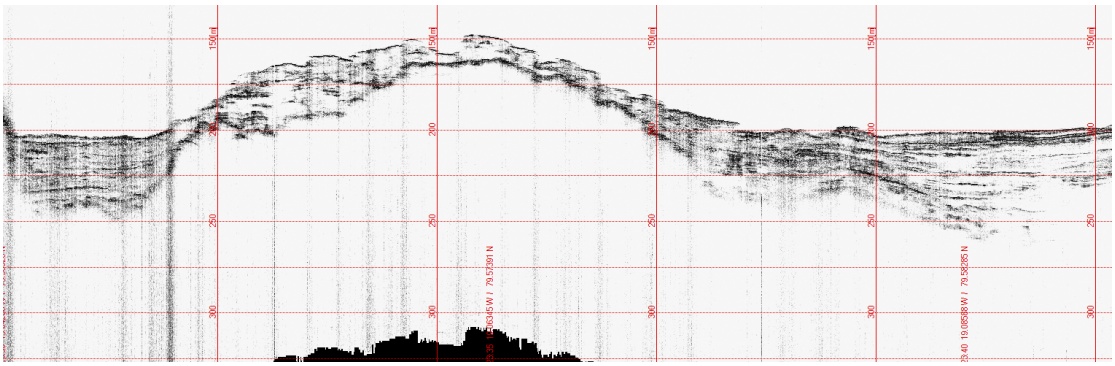

Fig. 7.5: Bedrock high and thick basin fills of acoustically stratified sediment from the embayment in front of 79N Glacier. Note the geometry of the stratified sediments which drape the bedrock highs and thicken in the intervening basins. The stratified sediments are typically composed of banded red and grey clays. Note also that stratification is better developed in the basins and is more chaotic and disturbed over the bedrock highs. Horizontal bars are 25 m apart.

Norske Trough

Geophysical data collection and coring focused mainly on the mid-inner part of Norske Trough (Fig. 7.1). Two multibeam surveys immediately west of the islands of Norske Oer and Franske Oer acquired data on seafloor morphology (Fig. 7.6). Drumlins merge southeastwards in Norske Trough with well-developed mega-scale glacial lineations recording flow of grounded ice through the trough towards the outer shelf (Fig. 7.7). Parasound records from the central and eastern part of the inner Norske Trough imaged acoustically homogenous to transparent facies overlying a prominent basal reflector and, in places, overlain in turn by a stratified drape (Fig. 7.8). Such acoustic stratigraphy was also observed in Westwind Trough and is a common feature of many glacially eroded cross-shelf troughs. This stratigraphy has typically been interpreted as representing a glacial advance-retreat sequence with the homogeneous unit representing a subglacial deforming bed till overlying bedrock or over-compacted till, and overlain in turn by deglacial glacimarine sediments (Evans et al., 2005; Ó Cofaigh et al., 2007; Dowdeswell et al., 2014). Cores from these acoustic facies bottomed out in the homogeneous unit and showed that it comprised soft massive diamicton. Further southeast towards the shelf edge the mid-trough area is characterised by grounding-zone wedges marking ice sheet retreat as well as streamlined subglacial bedforms. These were a focus of investigation during PS100. Multibeam and Parasound data were acquired across the outer trough region of Norske Trough and confirmed results from PS100 in showing that this region is heavily iceberg scoured.

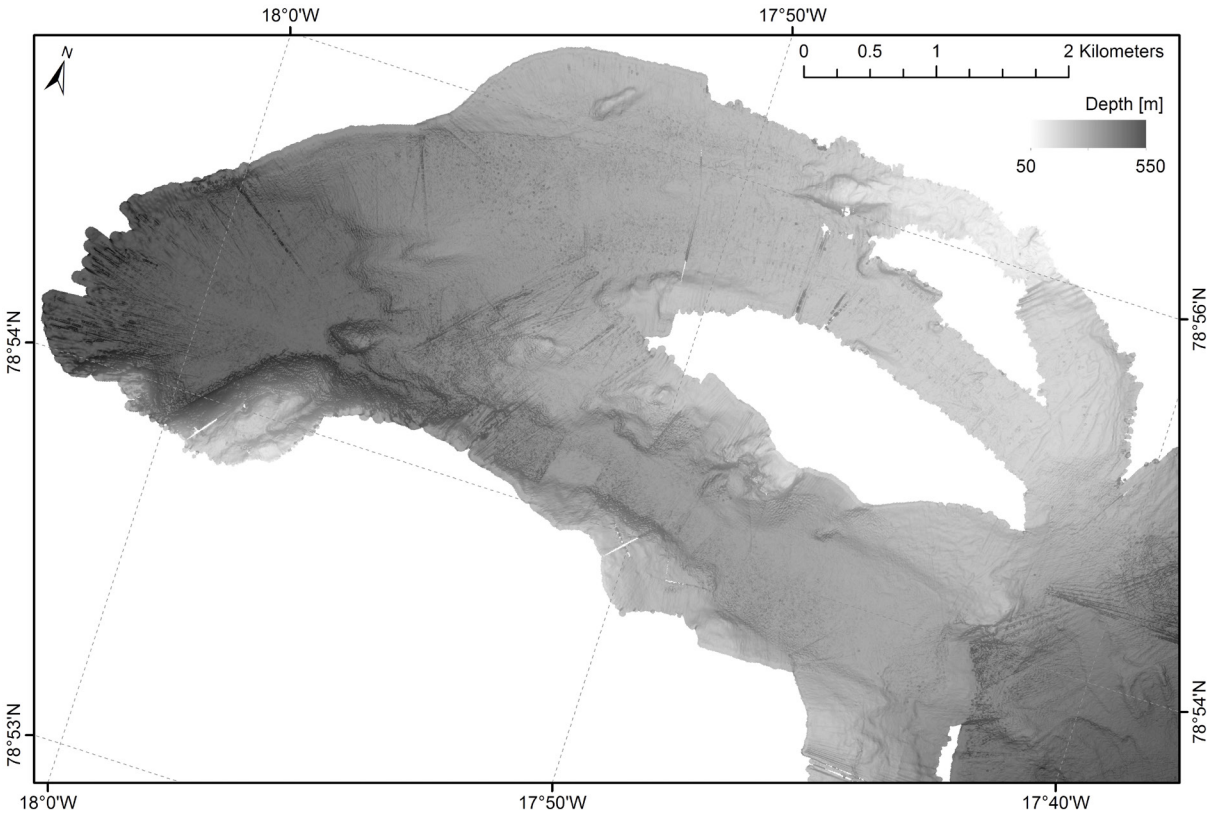

Fig. 7.6: Hydrosweep multibeam swath bathymetric record of seafloor morphology in inner Norske Trough east of Franske Oer

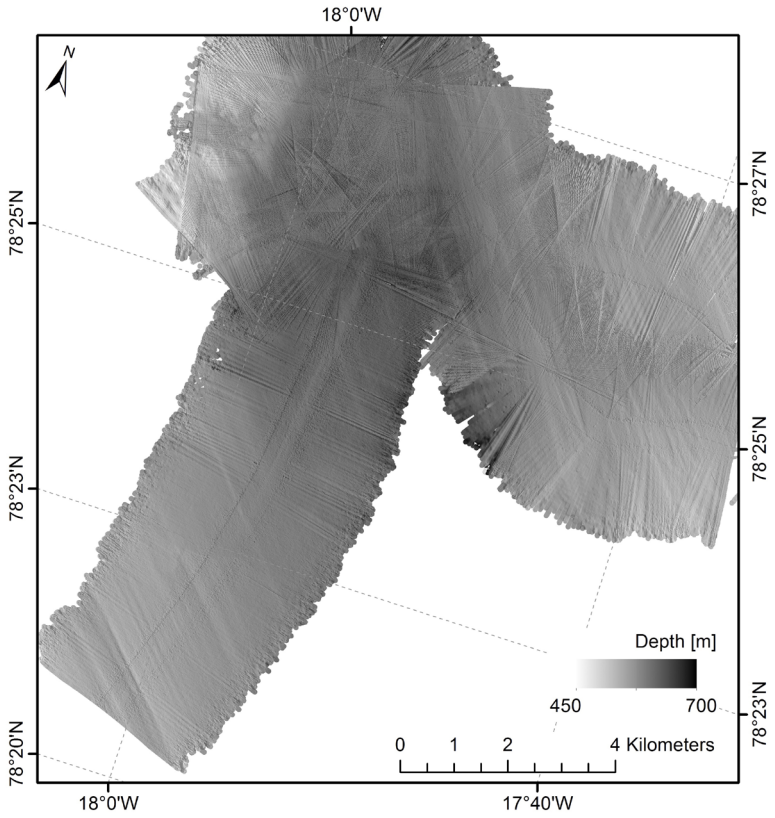

Fig. 7.7: Well-developed mega-scale glacial lineations in inner Norske Trough recording flow of a grounded ice sheet along the trough towards the outer shelf.

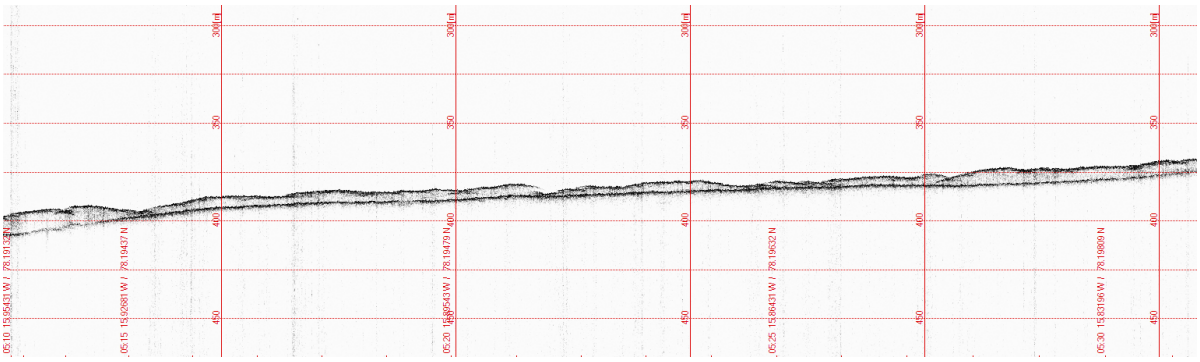

Fig. 7.8: Parasound record of acoustically homogeneous to transparent sediment unit underlain by a prominent basal reflector from inner Norske Trough. This unit is interpreted as a till sheet deposited by grounded ice flow along Norske Trough. The prominent basal reflector beneath the till represents a transition into an underlying stiffer till or bedrock.

Continental slope in front of Norske Trough

Parasound investigations of acoustic stratigraphy on the continental slope offshore of the mouth of Norske Trough imaged distinctive lenticular units of, typically, acoustically homogeneous sediment ranging in thickness from a few metres to over 10 m. These units commonly thin and pinch out downslope (Fig. 7.9) and they were observed from the upper continental slope in water depths of 500 m to the lower slope in water depths of greater than 2,800 m. The location of these deposits in front of a cross-shelf bathymetric trough containing clear evidence of

fast-flowing grounded ice in the form of streamlined subglacial bedforms and their acoustic characteristics are consistent with these lenses being glacigenic debris flows. Debris flow delivery onto the slope occurred when the ice sheet was grounded at the shelf edge in Norske Trough and delivered glacigenic sediment onto the upper slope which was then remobilized downslope by debris flow processes (Laberg and Vorren, 1995, 2000). A series of sediment cores targeted these debris flow lenses in water depths of 600-2,220 m (Fig. 7.1). Core recovery was variable but cores up to 3 m in length were recovered which bottomed out in poorly-sorted, massive grey pebbly mud consistent with a glacigenic debris flow interpretation.

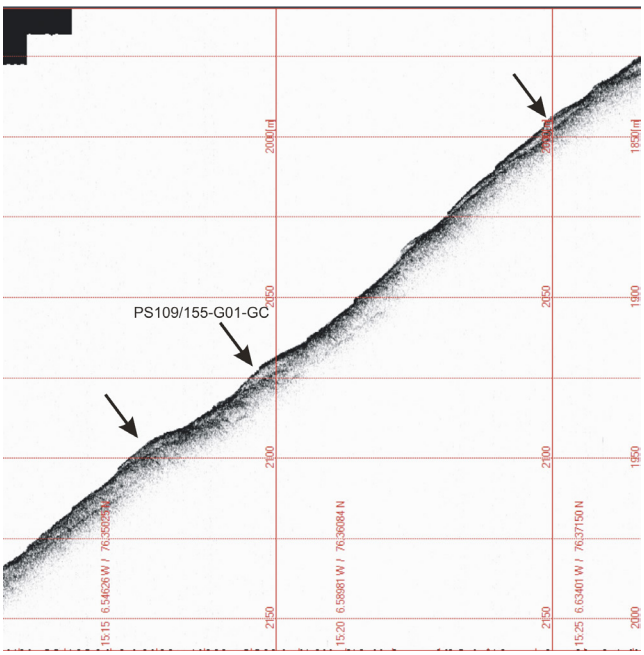

Fig. 7.9: Parasound image of the continental slope in front of Norske Trough in 1975-2150 m water depth. Note lenticular homogeneous sediment units (arrowed) that are interpreted as glacigenic debris flows. The location of core PS109/155-01-GC is indicated. Horizontal bars are 25 m apart.

Data management

The majority of cores collected during PS109 were split onboard, and logged and described sedimentologically during the cruise. The cores will be shipped to Durham University for multi-sensor core logger (MSCL) measurements (e.g. bulk density, porosity, grainsize, P-wave velocities and water content), XRF and XCT 3D X-ray analysis. Foraminiferal, stable isotope analyses and sediment geochemistry (TOC, TN, C/N analysis) will also be conducted at Durham. The cores will be archived at AWI post analysis. Sample processing for radiocarbon dates (^{14}C) will be carried out at the NERC Radiocarbon Laboratory, UK. All data will be uploaded to the PANGAEA database. Unrestricted access to the data will be granted after about three years from the end of the cruise, pending analysis and publication.

Tab. 7.1: Core sample names and locational information details from PS109

Site Number	Equipment	Latitude (N)	Long (W)	Water Depth [m]	Recovery [cm]
PS109/ 19-02	Multi-Corer	80° 08.839’	07° 57.019’	316	28
PS109/ 21-01	Gravity Corer	80° 10.301’	07° 36.573’	301	128
PS109/ 22-01	Gravity Corer	80° 11.018’	07° 26.587’	329	265
PS109/23-01	Gravity Corer	80° 12.767’	06° 53.077’	289	221
PS109/ 24-01	Gravity Corer	80° 12.688’	06° 45.169’	289	331

Site Number	Equipment	Latitude (N)	Long (W)	Water Depth [m]	Recovery [cm]
PS109/25-01	Gravity Corer	80° 14.371’	05° 55.803’	397	268
PS109/28-01	Gravity Corer	80° 32.033’	07° 46.769’	259	304
PS109/36-02	Multi-Corer	80° 19.058’	10° 01.904’	317	29
PS109/37-01	Gravity Corer	80° 21.873’	10° 32.686’	324	124
PS109/38-01	Gravity Corer	80° 21.839’	10° 34.330’	319	80
PS109/39-01	Gravity Corer	80° 21.588’	10° 34.627’	308	38
PS109/40-01	Gravity Corer	80° 21.112’	10° 39.391’	291	152
PS109/46-02	Multi-Corer	80° 08.854’	17° 42.136’	210	34
PS109/72-01	Gravity Corer	79° 28.610’	19° 13.972’	438	500
PS109/73-01	Gravity Corer	79° 26.492’	19° 14.852’	185	500
PS109/74-01	Gravity Corer	79° 30.489’	18° 54.120’	480	502
PS109/75-01	Gravity Corer	79 ° 35.459’	19° 06.287’	168	351
PS109/76-01	Multi-Corer	79° 37.213’	19° 17.323’	367	40
PS109/85-02	Multi-Corer	79° 33.408’	19° 13.635’	156	44
PS109/97-01	Gravity Corer	78° 25.401’	18° 37.150’	211	500
PS109/ 98-01	Gravity Corer	78° 25.395’	18° 37.392’	206	484
PS109/99-01	Gravity Corer	78° 24.614’	18° 25.672’	412	500
PS109/105-01	Multi-Corer	78° 28.880’	18° 33.371’	440	51
PS109/108-01	Gravity Corer	78° 25.070’	17° 34.535’	560	489
PS109/109-01	Gravity Corer	78° 19.695’	17° 11.491’	507	368
PS109/121-01	Gravity Corer	78° 20.138’	16° 43.210‘	480	378
PS109/139-01	Multi-Corer	76° 48.107‘	08° 37.512‘	357	23
PS109/145-01	Gravity Corer	76° 19.073‘	06° 21.974‘	2240	0
PS109/146-01	Gravity Corer	76° 28.266‘	07° 03.337‘	1278	Bag sample core barrel
PS109/147-01	Gravity Corer	76° 33.024‘	07° 29.261‘	628	295
PS109/155-01	Gravity Corer	76° 21.402‘	06° 34.401‘	2030	201

References

AMAP (2011) Arctic Climate Issues 2011: Changes in Arctic Snow, Water, Ice and Permafrost. SWIPA 2011 Overview Report.

Bennike O, Weidick A (2001) Late Quaternary history around Nioghalvfjerdsfjorden and Jøkelbugten, North-East Greenland. Boreas, 30, 205-227.

Dowdeswell JA, Hogan KA, Ó Cofaigh C, Fugelli EM, Evans J and Noormets R (2014) Late Quaternary ice flow in a West Greenland fjord and cross-shelf trough system: submarine landforms from Rink Isbrae to Uummannaq shelf and slope. Quaternary Science Reviews, 92, p. 292-309.

Evans J, Pudsey CJ, Ó Cofaigh C, Morris P & Domack E (2005) Late Quaternary glacial history, flow dynamics and sedimentation along the eastern margin of the Antarctic Peninsula Ice Sheet. Quaternary Science Reviews, 24 (5-6), 741-774.

Laberg JS, Vorren TO, (1995) Late Weichselian submarine debris flow deposits on the Bear Island Trough Mouth Fan. Marine Geology, 127, 45–72.

Laberg JS & Vorren TO (2000) Flow behaviour of the submarine glacigenic debris flows on the Bear Island Trough Mouth Fan, western Barents Sea. Sedimentology, 47, 1105-1117.

Mouginot J, Rignot E, Scheuchl B, Fenty I, Khazendar A, Morlighem M, Buzzi A, Paden J (2015) Fast retreat of Zachariæ Isstrøm, northeast Greenland. Science, DOI: 10.1126/science.aac7111

Nick F, van Der Veen CJ, Vieli A, Benn D (2010) A physically based calving model applied to marine outlet glaciers and implications for the glacier dynamics. Journal of Glaciology, 56, 781–794.

Ó Cofaigh C, Evans J, Dowdeswell JA & Larter, RD (2007) Till characteristics, genesis and transport beneath Antarctic paleo-ice streams. Journal of Geophysical Research. 112, F03006, doi:101029/2006JF000606.

Seroussi H, Morlighem M, Rignot E, Mouginot J, Larour E, Schodlok M, Khazendar A (2014) Sensitivity of the dynamics of Pine Island Glacier,West Antarctica to climate forcing for the next 50 years. The Cryosphere, 8, 1699–1710.

Straneo F, Sutherland D, Holland D, Gladish C, Hamilton GS, Johnson HL, Rignot E, Xu Y, Koppes M (2012) Characteristics of ocean waters reaching Greenland's glaciers, Ann. Glaciol., 53(60), 202–210.

Wilson NJ, Straneo F (2015) Water exchange between the continental shelf and the cavity beneath Nioghalvfjerdsbræ (79 North Glacier). Geophys. Res. Lett., 42, 7648–7654.

Winklemann D, Jokat W, Jensen, Schenkeb WK (2010) Submarine end moraines on the continental shelf off NE Greenland – Implications for Lateglacial dynamics. Quaternary Science Reviews, 29, 1069-1077.

Yin J, Overpeck JT, Griffies SM, Hu A, Russell JL, Stouffer RJ (2011) Different magnitudes of projected subsurface ocean warming around Greenland and Antarctica. Nature Geoscience, 4, 524-528.

8. SEISMOLOGY

Vera Schlindwein[1] (not on board), Michaela Meier[1] [1]AWI

Grant-No. AWI_PS109_08

Objectives

At spreading ridges, new oceanic lithosphere is produced by upwelling of mantle material. Major differences between ridges spreading at different velocities have been observed (e.g. Dick et al, 2003). Ultraslow spreading ridges with spreading rates of 20 mm/y and less represent the melt-poor endmember of spreading ridges. Here, melt is suggested to travel to volcanic centres, where the lithosphere is thinner and it can erupt. Outside of volcanic centres the lithosphere is thicker and thereby inhibits the upwelling of magma. The Knipovich Ridge is an ultraslow spreading ridge. It was instrumented on a length of 160 km of ridge axis with 23 ocean bottom seismometers (OBS) during *Polarstern* cruise PS100. For an active experiment to map the structure of the Logachev Seamount, four additional OBS were deployed during PS109. The other stations ran out of power by early September. The active experiment includes seismic refraction and was successfully carried out on cruise MSM67 of *Maria S. Merian* in September 2017. The active experiment allows seismic tomography of Logachev Seamount. With this information we want to study how melts manage to travel through the thick cold lithosphere to the seafloor at the volcanic centres. All OBS will be recovered during MSM68 in October 2017.

Around the 79°N glacier unusually many seismic events are observed for a stable craton. This is especially obvious along the northern edge of the glacier and its mouth. We suspect that the seismicity is partly of cryogenic origin, but to study the provenance and the source mechanisms of the evens in more detail, local networks are necessary. Otherwise the station coverage is too sparse to allow detailed studies. Small icequakes produced by the glacier itself are potentially caused by fracturing at the grounding line. With data from a local network we want to study the relation of events to the tides and flow speed of the glacier as well as seasonal effects. Following a pilot experiment during PS100 in 2016, we will now deploy a specifically dimensioned local seismic network consisting of four seismometer stations. After one year of recording, the stations will be recovered during a field campaign in summer 2018.

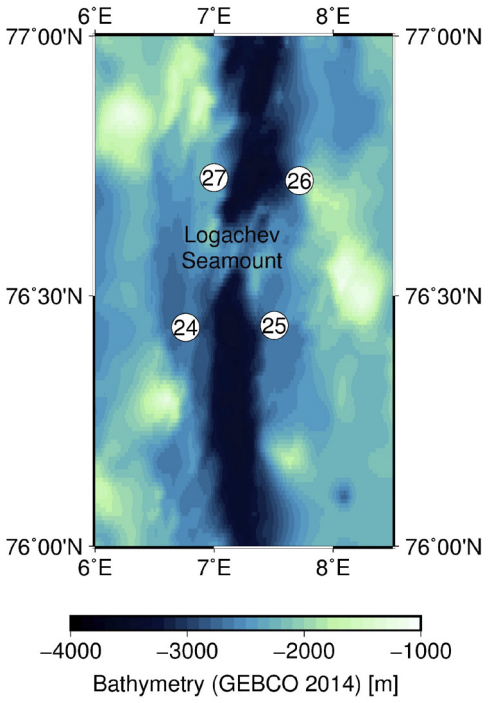

Fig. 8.1: Locations of ocean bottom seismometer deployment positions along the Knipovich Ridge

Work at sea and land

The OBS were assembled in port in Tromsø and stored on deck, ready to be dropped at the planned positions. Areas with flat topography were chosen based on bathymetry data. Around two days after leaving port in Tromsø, these positions were reached. The instruments were deployed in free-fall mode. The deployment positions are summarised in Table 8.1 and shown on the map in Fig. 8.1.

Tab. 8.1: Ocean bottom seismometer deployment sites and recording parameters

OBS No	Latitude	Longitude	Depth [m]	Deployment Time	Sample Rate [sps]	Autorelease Time
24	76° 26.26' N	006° 45.655' E	2729	14.09.2017 09:29	100	12.10.2017 06:00
25	76° 26.499' N	007° 30.293' E	2699	14.09.2017 11:30	100	12.10.2017 11:00
26	76° 43.419' N	007° 42.997' E	2499	14.09.2017 13:34	100	12.10.2017 16:00
27	76° 43.770' N	006° 59.960 E	2361	14.09.2017 15:06	100	12.10.2017 21:00

The four stations of the seismic network at the 79°N glacier were installed during one helicopter flight. It was installed on a nunatak close to the grounding line of the glacier. The network consists of one central station and three stations around the centre. The distance between stations is around 700 m. Table 8.2 summarises the station information and the positions are also shown in Fig. 8.2. Fig. 8.3 shows a photo of station 79N12. The entire operation took around 4.5 - 5 hours. Stations will stay at their positions until summer 2018.

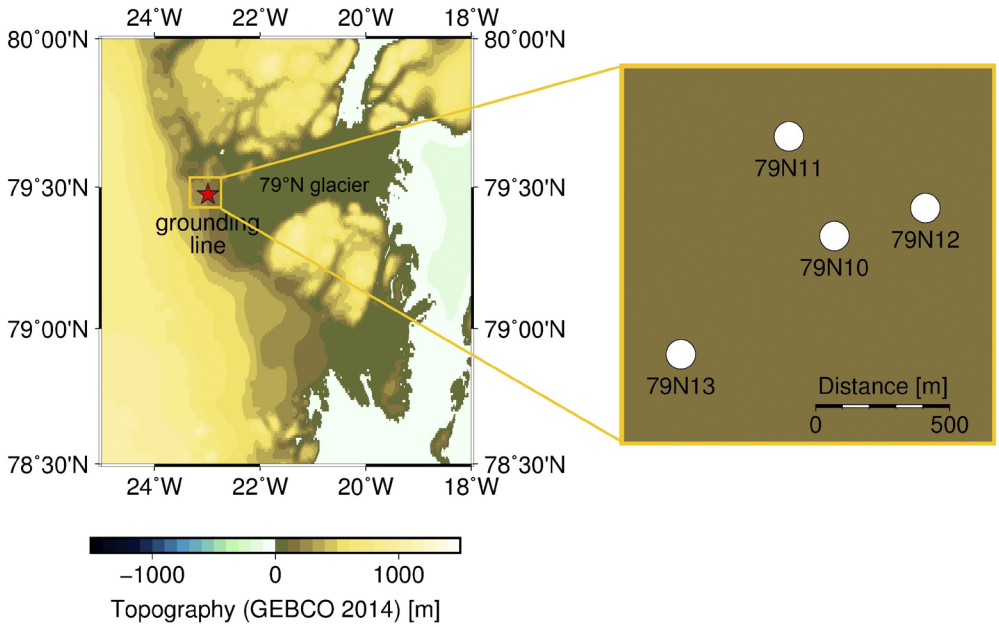

Fig. 8.2: Locations of land seismometer stations at the 79°N glacier

Tab. 8.2: Land seismic network deployment sites

Station No	Latitude	Longitude	Date	Time	Orientation wrt magnetic N
79N10	79° 28.48' N	22° 59.28' W	21.09.17	10:00	0
79N11	79° 28.67' N	22° 59.79' W	21.09.17	10:55	0
79N12	79° 28.53' N	22° 58.35' W	21.09.17	12:02	0
79N13	79° 28.25' N	23° 00.93' W	21.09.17	12:42	0

Preliminary (expected) results

The seismic data recorded at the Knipovich Ridge can only be accessed upon retrieval in October 2017. The OBS deployed during *Polarstern* cruise PS109 are expected to record a few hundred earthquakes and the rays of the active experiment. These data together with earthquake recordings of the other OBS stations will allow to study the seismicity and lithospheric structure of the area.

Based on a reconnaissance survey during *Polarstern* cruise PS100, we expect to record hundreds of icequakes with the small array near the grounding line. Most of these icequakes result from fracturing near the grounding line and their occurrence is tidally modulated. Our previous survey covered only few days. We now expect to see changes in seismicity not only on a diurnal but also on a seasonal basis that will help to constrain the source processes of the icequakes.

The seismic stations will run out of power in late autumn and should recover once sufficient daylight has recharged the batteries. We expect about 6 months of data. This more extended data set should include several regional seismic events that occur in the wider region of the 79°N glacier and are strong enough to be recorded by the entire network. We hope that we can determine focal depths and resolve the focal mechanisms of these earthquakes to understand their origin.

Fig. 8.3: Photo of station 79N12

Data management

Raw data will be archived in Pangaea. Continuous waveform data will be made available approximately three years after recovery through seismological data portals (GEOFON) that allow automatic data retrieval.

References

Dick H, Lin J, Schouten H (2003) An ultraslow-spreading class of ocean ridge. Nature, 426, doi:10.1029/2002JB001964.

9. GPS OBSERVATIONS IN NORTH-EAST GREENLAND TO DETERMINE VERTICAL AND HORIZONTAL DEFORMATIONS OF THE EARTH'S CRUST

Mirko Scheinert[1] (not on board), Christoph Knöfel[1], Susanne Lunz[1]

[1]TU Dresden

Grant-No. AWI_PS109_09

Objectives

Besides Antarctica, Greenland is the only place where a huge continental ice sheet is still present. Although it contains only 10 % of the global fresh-water storage in comparison to the Antarctic ice sheet, it still plays an important role for the global climate. Due to its location at high- and sub-polar latitudes it reacts to changes in the environmental and climate conditions in a very sensitive way. Therefore, the Greenland ice sheet has been subject to intensive geophysical and glaciological investigations for almost one century.

Mass changes of the ice sheet can be regarded as changing surface loads, which cause – due to the rheological properties of the upper layers of the Earth – long-term visco-elastic and immediate elastic reactions of the solid earth. Hence, the response of the Earth's crust contains indirectly the integral effect of all ice-mass changes during the glacial history and can be obtained by observing the vertical deformation of the surface of the Earth.

The area of North-East Greenland is characterized by a high variability of the ice edge with regard to its boundaries as well as its mass change. In addition, according to model predictions a visco-elastic signal due to deglaciation since the last glacial maximum reaches maximum values there. Deformations of tectonic origin can also not be excluded, which will be investigated by analysing the horizontal components.

Satellite-based positioning by means of Global Navigation Satellite Systems (GNSS) allows a precise geodetic determination of three dimensional coordinates and, with repeated observations, the determination of changes of the horizontal as well as of the vertical components with an accuracy in the sub-centimetre level. In order to ensure a high accuracy of repeated measurements, a stable base for the GNSS marker has to be chosen. Therefore, the stations are to be set-up at ice-free bedrock locations which are only available at the coastal regions of Greenland.

This project is a continuation of research work done during *Polarstern* cruises ARK-XXIII/1+2 (PS72, 2008), ARK-XXIV/3 (PS74, 2009) and PS100 (ARK-XXX/2, 2016). The main goal of the geodetic work was the re-observation of GNSS sites at up to 5 ice-free locations in the coastal area of Northeast Greenland between 78° and 81°N. These were installed and firstly observed during *Polarstern* ARK-XXIII/1 (PS72) and ARKXXIII/2 (PS72) cruises in 2008. Some of these stations could be re-observed in 2009 during cruise ARK-XXIV/3 (PS74) and in 2016 during cruise PS100 (ARK-XXX/2) as well as through the field campaign iGRIFF in July 2017.

In addition to the re-occupations of the stations on bedrock another GNSS site named NIO1 located on the floating part of the 79°N glacier (79NG) should be visited to perform a sensor upgrade, download the GNSS data and to measure ablation values. The station was set up in

July 2017 and is supposed to stay on the 79NG for one year to observe the influence of ocean tides on the glacier as well as the glacier velocity. Thus, the ground-based GNSS data are intended to be used to validate models of the glacier velocity and of the ocean tides.

Work at sea and land

Polarstern with its two helicopters served as basis for the realisation of the work. To reach the locations on land, *Polarstern* had to sail to positions close enough to Greenland's coast. The geodetic flight programme was adapted to the ship's route such that no additional shiptime was necessary.

The first activity took place during oceanographic station work close to the coastline of Greenland. The GNSS site HOLM was within long-range flight distance of the helicopter (80 nm) and the equipment could be re-installed on the position marked in 2008. Due to bad weather conditions, only two more stations, MUSK and FRAN, could be reoccupied during the next weeks. Except HOLM, the scientific equipment of all sites could be recovered successfully. Bad and locally varying weather conditions did not allow any other long-distance flights. A visit of the long-term glacier station NIO1 was also not possible during the vessels stay within flight distance of the station.

The setup of a geodetic GNSS site consists of a GNSS antenna which is screwed on a bolt permanently fixed to bedrock. This allows a forced centering of the antenna. The power supply is realised by solar modules and sealed batteries, specially adapted for usage with solar power. GNSS receiver, batteries and a charging controller are stored in an aluminium box, which protects the equipment from the influences of weather and animals. Fig. 9.1 shows an example of the GNSS site set-up. The receivers are supposed to collect data for at least three 24h-sessions with a data sampling rate of 15 s in order to ensure a sufficient accuracy of the obtained coordinates. A list of the GNSS sites is given in Table 9.1. Their locations are also shown in the overview map in Fig. 9.2.

Altogether, 3 GNSS sites were set up while two of them could be removed during the cruise. A successful re-observation of the 2008, 2009 and 2016 campaigns took place.

Tab. 9.1: List of GNSS sites with approximate coordinates and observation schedule.

ID	Longitude	Latitude	Ellips. H [m]	Geographical region	Start date	Stop date	24h Session
HOLM	16° 25‘ 53“ W	80° 16‘ 23“ N	410	Holm Land E	19.09.17	-	?
MUSK	22°43‘ 22“ W	79° 58‘ 46“ N	616	Skallingen	20.09.17	23.09.17	3.5
FRAN	18° 37‘ 38“ W	78° 43‘ 42“ N	337	Franske Øer S	27.09.17	30.09.17	2.5

Preliminary (expected) results

The GNSS observations will be post-processed based on latest standards of scientific GNSS data analysis using the Bernese GNSS Software (e.g. consistent and precise realisation of the global reference frame). The estimated site coordinates of each observation campaign allow the derivation of coordinate changes in both horizontal and vertical direction. These rates serve as an independent source for the validation and improvement of models on the glacial history and on the recent ice-mass balance of Northeast Greenland. Through testing the significance of horizontal deformations contributions to an improved analysis of the tectonic regime in the working area will be given.

The observations at 79NG would have been analysed in kinematic mode in order to investigate the tidal dynamics of the floating glacier.

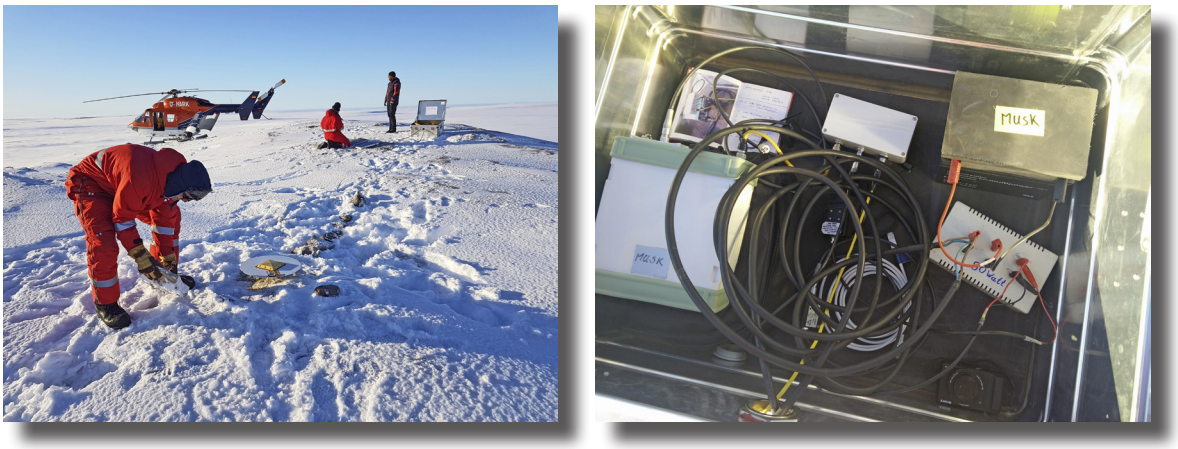

Fig. 9.1: Typical set-up of a GNSS site. Left: View at the final set-up of site MUSK (Skallingen).Right: View into the aluminium box with GNSS receiver, charging controller and a sealed battery.

Data management

The geodetic GNSS observation data will be archived in a similar database like the SCAR GNSS Database that is maintained at TU Dresden. The long-term preservation of the data will be maintained also through the close cooperation within the SCAR Scientific Programme SERCE (Solid Earth Responses and Influences on Cryosphere Evolution). A common structure of the data holdings is ensured through the application of the same scientific software package utilised to analyse geodetic GNSS measurements at TU Dresden (i.e., the Bernese GNSS Software). Further products and resulting models will be archived in the PANGEA database at AWI.

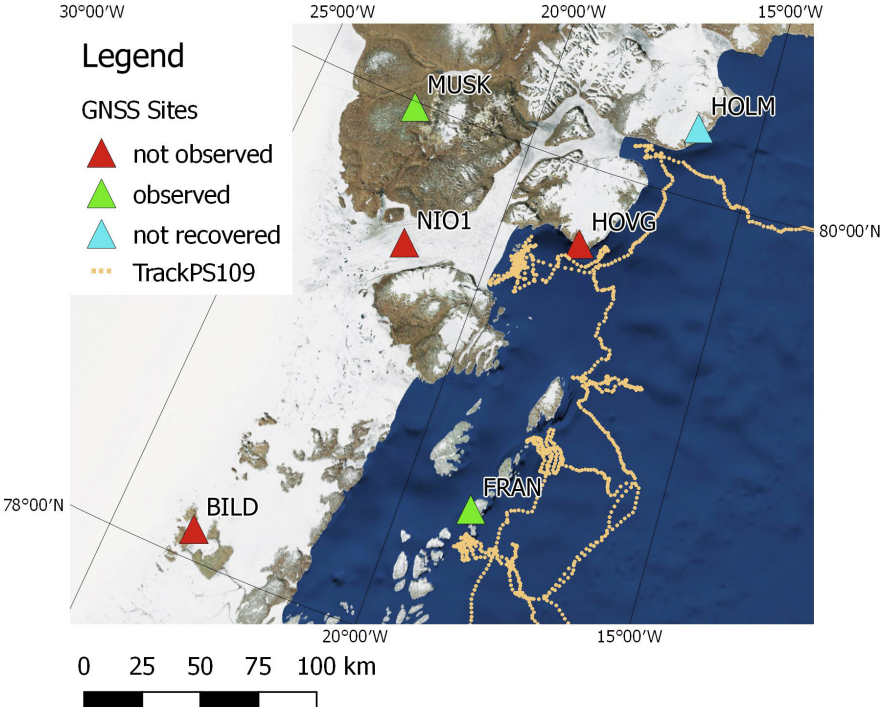

Fig. 9.2: Overview map showing the locations of GNSS sites in the area of investigation
(Map: ArcGIS World_Imagery; mapping software: QGIS)

Acknowledgements

The geodetic programme could be realised successfully due to the great support by numerous colleagues in the preparation and realisation of the expedition as well as by the crew of *Polarstern*. Especially we like to thank: Torsten Kanzow (chief scientist), Lars Vaupel and Jan Kendzia (helicopter pilots) and their crew and Thomas Wunderlich (Master of RV *Polarstern*).

10. BENTHIC BIOGEOCHEMICAL PROCESSES

Janine Felden[1], Ulrike Braeckman[2],
Frank Wenzhöfer[3] (not on board),
Volker Asendorf[3], Jakob Barz[3]

[1]UHB
[2]Uni Ghent
[3]MPIMM

Grant No AWI_PS109_10

Objectives

Benthic communities are strictly dependent on carbon supply through the water column, which is determined by temporal and spatial variations in the vertical export flux from the euphotic zone but also by lateral supply from shelf areas. Most organic carbon is recycled in the pelagic, but a significant fraction of the organic material ultimately reaches the seafloor, where it is either re-mineralized or retained in the sediment record. Benthic oxygen fluxes provide the best and integrated measurement of the metabolic activity of surface sediments. They quantify benthic carbon mineralization rates and thus can be used to evaluate the efficiency of the biological pump (export of organic carbon from the photic zone). Arctic shelf sediments reveal high fauna abundance and biomass and show high benthic microbial activities. Changes in sea ice extent and thickness, precipitation and river discharge, as well as melt water input alter the light and nutrient availability in the shelf zone and are expected to affect productivity. However, how benthic communities respond on climate induced environmental shifts, as increased melt water input, is not known. During *Polarstern* expedition PS109, benthic lander measurements and TV-guided Multicorer samples have been used to investigate how increased melt water input affects benthic biogeochemical processes and community composition.

Work at sea

Benthic exchange and mineralization rates were measured *in-situ* with 2 Benthic Lander systems at selected stations and *ex situ* on TV-MUC cores from all stations (Fig. 10.1). Each of the used Lander systems was equipped with three benthic chamber modules and one X-Y Microprofiler. The benthic chambers were used to measure total oxygen uptake (TOU) and nutrient exchange of the sediment integrating all relevant solute transport processes (diffusion, advection and fauna-mediated transport) covering an area of 400 cm^2. During the deployment an oxygen optode measured changes in oxygen concentration and 7 syringes took water samples in pre-programmed time intervals for analyses of dissolved inorganic carbon (DIC) and nutrients. Furthermore, the enclosed and retrieved sediments were sampled for pigments, total organic carbon content (TOC), abundances of microbes, meio- and macrofauna and community composition. The X-Y microprofiler was used to quantify diffusive oxygen uptake (DOU), which is generally assigned to microbial respiration. The difference between TOU and DOU is then attributed to the activity of meio- and macrofauna (respiration and stimulation

of microbial oxygen consumption). Each microprofiler was equipped with nine oxygen, one temperature and two resistivity microsensors. The measurements across the sediment-water interface were performed with a vertical resolution of 100 µm and a total length of 15 cm. During the deployments the microprofiler performed five vertical profiles horizontally separated by 10 cm.

Ex-situ oxygen microprofiles were measured with a motorized micromanipulator set up at *in-situ* temperature in an oxygenated water bath on board. Afterwards, *ex situ* incubations were run on sediment cores with ~10 cm overlying water to estimate the total oxygen uptake. Firesting optode microsensors were used to monitor the oxygen concentration in the overlying water of the incubated cores. At start and end of the incubations, additional water samples were taken to quantify nutrient and DIC exchange across the sediment-water interface.

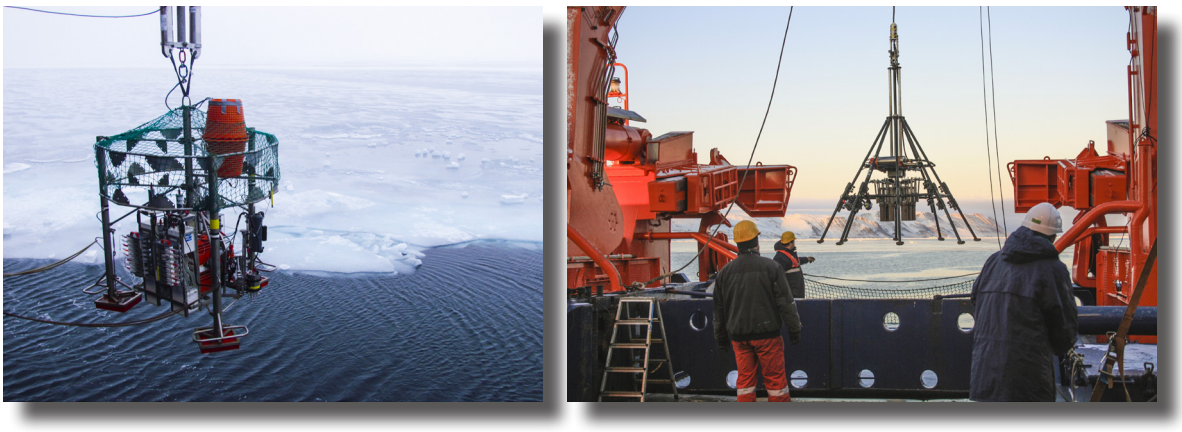

Fig. 10.1: Benthic lander (left) and TV-MUC (right) upon deployment

The Multicorer was equipped with a video camera (TV-MUC) and videos of the seafloor are available for most stations. Multicorer cores were subsampled in 0.5 centimeter step interval (0-5 cm), one centimeter interval (5-10 cm) and in two centimeter step intervals (10-20 cm) for granulometry, porosity and ^{210}Pb. The latter analyses will provide insight in the sediment deposition rate and biogenic mixing depth. Microbial and meiofaunal abundances and community composition, pigments and TOC will be investigated in the upper 0-5 cm at 1 cm intervals. Macrofauna communities will be characterized in the 0-5 cm and 5-10 cm sediment layers. Sediment samples were fixed for several faunal microbiological, and geochemical analyses that will be conducted in the home laboratory. A list of all Multicorer and Lander stations is given in Table 10.1.

Table 10.1: List of stations sampled with TV-MUC and benthic lander during PS109

Station	Gear	Date [Deploy-ment]	Latitude [N]	Longitude [W]	Depth [m]	Site/Area
PS109_19-2	TV-MUC	2017-09-17 12:38	80° 08,839‘	007° 57,019‘	313	Westwind Trough
PS109_19-4	TV-MUC	2017-09-17 15:16	80° 08,049‘	007°55,904‘	315	Westwind Trough
PS109_19-3	Lander	2017-09-17 14:29	80° 08,840‘	007° 56,861‘	315	Westwind Trough

Station	Gear	Date [Deploy-ment]	Latitude [N]	Longitude [W]	Depth [m]	Site/Area
PS109_36-2	TV-MUC	2017-09-19 06:09	80° 19,058‘	010° 01,904‘	317	Westwind Trough
PS109_36-3	TV-MUC	2017-09-19 06:55	80° 18,779‘	010° 05,185‘	310	Westwind Trough
PS109_45-3	TV-MUC	2017-09-20 19:25	80° 08,057‘	017° 42,178‘	206	Djimphna Sund
PS109_45-4	TV-MUC	2017-09-20 20:05	80° 08,062‘	017° 42,630‘	219	Djimphna Sund
PS109_53-1	TV-MUC	2017-09-21 22:30	79° 34,128‘	019° 27,534‘	556	at 79° Glacier
PS109_61-1	TV-MUC	2017-09-22 22:17	79° 33,393‘	019° 13,249‘	162	at 79° Glacier
PS109_62-1	TV-MUC	2017-09-22 23:37	79° 30,400‘	019° 19,315‘	301	at 79° Glacier
PS109_68-1	Lander	2017-09-23 09:35	79° 33,371‘	019° 13,186‘	169	at 79° Glacier
PS109_69-1	Lander	2017-09-23 11:30	79° 30,316‘	019° 19,023‘	301	at 79° Glacier
PS109_76-1	TV-MUC	2017-09-24 01:23	79° 37,200‘	019° 17,488‘	366	at 79° Glacier
PS109_76-2	TV-MUC	2017-09-24 02:41	79° 37,213‘	019° 17,323‘	367	at 79° Glacier
PS109_84-2	TV-MUC	2017-09-24 23:03	79° 30,376‘	019° 19,093‘	309	at 79° Glacier
PS109_85-1	TV-MUC	2017-09-25 00:25	79° 33,408‘	019° 13,635‘	156	at 79° Glacier
PS109_93-2	TV-MUC	2017-09-26 12:27	79° 11,349‘	017° 07,199‘	386	Norske Trough
PS109_93-3	TV-MUC	2017-09-26 13:37	79° 11,045‘	017° 08,791‘	389	Norske Trough
PS109_105-1	TV-MUC	2017-09-28 12:26	78° 28,088‘	018° 33,371‘	440	Joekelbochten
PS109_105-2	TV-MUC	2017-09-28 13:29	78° 28,865‘	018° 33,312‘	441	Joekelbochten
PS109_107-1	Lander	2017-09-28 17:59	78° 27,520‘	017° 54,932‘	645	Norske Trough
PS109_115-2	TV-MUC	2017-09-29 23:02	78° 01,969‘	016° 32,436‘	503	Norske Trough
PS109_115-3	TV-MUC	2017-09-29 23:48	78° 01,989‘	016° 31,017‘	502	Norske Trough
PS109_116-2	TV-MUC	2017-09-30 09:03	78° 25,666‘	017° 56,211‘	669	Norske Trough
PS109_122-1	TV-MUC	2017-10-02 15:42	77° 54,688‘	013° 10,456‘	140	Norske Trough

Station	Gear	Date [Deploy-ment]	Latitude [N]	Longitude [W]	Depth [m]	Site/Area
PS109_125-1	TV-MUC	2017-10-03 00:30	77° 47,965‘	013° 37,915‘	388	Norske Trough
PS109_125-2	TV-MUC	2017-10-03 01:10	77° 47,918‘	013° 37,667‘	391	Norske Trough
PS109_125-3	TV-MUC	2017-10-03 02:09	77° 47,747‘	013° 37,530‘	392	Norske Trough
PS109_129-1	TV-MUC	2017-10-03 09:01	77° 54,753‘	013° 10,630‘	139	Norske Trough
PS109_139-2	TV-MUC	2017-10-04 19:13	76° 47,945‘	008° 39,624‘	354	Norske Trough
PS109_139-3	Lander	2017-10-04 21:35	76° 48,046‘	008° 38,232‘	357	Norske Trough
PS109_139-4	TV-MUC	2017-10-04 22:10	76° 48,107‘	008° 37,512‘	357	Norske Trough
PS109_154-1	TV-MUC	2017-10-07 02:06	76° 29,214‘	007° 07,921‘	1175.6	Greenland Shelf slope
PS109_154-2	TV-MUC	2017-10-07 03:28	76° 29,182‘	007° 06,561‘	1200.2	Greenland Shelf slope

Preliminary (expected) results

During the TV-MUC surveys, feather stars Comatulida (Crinoidea, Echinodermata) were observed at PS109_19-2 (outer Westwind Trough), and sea pens (Pennatulacea, Anthozoa, Cnidaria) at PS109_61-1 and PS109_62-1 (in front of the 79N Glacier) (Fig. 10.2). At the other locations, there were sporadic observations of tube worms, burrows and pits (not shown here).

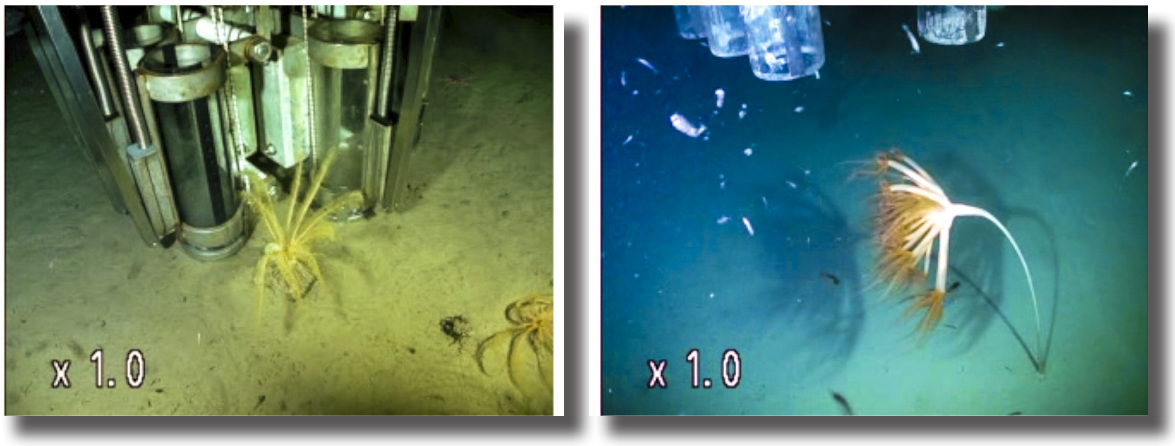

Fig. 10.2: Comatulida observed at Station PS109_19-2 (left) and Pennatulacea (right) observed at PS109_61-1, respectively in Westwind Trough and in front of the 79N Glacier.

The Total Oxygen Uptake (TOU) rates measured on the NE Greenland shelf ranged between 1.18 ± 0.20 mmol O_2 m^{-2} d^{-1} in mid Norske Trough and 2.4 ± 0.35 mmol O_2 m^{-2} d^{-1} on the outer Norske Trough (Fig. 10.3). The lowest TOU was recorded at the 1,200 m deep station on the Greenland slope (0.58 ± 0.06 mmol O_2 m^{-2} d^{-1}). The TOU rates in Westwind Trough and in

front of the 79N Glacier range between the above mentioned values. Generally, the measured TOU rates on the NE Greenland shelf are similar to or slightly higher than the TOU rates in the deep Arctic Fram Strait (Cathalot et al., 2015, Hoffmann et al., in prep.). This suggests that the benthic system of the NE Greenland shelf is oligotrophic. Similarly low TOU rates were observed by Rowe et al. (1997) during a first survey of the NE Greenland shelf in the 1990s. Further habitat characterization and description of benthic communities will be done after sample analysis in the home laboratory.

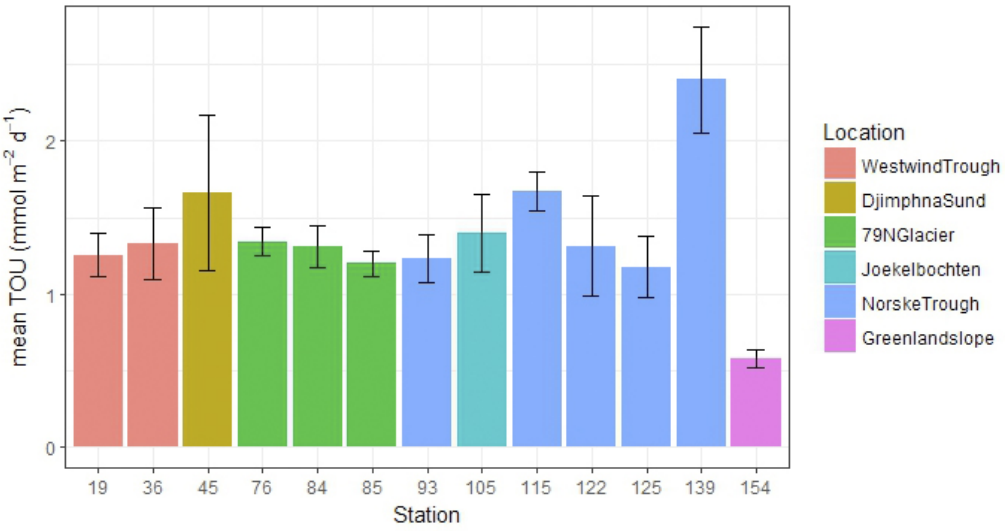

Fig. 10.3: Average Total Oxygen Uptake ± se measured during ex situ incubations. Station metadata can be found in the Station List.

Data management

The station list and all metadata from sampling and observations will be stored in the data base of the Data Publisher for Earth & Environmental Science PANGAEA (http://www.pangaea.de). Further scientific data retrieved from observations, measurements and home-based data analyses will also be submitted to PANGAEA either upon publication, or with password protection by the individual P.I.s as soon as the data are available and quality-assessed. This includes also biological data, for most of which parameters are already defined in PANGAEA. Molecular data will be deposited in globally accessible databases such as the European Nucleotide Archive (ENA). All zoological samples will be stored at Ghent University (Macro- and Meiofauna), and all microbiological samples are stored deep frozen or fixed at the Max Planck Institute for Marine Microbiology in Bremen.

References

Cathalot C, Rabouille C, Sauter E, Schewe I, Soltwedel T, Vopel KC (2015) Benthic Oxygen Uptake in the Arctic Ocean Margins - A Case Study at the Deep-Sea Observatory HAUSGARTEN (Fram Strait), PLoS ONE, 10, e0138339, doi:10.1371/journal.pone.0138339.

Hoffmann R, Braeckman U, Krumpen T, Schewe I, Hasemann C, Wenzhöfer F (in prep.) Benthic oxygen fluxes and benthic communities under contrasting sea-ice conditions in the deep Arctic Ocean.

Rowe GT, Boland GS, Escobar Briones EG, Cruz-Kaegi ME, Newton A, Piepenburg D, Walsh I, Deming J (1997) Sediment community biomass and respiration in the Northeast Water Polynya, Greenland: a numerical simulation of benthic lander and spade core data. Journal of Marine Systems, 10, 497-515.

11. SEA ICE BIOLOGY AND BIOGEOCHEMISTRY IN RELATION TO ATMOSPHERIC EMISSIONS

Ilka Peeken[1] (not on board), Falk Pätzold[2], Ulrike Dietrich[3], Thomas Krüger[2], Josefa Verdugo[1], Julia Ehrlich[1], Sarah Maes[1],
not board: Hauke Flores[1], Astrid Lampert[2], Ellen Damm[1]

[1]AWI
[2]TUB
[3]UIT

Grant No. AWI_PS109_11

Objectives

Sea ice is of major importance in the polar oceans since it affects the solar radiation fluxes due to its reflective properties and it is a habitat and feeding ground for various organisms of the polar ecosystem. The Arctic Ocean is in a state of rapid transition that is best exemplified by the marked reduction in age, thickness and extent of the sea ice cover, at least in summer. The European Arctic margin is largely influenced by drift ice formed on the Siberian shelves and carried to the Fram Strait via the Transpolar Drift. Sea ice thickness for the various regions of the Transpolar Drift between 1991 and 2007 showed a reduction in modal ice thickness from 2.5 m towards 0.9 m.

General Sea Ice Work

A long-term trend towards thinner sea ice has profound implications for the timing and position of the Seasonal Ice Zone. Future ice free summers will have major implication for the entire ecosystem and thus alter current biogeochemical cycles in the Arctic. Due to the decrease in ice thickness, new evolving habitats for sea ice algae have been observed in surface melt ponds (Fernández-Méndez et al., 2014) and under the ice (Assmy et al., 2013). Observed algal aggregates in melt ponds and under the ice might have consequences for the carbon budget, leading to major implications for the sympagic-benthic and sympagic-pelagic coupling of the Arctic Ocean.

Furthermore, sea ice offers an attractive substrate for sea ice associated species known as sea ice fauna. Sea ice fauna refers predominantly to heterotrophic protists and ectotherm metazoans living either inside channels or cavities of sea ice or using the ice-water interface temporarily as habitat. It is anticipated that the decline of the sea ice will alter the composition and biodiversity of the sea ice fauna and flora. Recent studies show a reduction of biodiversity from multi to first year ice (Hardge et al., 2017). Biodiversity in turn plays a vital role for the stability of ecosystem processes, and is positively coupled with the efficiency of ecosystem functions such as fluxes of energy, nutrients and organic matter through an environment. Thus, understanding the relationship between biodiversity and ecosystem functions is important for predicting consequences of climate change in the Arctic ecosystem.

Within the ice, exopolymeric substances (EPS) are an important component of the carbon pool. They are excreted by bacteria and algae and protect those same organisms from high salinity and low temperature stress. Two classes of EPS, transparent exopolymeric particles (TEP; acidic sugars) and Coomassie stainable particles (CSP; proteins), will be studied quantitatively and qualitatively,

Off the coast of East Greenland, detailed studies on the sea ice and adjacent ecosystems are restricted to the subarctic region in Young Sound at 74° N. Little is known about land fast sea ice biology north of 74°N and preliminary results from the recent *Polarstern* PS 85 (ARK-XXVIII/2) cruise indicated very low standing stocks of sea ice algae in spring. Therefore, the anticipated cruise will allow for first sea ice related biological studies in an under-sampled area.

During PS109 (ARK-XXXI/4) we aim to achieve the following objectives:

- Investigate sea ice biota at the end of the Transpolar drift and compare with historic data
- Reveal the role of melt pond associated communities for the ecosystem
- Using molecular and isotopic biomarkers to trace sea ice-derived carbon
- in pelagic food webs
- Understand the variability and biodiversity of the sea ice-associated biomass with respect to the sea ice conditions and nutrient availability, to quantify their ecosystem functions
- Identify drivers of EPS excretion, EPS concentration and chemical composition

Polar cod

Polar cod (*Boreogadus saida*) is the most abundant fish species in the high Arctic and the staple food of numerous Arctic seabirds and seals and also strongly depends on the sea ice algae derived carbon (Kohlbach et al., 2016). On the broad shelves inhabited by the spawning populations, a part of the first-year population associates with the under-ice habitat at the end of summer. Recent studies showed that juvenile polar cod residing in the ice-water interface layer are practically ubiquitous in the Eurasian Basin, and probably throughout the Arctic Ocean. Satellite-based sea ice back-tracking enabled to identify the potential areas on the Siberian shelf from where juvenile polar cod associated with sea ice possibly followed the Transpolar Drift across the central Arctic Ocean, potentially reaching spawning populations in northern Greenland (David et al., 2016). Hence, the Transpolar Drift may act as a vector enabling genetic exchange between coastal populations, and contributing to their recruitment. Further decline in extent and duration of sea ice may thus compromise genetic exchange, juvenile survival and recruitment of shelf populations. To assess the importance of the connectivity of Siberian and Greenland populations, the genetic relationship between potential Siberian spawning populations and stocks on the Greenland shelf must be elucidated.

During PS109 we aimed to achieve the objective to sample larval polar cod on the shelf to investigate the genetic connectivity of the Greenland populations with other Arctic populations.

Our work on polar cod will help to assess whether the Transpolar Drift is important for the genetic exchange and the recruitment of populations around the Arctic Ocean, and study the implications of sea ice decline for the resilience of an Arctic ecological key species to climate change.

Trace gases

Summer sea ice retreat alters water mass formation and convection, which may have profound effects on natural biogeochemical cycles between sea ice and seawater. Especially feedback effects to pathways of climatically relevant trace gases will loom large in the equation of change. Increasing water stratification during sea ice melting is likely to limit nutrient availability in near-surface water, which in turn hampers the enhancement of primary production. A characteristic feature of the Arctic Ocean is distinct post-bloom nutrient limitation. Nutrient limitation may be

also a possible regulator of methane (CH_4) production in surface water. Methanogens form CH_4 via various pathways commonly classified with respect to the type of carbon precursor utilized, e.g. the methylothrophic pathway indicates the intact conversion of a methyl group to CH4. The contribution of methylated substrates is potentially large in sea ice, and methylothrophic methanogenis may be a principal pathway from which CH4 is readily formed by microbial activity. However, the direct evidence of this role of methylated substrates in sea ice is still lacking.

Therefore, the main objective of this cruise is to identify the main triggering processes for climate-relevant compounds (CH_4) in sea ice and in the underlying water column following the melting cycles in the Arctic Ocean.

Atmospheric measurements

Methane's (CH_4) global warming potential is large (e.g. Shindell et al., 2005; 2009). Although less than carbon dioxide (CO_2) on a century timescale, CH_4 is 100 times more potent than CO_2 on a decadal time scale (Solomon et al 2007) producing a near-future, greater overall impact on the atmospheric radiative balance (IPCC 2007; Fig. 2.21). Moreover, global warming feedbacks and rising anthropogenic emissions likely will increase CH_4 emissions (Wunch et al 2009). Yet, current knowledge of CH_4 sources remains inadequate, in part due to the lack of sufficiently accurate assessments of the temporal and spatial behaviour of highly variable anthropogenic and natural CH_4 surface fluxes (IPCC 2007).

The role of the polar regions in the CH_4 budget is subject to discussion, facing inconsistencies of the very few surface network data and satellite data indicate significant source regions above the polar oceans (Yurganov et al., 2014), which remain poorly quantified. There is a critical need for field data to validate satellite measurements. Various parameters influencing on the emission of polar CH_4 into the atmosphere include the atmospheric stability, sea ice fraction, and air - sea temperature difference, but the mechanisms remain unclear. Generally speaking, the origin of atmospheric methane in Antarctica is uncertain.

The main objectives of the project ALICE (Airborne tool for methane isotopic composition and polar meteorological experiments) are to measure the vertical structure of the atmosphere up to an altitude of 1000 m and to take air samples for methane isotopic analyses using a remotely piloted aerial system (RPAS, or unmanned aerial vehicle – UAV). The stability of the atmosphere strongly influences vertical mixing processes and the exchange of heat, moisture and trace gases between the surface and the atmosphere. Based on these measurements the methane sources and the distribution of the released methane in the lower atmosphere shall be investigated.

While PS109 (ARK-XXXI/4) the initially tested system prototypes shall be investigated regarding safe and efficient operations in arctic weather and vessel caused constrains. After successful system approval as many as possible vertical air sample and air data profiles shall be obtained.

Work at sea

General Sea Ice Work

The sea ice work during this expedition was hampered by unfavorable weather and ice conditions, not allowing us to reach the goal of carrying out the anticipated ice station work. The far distances to the ice edge away from the coast of Greenland and massive new ice formation close to the coast, did not allow using the zodiac for general transportation to the ice stations. The use of the helicopter was further limited by unstable weather conditions, low cloud ceiling, and short day time in autumn combined with a high helicopter request by other

groups. Several attempts to make a full ice station in drifting ice fields, Diphnasound and in the passage to Jøkelbugten were not successful due to unexpected strong new ice formation, or the opposite, extreme thick sea ice, making it impossible to drill enough cores for the sampling of the anticipated variables.

Alternatively, newly formed sea ice of different thickness was sampled at one station towards the end of the cruise. Samples were taken with the mummy chair. By submerging the mummy chair, new ice could safely be sampled and transported on board of the ship. Samples will be used for the analysis of the microbial community composition associated with new ice and its biological and chemical properties. New ice was melted in closed plastic barrels at 4°C. Melted samples were subsequently split into aliquots for chlorophyll a, pigment, POC, EPS, DNA, fluorescent *in-situ* hybridization (FISH), flow cytometry, nutrient, and biogenic silica analysis. Salinity was determined with a WTW 315i conductivity probe.

Despite the occurrence of open and refrozen melt ponds in the ice fields on the way to Greenland, sampling of the ponds was not possible due to the general small floe size and uneven surface of the ice floes, which did not allow for safe working conditions on the ice.

Fig. 11.1: Mummy chair based new ice sampling (Foto: A. Preusser)

In addition to the sea ice work, six CTDs were randomly sampled on the shelf. DNA and FISH samples from the surface, chlorophyll a maximum, and bottom will be studied by Brandon Hassett (UiT) for the presence of chytrids, a class of fungi.

Tab. 11.1: List of CTD casts and ice sampling during PS109 (ARK-XXXI/4)

Date	Time [UTC]	Station #	Action	Lat	Lon
09/28/2017	05:14	100_1	CTD	78°26,763`N	18°33,467`W
09/29/2017	22:31	115_1	CTD	78° 01.868' N	16° 34.447' W
09/30/2017	14:10	118_1	Mummy chair	87°34,531`N	17°51,617`W
10/03/2017	03:20	125_4	CTD	77°47,812`N	13°38,504`W
10/04/2017	01:36	134_1	CTD	77°54,501`N	7°59,201`W
10/06/2017	20:50	151_1	CTD	76°36,313`N	7°38,514`W
10/07/2017	00:31	153_1	CTD	76°34,453`N	7°29,779`W

Polar cod

To sample larval and post-larval polar cod we conducted 14 oblique hauls with a bongo net (mesh size 1,000 µm) in the upper water column (80-0 m). Twelve of those hauls were located at the Greenland shelf region and two at the 0-meridian of Fram Strait. An overview of the sampling locations is given in Fig. 11.1 and Table 11.2.

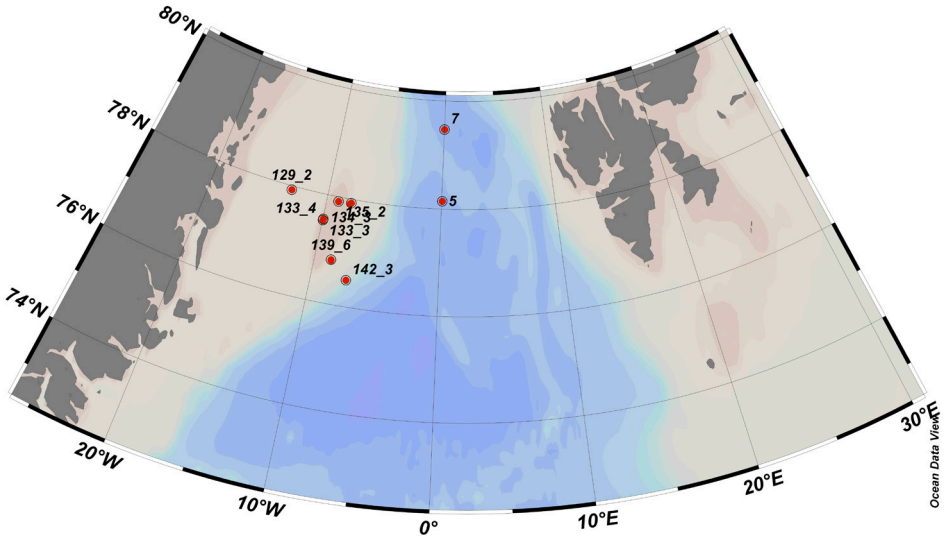

Fig. 11.2: Conducted bongo net stations during PS109 (ARK-XXXI/4).

CTD stations were conducted close to the bongo net stations to maintain information about physical properties of the sampled water column (Table 11.2).

Fish larvae were extracted from the zooplankton catch and frozen individually at -80°C for subsequent analyses of trophic biomarkers, genetics and otolith chemistry (Fig. 11.3). The rest of the catch was immediately preserved in formalin (4%) buffered with hexamethylentetramin.

Tab. 11.2: List of bongo net stations, hauls, and positions during PS109 (ARK-XXXI/4)

Date	Station	Haul	Lat (Start-End)	Long (Start-End)
09/15/2017	5_2	1	78°09,023'N-78°08,247'N	0°02,081'E-0°05,555'E
09/15/2017	7_1	2	79°28,786'N- 79°27,861'N	0°00,489'E-0°01,951'E
09/18/2017	30_02	3	80°21,529'N-80°22,318'N	7°46,798'W-7°44,589'W
10/03/2017	129_2	4	77°54,763'N-77°56,281'N	13°10,715'W-13°9,571'W
10/03/2017	133_3	5	77°30,269'N-77°31,383'N	9°57,898'W-9°57,693'W
10/03/2017	133_4	6	77°31,678'N-77°32,784'N	9°57,608'W-9°57,005'W
10/04/2017	134_2	7	77°54,579'N-77°55,217'N	7°58,645'W-7°54,015'W
10/04/2017	134_3	8	77°55,336'N-77°55,970'N	7°53,138'W-7°48,811'W
10/04/2017	135_2	9	77°54,500'N-77°55,105'N	9°00,051'W-8°57,122'W
10/04/2017	139_5	10	76°48,140'N-76°48,958'N	8°37,907'W-8°39,158'W
10/04/2017	139_6	11	76°49,070'N-76°49,952'N	8°39,192'W-8°39,341'W
10/05/2017	142_3	12	76°29,404'N-76°29,997'N	7°11,412'W-7°14,857'W
10/06/2017	152_2	13	76°36,672'N-76°37,670'N	7°38,815'W-7°39,130'W
10/07/2017	155_2	14	76°21,476'N-76°21,529'N	6°30,922'W-6°26,207'W

Tab. 11.3: List of CTD stations, positions and related bongo net hauls during PS109 (ARK-XXXI/4)

Date	Station	Bongo haul	Lat (Start-End)	Long (Start-End)
09/15/2017	5_1	1	78°09,137'N-78'09,220'N	0°00,258'E-0°00,650'E
09/15/2017	7_1	2	79°28,846'N-79°28,816'N	0°01,460'E-0°00,820'E
09/18/2017	30_1	3	80°22,969'N-80°22,690'N	7°56,668'W-7°55,683'W
10/03/2017	128_1	4	77°54,445'N-77°54,498'N	13°16,132'W-13°16,817'W
10/03/2017	133_2	5,6	77°29,699N-77°29,650'N	9°57,556'W-9°57,761'W
10/04/2017	134_1	7,8	77°54,382'N-77°54,501'N	7°59,766'W-7°59,201'W
10/04/2017	135_1	9	77°54,363'N-77°54,422'N	9°00,325'W-9°00,296'W
10/04/2017	138_1	10,11	77°03,976'N-77°04,076'N	9°59,486'W-9°59,829'W
10/05/2017	142_2	12	76°29,204'N-76°29,186'N	7°08,010'W-7°08,858'W
10/06/2017	152_1	13	76°36,231'N-76°36,310'N	7°37,943'W-7°38,490'W
10/07/2017	156_1	14	75°49,327'N-75°49,116'N	4°51,103'W-4°51,586'W

Trace gases

Water samples for all gas analysis and nutrient measurements have been collected at 54 stations. Samples were taken from Niskin bottles mounted on a rosette sampler at discrete depths throughout the water column down to 600 m or on the shelf depending on the water depth close to the bottom. The number of sampling depths varied as a function of the fluorescence and the O_2- sensor signal.

Methane was immediately measured on board, using a gas chromatograph equipped with a flame ionization detector (FID). Methane gas samples are stored at +4°C for analyses of the $d^{13}C_{CH4}$ values in the home laboratory. Nutrient samples were taken at almost all sampling stations in falcon tubes (15 ml) and stored at -20°C for further analysis at the home laboratory.

Tab. 11.4: List of CTD stations taken during PS109 (ARK-XXXI/4) for trace gases and nutrients

Date	Station	Cast	CH4 conc.	$d^{13}C_{CH4}$	Nutrients	Deployment
09/15/2017	5	1	x	x		CTD
09/15/2017	6	1	x	x		CTD
09/15/2017	7	1	x	x		CTD
09/16/2017	11	1	x	x	x	CTD
09/16/2017	15	1	x	x		CTD
09/17/2017	19	1	x	x		CTD
09/18/2017	26	1	x	x		CTD
09/18/2017	29	1	x	x	x	CTD
09/18/2017	31	1	x	x		CTD
09/19/2017	36	1	x	x	x	CTD
09/20/2017	41	1	x	x		CTD
09/20/2017	42	1	x	x	x	CTD
09/20/2017	43	1	x	x	x	CTD
09/20/2017	44	1	x	x	x	CTD
09/20/2017	45	1	x	x	x	CTD

Date	Station	Cast	CH4 conc.	$d^{13}C_{CH4}$	Nutrients	Deployment
09/20/2017	46	2	x	x	x	CTD
09/21/2017	48	1	x	x	x	CTD
09/21/2017	52	2	x	x	x	CTD
09/22/2017	54	1	x	x	x	CTD
09/22/2017	55	1	x	x		CTD
09/22/2017	57	1	x	x	x	CTD
09/23/2017	63	1	x	x	x	CTD
09/23/2017	65	1	x	x	x	CTD
09/23/2017	67	1	x	x	x	CTD
09/24/2017	77	1	x	x		CTD
09/24/2017	78	1	x	x		CTD
09/24/2017	79	1	x	x	x	CTD
09/24/2017	80	1	x	x		CTD
09/24/2017	82	1	x	x	x	CTD
09/25/2017	87	1	x	x	x	CTD
09/25/2017	89	1	x	x	x	CTD
09/26/2017	90	1	x	x	x	CTD
09/26/2017	91	1	x	x	x	CTD
09/26/2017	92	1	x	x	x	CTD
09/26/2017	93	1	x	x	x	CTD
09/26/2017	94	1	x	x	x	CTD
09/28/2017	100	1	x	x	x	CTD
09/28/2017	103	1	x	x	x	CTD
09/28/2017	104	1	x	x		CTD
09/28/2017	101	1	x	x	x	CTD
09/28/2017	102	1	x	x		CTD
09/29/2017	114	1	x	x	x	CTD
09/29/2017	115	1	x	x	x	CTD
09/30/2017	116	1	x	x	x	CTD
10/01/2017	119	1	x	x	x	CTD
10/02/2017	124	1	x	x	x	CTD
10/03/2017	125	4	x	x	x	CTD
10/03/2017	126	1	x	x	x	CTD
10/03/2017	128	1	x	x	x	CTD
10/03/2017	130	1	x	x	x	CTD
10/03/2017	132	1	x	x	x	CTD
10/04/2017	134	1	x	x	x	CTD
10/04/2017	135	1	x	x	x	CTD

Atmospheric measurements

The complete system consists of the carrying system (RPAS) and the scientific payload which combines the air sampling and the meteorological measurement subsystem:
As carrying system a quadrocopter configuration was chosen. For the weight of the scientific payload of 6 to 7 kg and its corresponding size no of the shelf solutions are available so the

RPAS was designed complete new at the Institute of Flight Guidance at TU Braunschweig, based on the experience of other special application RPAS designs. While the maximum design take-off weight for the designed system is 25 kg, the current mission take-off weight is 19 kg. The thrust to weight ratio is high compared to other RPAS systems to operate the RPAS in wind speeds up to 70 km h^{-1}.
The air sampling subsystem consists of twelve 100 ml glass flask each equipped with a magnet valve and a pressure sensor. At the desired altitudes the evacuated flasks are filled pairwise by an operator triggered 2 sec opening of the magnet valves. The meteorological measurement subsystem includes four different temperature sensors, two different capacitive humidity sensors, an upward and a downward looking pyranometer, an infrared surface temperature sensor, pressure sensors and a position and attitude determination system.

The designed standard mission starts with a fast climb to the maximum set altitude. During climb the distribution of humidity and temperature is transmitted to the operator to set – combined with available a priori information from radio sondes and/or LIDAR systems – the air sampling altitudes with respect to the vertical stratification (expectable vertical mixture). Air samples shall be taken while descend. The air samples shall be partly analysed at *Polarstern* right after the sampling flights, partly after the expedition with the mass spectrometer at the AWI laboratory.

The current expedition was the first field campaign with the initially tested system prototypes. At the beginning the focus was on operational safety and system integrity. After demonstrating a safe system operation and appropriate data quality the targeted air sampling mission shall be flown as often as possible. The following work was done in the listed order:

1. System handling non-flying on board of *Polarstern*.
2. Stability of telemetry between RPAS and ground station in the presence of the vessel.
3. Stability and repeatability of alignment of RPAS attitude system at the helicopter deck of *Polarstern*.
4. Integration of safe RPAS flight operation on board as part of *Polarsterns* scientific programme.
5. Integration of safe RPAS flight operation to the *Polarstern* based helicopter operations.
6. Practical handling of airspace allocation procedures.
7. Deploying test of parachute rescue system, on the ground (non-flying).
8. Flight mechanical stability in the turbulent wind field behind the vessel.
9. Testing of the autopilot system for horizontal and vertical mission profiles.
10. Testing of flight mode transitions (manual take-off and landing, automated vertical profiling).
11. Testing of handling procedure of gas sampling flasks (preparation, in-flight filling, post flight handling).
12. Testing of usability of meteorological measurements.
13. Methane concentration analyses of taken air samples using a gas chromatograph.
14. Executing regular vertical profiling as intended and assessing the prototype system in a “proof of concept” sense.

During the PS109 (ARK-XXXI/4) cruise, 8 flights were conducted safely using one of the two system prototypes (table 11.5). For the duration of flight system initialization and the flight itself the vessel had to be stationary. Additionally the wind and the subjectively assessed turbulence had to be at a moderate level. Flights into clouds and at relative humidity above 95% were excluded to keep visual contact to the RPAS and to avoid propeller icing.

Fig.11.3: Air sampling RPAS in flight

All items described above were handles successfully, except items 11 and 14. Flights to investigate and carry out items 11 and 14 were cancelled due to improper weather conditions during the second part of the expedition.

Tab. 11.5: RPAS flight during PS109 (ARK-XXXI/4)

Flight No.	Date	Location Lat	Location Lon	Take off UTC	Landing UTC	Duration [min]	Description
1	09/23/17	N79°33,756'	W19°26,400	18:29:00	18:42:00	0:13	Hover test above Helicopter deck
-	09/24/17	N79°33,331'	W19°12,955	18:30:00	-	-	Flight aborted while take off due to abnormal behavior, later identified as technical issue
2	09/25/17	N79°22,284'	W17°11,040	20:51:00	20:54:00	0:03	Manual flight at approx. 50 m to a position 100 m behind the vessel and back
3	09/25/17	N79°22,284'	W17°11,040	20:17:00	20:26:00	0:09	Manual takeoff and landing, horizontal mission at 70 m to three different waypoints behind the vessel

Flight No.	Date	Location Lat	Lon	Take off UTC	Landing UTC	Duration [min]	Description
4	09/26/17	N79°03,234'	W16°44,220	20:59:00	21:06:00	0:07	Manual takeoff and landing, automated flight up to 300 m
5	09/30/17	N78°27,390'	W17°54,180	13:28:00	13:37:00	0:09	Manual takeoff and landing, automated flight up to 600 m
6	10/01/17	N78°52,710'	W17°10,740	18:59:00	19:06:00	0:07	Manual takeoff and landing, automated flight up to 250 m (aborted due to cloud layer), gas sampling flasks filled inflight
7	10/01/17	N78°52,710'	W17°10,740	19:14:00	19:19:00	0:05	Manual takeoff and landing, automated flight up to 200 m (limited by low cloud layer)
8	10/01/17	N78°52,710'	W17°10,740	19:46:00	20:00:00	0:14	Manual takeoff and landing, automated flight up to 1000 m

Preliminary (expected) results

General Sea Ice Work

Ice observation from helicopter and the vessel

Ice fields on the way to Greenland were characterized by small and thick floes (larger ones of about 20 m in diameter, thickness >2m) with a high coverage of open and refrozen meltponds and ridges. Many of the unfrozen meltponds showed a green-brownish color indicating algal presence.

The samples will be used for the biological and chemical characterization of newly formed sea ice. This will give insights into the seeding community composition of new sea ice and the microbial community succession of ice of different thickness and structure. The current data set will be implemented in the long term biological observatory for sea ice in the Central Arctic.

Polar cod

Fish larvae were caught during five bongo net hauls at station *30, 133, 134, 135*, and *139*.

The catch of the bongo net generally included copepods such as *Calanus spp.*, amphipods such as *Themisto libellula* and *T. abyssorum*, the gastropod *Clione limacina*, chaetognaths, gelatinous species such as *Merstensia spp* and *Beroe cucumis*, and euphausiids such as *Thysanoessa longicaudata* and *T. inermis*. Amphipods such as *Apherusa glacialis*, *Gammarus wilkitzkii*, *Onisimus glacialis* and *Onisimus nanseni* were rare species and only present in single hauls.

Post-expedition analysis of biological samples will comprise otolith studies, and genomics of the fish larvae as shown in Fig. 11.2. Information from otoliths (trace elements) and DNA (obtained from fin clips) will primarily be used to infer genetic population structure and connectivity patterns. Together with specimen metadata and environmental parameters these insights are used for predictive modelling. The resulting datasets will enable us to

1. identify habitats favourable for species in terms of physical properties, prey availability and biodiversity
2. identify critical habitats for the viability of polar cod stocks and assess their vulnerability to climate change.

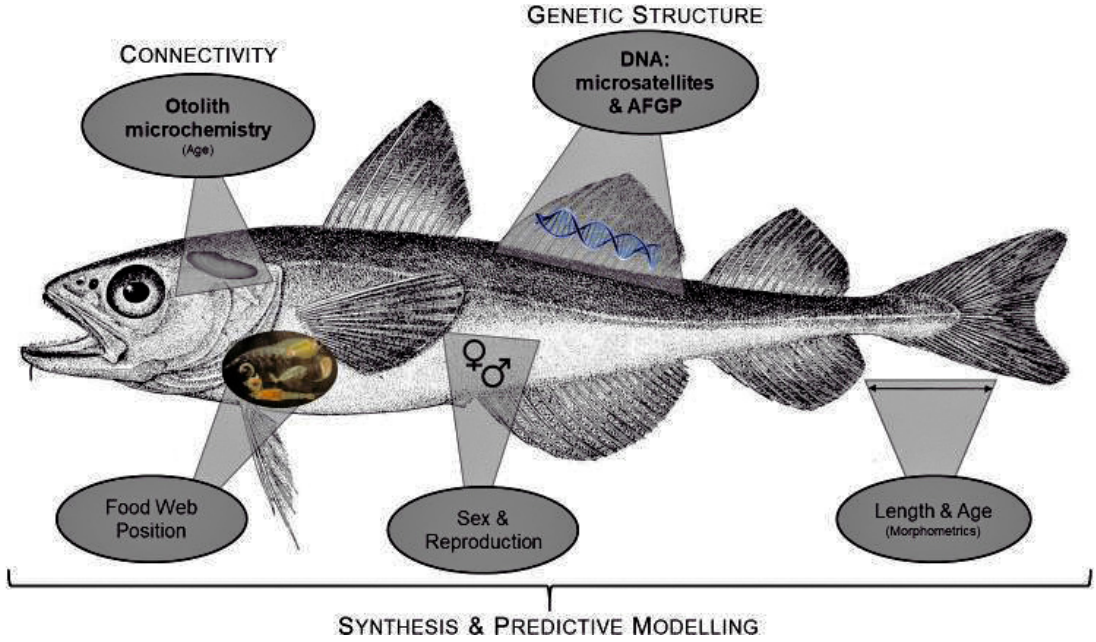

Fig. 11.4: Post expedition processing of polar cod samples

Trace gases

In the study area, methane concentrations are heterogeneous and correspond to both, a clear under-saturation and a clear super-saturation with respect to the atmospheric equilibrium concentration. The equilibrium concentration is calculated as a function of the gas solubility on the basis of the measured temperature and salinity properties and varies between 3.2 to 3.9 nM. Methane super-saturation was detected in the winter mixed layer and surface waters. Methane under-saturation was revealed in inflowing Atlantic water.

Atmospheric measurements

Although fewer flights than planned were possible, comprehensive conclusions can be drawn from the 8 conducted flights. After the experience with the on-board possibilities and weather conditions, several improvements for handling the system are recommended and will be implemented for future applications. The results are outlined in detail to support other RPAS applicants in the near future with these basic findings.

1. System handling non-flying on board of *Polarstern*

One unique design feature of the RPAS is the quick assembly of the rotor arms and a compact main frame carrying the scientific payload. This feature was realized in view of the limited space and door width at polar research stations and as well at *Polarstern*. For the experimental flight trials carried out while PS109 (ARK-XXXI/4) it was acceptable to transport the equipment

from a dry lab at E-deck to the helicopter hanger through doors with high doorsteps and using an elevator. The final preparation of the system for each flight inside the helicopter hanger was very helpful including easy access to the helicopter deck.

Recommendation: For regular operation of such an air sampling system a permanent placing near the take-off and landing site at the vessel is strongly recommended.

2. Stability of telemetry between RPAS and ground station in the presence of the vessel. At least five different radio links have to be considered:

- 2.4 GHz primary control link, bidirectional: This link was stable without indications of data losses.
- 868 MHz autopilot data link, bidirectional: While flight 4 this link became unstable at altitudes between 150 and 250 m. The antenna position at the RPAS was changed after tis flight and the problem disappeared.
- 433 MHz meteorological data downlink: After nonstable behavior observed while flight 5 the antenna position was improved. While flight 8 the instability was mostly at altitudes between 600 and 1,000 m. The telemetry module was changed after flight 8 using an 868 MHz module, but this improvement could not be tested because of unfavourable weather conditions.
- 5 GHz video downlink: This downward looking video is intended as backup system allowing the pilot to stabilize the yaw movement of the RPAS in case of a loss of heading information in the autopilot system. The link was stable only up to 400 m. Since this system is supposed to work until ranges up to 1 km, this could be due to antenna positioning or due to an interaction of radio signals with the ship. Unfortunately, this could not be further investigated because of unfavourable weather conditions.
- 868 MHz parachute rescue system activation link: This secured link was only tested on helicopter deck. Restrictions of functionality could not be detected or analysed.

Conclusion: The stability of the telemetry links between the RPAS and vessel based ground station must be improved. Appropriate tools and methods to observe and analyse instable phases must be established.

3. Stability and repeatability of alignment of RPAS attitude system at the helicopter deck of *Polarstern*

As the autopilot uses earth's magnetic field information, its disturbance by the vessel is essential for the heading alignment. Based on the autopilot data it was observed that *Polarst*ern increases the vertical magnetic intensity of earth's magnetic field by about 20% but does effect the horizontal components only in a minor manner, so a sufficient alignment heading can be derived.

It depends on the used autopilot system and the used flight mode whether the change in the total magnetic intensity while leaving the vessels radius of influence is critical for the flight. The manual take-off and manual flight to a position at minimum horizontal 100 m away from *Polarstern* does avoid problems as the navigation filter in the used autopilot did correct the magnetic field changes while the manual flight in form of an inflight-calibration after detecting a ground-anomaly.

Recommendation:

- Beside the magnetic heading determination the use of GNSS heading systems is discussed. Both options have relevant disadvantages so a systematic infield investigation of heading alignment and determination methods appropriate for RPASs below 25 kg maximum take-off weight is proposed.
- If the magnetic heading measurement is essential for future operations the vessels magnetic vectorial interfering field shall be determined.

4. Integration of safe of RPAS flight operation on-board as part of *Polarstern's* scientific programme

   and

5. Integration of safe of RPAS flight operation into the *Polarstern* based helicopter operations

The RPAS was operated from the helicopter deck while *Polarstern* was stationary, the helicopters were inside the hangar and ceiling, humidity, wind speed and turbulence were within acceptable limits. The number of factors that must be fulfilled resulted in a small number of usable time slots while PS109 (ARK-XXXI/4). As this is acceptable for a “proof of concept” expedition it is marginal for regular scientific investigations.

(The option to fly the copter when the helicopter was on ground while out on a mission was not used.)

Conclusions/Recommendations: To expand the usable operation time the following aspects shall be investigated regarding their feasibility and the gain-cost-ratio:

- Vessel following mode: The RPAS follows the track of the vessel within a preset distance. This feature is in principle implemented in the autopilot, but must be investigated regarding integrity and additional propulsion power consumption. Additionally the determination of the vessels accurate position and the data uplink must be very reliable.
- Flights outside the operators view: This option allows flying in clouds. This implies to change the roll of the safety pilot; in general this changes the whole safety concept.
- Flights in icing conditions: In sea ice conditions the temperature and humidity in the lower atmosphere is prone for propeller icing. Propeller de-icing solutions for the small scales of the used RPAS can be derived from well-known solutions for manned aircraft. The scientific payload must be upgraded for icing/condensing conditions as well.
- Take-off and landing site at the vessel apart from the helicopter deck. This would allow using time slots when the helicopter is on the helicopter deck for turnaround or is waiting for immediate take-off in marginal weather conditions.

6. Practical usability of airspace allocation procedure

Prior to the expedition a huge restricted area was arranged by the Danish aviation authority covering the whole planned cruise track in the Danish administrated area (Greenland AIP, Supplement 03/17). The restricted area was activated on daily basis by a phone call to Sondrestrom flight information centre (FIC). The activation was always possible because no other traffic was operating in this remote area. Nevertheless one single aircraft inside the designated restricted area would lead to a rejection of its activation. So this size of reserved airspace did only work in such a remote polar area but will be no option in other regions.

The helicopter operation on board *Polarstern* was not affected by this airspace allocation as the restricted area was considered in the helicopter operation permission.

Conclusion/Recommendation: For future operations of this specialized RPAS system all current and future options to for an economical and guaranteed airspace usage shall be used, e.g. an ADSB-transponder installed in the RPAS. Ideally the needed cylindrical airspace with a radius of about 2..5 NM and up to an altitude of 1,000 m is no longer allocated than 20 min for one flight.

7. Deploying test of parachute rescue system, on the ground (non-flying)

The commercial parachute rescue system was deployed while the system was non-flying at the helicopter deck. The system worked as expected.

8. Flight mechanical stability in the turbulent wind field behind the ship

The first flight at September 24th was used to test hovering above the helicopter deck up to 5 m altitude at a wind speed of about 7 m s-1. The RPAS was fully controllable.

9. Testing of autopilot system for horizontal and vertical mission profiles

For testing the functionality of the autopilot a horizontal and vertical missions with increasing maximum altitude were flown. No limitations or abnormal behaviour was found.

10. Testing of flight mode transitions (manual take-off and landing, automated vertical profiling)

The transition between the different modes of operation was possible without any findings or limitations.

11. Testing filling procedure of gas sampling flasks (preparation, in-flight filling, post flight handling)

The gas sampling flasks to be used in this project are equipped with two manually plastic valves. For the use at the RPAS one plastic valve is kept open and a magnet valve is installed. The nylon fitting between the valve and the glass flask contains a pressure sensor to observe the inside pressure. The designed procedure is to evacuate the flasks before assembling into the payload, open the magnet valves while descend manually via telemetry and close the second plastic valve after the flight. In practical operation while PS109 (ARK-XXXI/4) two problems occurred: 1. Telemetry instability and 2. Leak tightness.

The telemetry issue was discussed right before in detail. Due to the instabilities of the telemetry link the manual magnet valve triggering was disturbed. In the future the magnet valve trigger routine will be changed to a more a prior based approach with predefined altitudes that can be changed by the operator if needed while flying. Without any operators input the predefined altitudes will be used.

The leak tightness of the plastic valves was under investigation since the beginning of the project. To use the given sampling flasks follows the idea to stay compatible to the AWIs gas analysing infrastructure. Nevertheless the plastic valves seemed not to be designed to withstand vacuum in open state. Several attempts to improve the given valves were investigated in a temperature chamber at -30°C and simultaneously under vibrations as measured at the RPAS. These tests were done at a limited number of about 10 gas sampling flasks due to limited time. The solution worked out in the laboratory showed up to be improper under real conditions. Applying another prepared but untested valve augmentations option the leak tightness issue was fixed while the expedition, using the -20°C cold storage room and a very time consuming five stage selection

process with a positive selection rate of less than 50% of the given sampling flasks. Even two prototypes of gas sampling flasks with much more sophisticated designed valves did fail in real conditions.

Recommendation: Although the leak tightness issue itself can be declared as fixed it is strongly recommended to review the design of the gas sampling system and reengineer the manual valves. The magnet valve trigger routine shall be redesigned to a predefinition oriented mode.

12. Testing of integrity of meteorological measurements

The meteorological measurement system consist auf four different types of temperature sensors, where two types are realized twice. The very different spectral behaviour provides enough data to identify the different transfer functions and the best setting for calculation a most likely complementary temperature.

The fast and the slow humidity sensor are both of capacitive measuring type but show dynamic differences as expected. These differences are amplified at lower temperatures due to the sensor principle. As next step a chilled mirror e.g. Meteolabor SnowWhite is recommended to improve the post processing. Sensors based on a radiation absorbing measuring principle are usually not light enough for RPASs today.

An experimentally installed downward looking infrared surface temperature sensor shows good agreement with the measurements of air and water temperature at *Polarstern*. The air temperature is equivalent with the helicopter deck surface temperature and can be compared while take-off and landing. The water temperature measured at the RPAS is disturbed by the ice coverage ratio as the IR surface sensor has a field of view of 10°. A very rough ice coverage rate can be derived.

The measurements of the body fixed upward and downward looking pyranometer show consistent results with the measurement at *Polarstern* and the rough ice coverage estimation from the IR surface temperature sensor.

Conclusions: The measured meteorological data are of high quality with a recommended improvement of humidity measurement.

13. Methane concentration analyses of taken air samples using a gas chromatograph

The air samples taken during flight 6 were analysed for methane concentration using an Agilent 7890B gas chromatograph. The handling of the air samples is without any findings.

14. Executing regular vertical profiling as intended and assessing the prototype system in a “proof of concept” sense.

After finishing the first 1,000 m vertical climb flight – what is the aspired normal operation profile – on October 1st, the weather did not allow further flights within the scientific phase of the cruise due to low ceiling, high wind speed or both.

Other flight mechanical and operational findings

While flight 8 the wind speed above 750 m above sea level increase to 15-18 m s^{-1}, based on an earlier radio sonde probing and later LIDAR measurements. In the commanded 8 m s^{-1} climb the load distribution onto the four propulsions almost reached the limitations of the RPAS. An automated reduction of the climb speed with increasing wind speed will improve the safety margin. Although the limits were not reached this event indicates that the RPAS is

operable up to the designed maximum wind speed of 20 m s-1.

One major safety item is the temperature of the lithium batteries as their usable capacity degrades dramatically at low temperatures. For our flight operations the batteries were heated up to 40°C some hours before the flight. At the RPAS the batteries are carefully insulated but not actively heated. The measurement of the temperature at the batteries shows that this approach is well appropriate.

For estimating the needed battery capacity for RPASs covering a larger altitude range it must be kept in mind, that the decreasing air density requires a more propulsion power.

In summary the tested prototype system shows the feasibility of safe RPAS based air sampling. For an efficient scientific operation some improvements are recommended. This RPAS based air sampling is in principle comparable to the regular CTD probing in oceanography ("airborne CTD"). In case of a high need to obtain atmospheric data and air samples to link it to the CTD data it seems to be feasible to establish a regular RPAS based air sampling system.

Data management

General Sea Ice Work

No results were obtained at sea. Data from Ice work and the CTD will be analysed after the cruise in the home laboratory. The entire data set will be submitted to PANGAEA within 1-2 years. The unrestricted availability from PANGAEA will depend on the progress of a PhD thesis based on the data.

Polar cod

Almost all sample processing, such as chemical measurements and species identifications and quantifications, will be carried out in the home laboratories at AWI. As soon as the data are available they will be accessible to other cruise participants and research partners on request. Depending on the finalization of PhD theses and publications, data will be submitted to PANGAEA, and will be open for external use.

Trace gases

All data collected during the expedition will be stored in the PANGAEA data repository at the AWI within three years after the cruise.

Atmospheric measurements

The atmospheric data and air samples obtained while the RPAS flights are used to evaluate the total approach, using intrinsic data assessment and comparisons with the regular radio sondes (air data profiles) released from *Polarstern*, data from the *Polarstern* data system (water temperature, continuous air data) and Lidar-data, see chapter 12. All data collected during the expedition will be stored in the PANGAEA data repository at the AWI within three years after the cruise.

References

Assmy P, Ehn JK, Fernandez-Mendez M, Hop H, Katlein C, Sundfjord S, Bluhm K, Daase M, Engel A, Fransson A, Granskog MA, Hudson SR, Kristiansen S, Nicolaus M, Peeken I, Renner AHH, Spreen G, Tatarek A, and Wiktor J (2013) Floating ice-algal aggregates below melting Arctic sea ice. PLOS ONE 8(10), e76599.

David C, Lange BA, Krumpen T, Schaafsma F, van Franeker JA, Flores H (2016) Under-ice distribution of polar cod *Boreogadus saida* in the central Arctic Ocean and their association with sea-ice habitat properties. Polar Biology 39(6), 1-14.

Fernández-Méndez M, Wenzhöfer F, Peeken I, Sørensen H, Glud RN, and Boetius A (2014) Composition, buoyancy regulation and fate of ice algal aggregates in the Central Arctic Ocean. PLoS ONE 9.

Hardge K, Peeken I, Neuhaus S, Lange BA, Stock A, Stoeck T, Weinisch L, and Metfies K (2017) The importance of sea ice for exchange of habitat-specific protest communities in the Central Arctic Ocean. Journal of Marine Systems 165, 124-138.

IPCC, Solomon S, Qin D, Manning M, Chen Z, Marquis M, Averyt KB, Tignor M, Miller HL (2007) Contribution of Working Group I to the Fourth Assessment Report of the Intergovernmental Panel on Climate Change. Cambridge University Press, Cambridge, United Kingdom and New York, NY, USA.

Kohlbach D, Graeve M, Lange BA, David C, Peeken I, Flores H (2016) The importance of ice algae-produced carbon in the central Arctic Ocean ecosystem: food web relationships revealed by lipid and stable isotope biomarker analyses. Limnol Oceanogr. 61(6), 2027–2044.

Shindell DT, Faluvegi G, Bell N, Schmidt GA (2005) An emissions-based view of climate forcing by methane and tropospheric ozone. Geophysical Research Letters 32, L04803.

Shindell DT, Faluvegi G, Koch DM, Schmidt GA, Unger N, Bauer SE (2009) Improved attribution of climate forcing to emissions. Science 326, 716-718.

Wunch D, Wennberg PO, Toon GC, Keppel-Aleks G, Yavin YG (2009) Emissions of greenhouse gases from a North American megacity. Geophysical Research Letters 36(15) L039825.

Yurganov L, Leifer I, XiongX (2014) Atmospheric Methane over the Arctic Ocean: Thermal IR Satellite and Ship-Based Observations. Greenhouse Gas Measurement and Management. Seventh International Symposium on Non-CO_2 Greenhouse Gases (NCGG7), November 5-7, 2014.

12. MEASUREMENT OF THE ATMOSPHERIC BOUNDARY LAYER USING A WIND LIDAR

Andreas Preußer[1], Günther Heinemann[1] [1]Uni Trier
(not on board)

Grant-No. AWI_PS109_12

Objectives

The atmospheric boundary layer (ABL) in the polar regions is a major challenge for numerical weather forecast models, regional climate models as well as atmospheric reanalysis due to the high variance of small scale surface features (open-water, thin-ice in leads/polynyas, ridges and elevated floe-rims, etc.). In particular over ocean areas, useful reference data sets are sparse and hence mostly recorded at nearby land stations, thereby leaving extensive gaps in spatial coverage and hence confidence. The objectives of the group of the Dept. of Env. Meteorology, University of Trier, were to measure vertical and horizontal profiles of wind, turbulence and aerosols in the Fram Strait and Greenland Sea area in order to perform a bias-evaluation and verification of the regional climate model COSMO-CLM (e.g. Gutjahr et al., 2016), get reference data for process studies as well as potential model assimilation purposes in the context of the international Year of Polar Prediction (YOPP; WMO Initiative). The measurements are part of the BMBF-funded project CATS (“The Changing Arctic Transpolar System”; BMBF Grant-No. 03F0776D).

Work at sea

The main instrument that was used on board is a “Halo-Photonics Streamline“ wind LiDAR (“Light Detection And Ranging”), a ground-based scanning device that can operate at maximum ranges up to 10 km. However, on the cruise it was configured to measure up to a maximum range of approximately 2,700 m due to the low aerosol concentration in the Arctic. The operation principle of the LiDAR (Fig. 12.1b) is backscattering at aerosol particles and the use of the Doppler-effect. Values have been averaged for 1 to 15 seconds, depending on the signal strength. In addition to the number of pulse averages the beam focus was also adjusted in order to optimize the signal-to-noise ratio (SNR) (Hirsikko et al., 2014). The main characteristics of the LiDAR system are listed in Table 12.1.

In the 2017 expeditions with participation from our group (PS106.1/.2, PS109), the LiDAR instrument has been installed on the portside of the lower monkey deck, at a height of approximately 19 m above sea-level (Fig. 12.1a). Likewise to the Starboard-side measurements of Heinemann and Zentek (2016), the ships superstructure (mainly the bridge, the crow nest and the exhaust-chimney) prohibited the possibility of using certain azimuth-angles for scan-mode definitions.

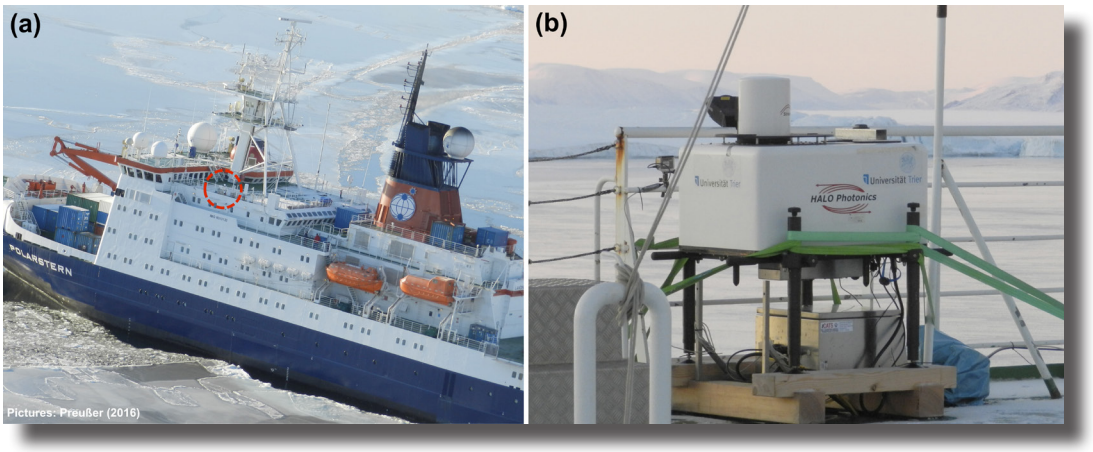

Fig. 12.1: (a) Position of the LiDAR (red circle) on the portside of Polarstern. (b) Photo of the LiDAR with all connected devices.

Tab. 12.1: Overview of the wind LiDAR characteristics during PS109 (modified from Heinemann and Zentek, 2016).

Wavelength	1.5 µm (eye-safe, class 1m)
Gate length	30 m
Points per Gate	10 (overlapping)
Band width	±19.4 m/s
Resolution	0.038 m/s
Threshold for Signal-to-Noise (SNR) ratio	variable (default -20 dB)
Measurement error	Approx. 0.1 m/s (depending on SNR)
Pulse rate	10 kHz
Beam range	30 - 2700 m
Beam focus	300 – 1750 m
Pulse averages	10000 – 150000
Scanning horizontal (azimuth)	0° to 360°
Scanning vertical (elevation)	-15° to 90°

In principle, the LiDAR is programmable and has the ability to perform vertical and horizontal scans in every direction (hemispheric). However, the primary scan patterns can be subdivided into the vertical azimuth display (VAD), the range-height indicator (RHI) as well as horizontal scans with fixed azimuth angles (STARE). A built-in 'Wind-Profile' mode (VAD-6) was used in addition. Since the measured wind signal of a single beam is only the radial wind component (i.e., line-of-sight (LOS) wind), at least two different scan angles with respect to the wind vector are needed. We applied an overlapping mode, i.e. the data are available at the original 3 m resolution of the pulses (Zentek and Heinemann, 2016). The VAD is used for the determination of wind profiles above the LiDAR with eight scans with an elevation angle of 75° and 45° azimuth steps. The Wind-Profile mode is, as the name implies, also designed for measurements of the

vertical wind profile, but uses only six directions for the calculation. A horizontal STARE mode was used mainly at several set-ups with two different azimuth angles, which were adjusted to the heading/course of the ship and the present wind direction. RHI scans were performed with different elevation angles up to 40°. This potentially allowed for measurements of e.g. the internal boundary layer at the sea ice edge or cold-air downdrafts at the glacier-front of the 79°North-Glacier (79NG; orig. name “Nioghalvfjerdsfjorden”).

Besides the LiDAR, two high-resolution camera-systems (GoPro Hero 4 Black) were installed on both sides of the lower monkey deck in order to document ambient weather-conditions throughout the total measurement-period (in total around 55.000 images; Fig. 12.2). An external Altitude Heading Reference System (AHRS; XSENS MTi-G-700-GPS/INS) was installed for higher frequency (sampled with 10 Hz) recordings of the ship’s pitch and roll, in addition to lower frequency (1 Hz) navigation data from the ship’s internal systems (Heinemann and Zentek, 2016).

Everyday work included an initial quality check of the recorded wind data of the previous day and comparisons to available radiosonde data (*Polarstern* meteorological office; Vaisala RS92, accents up to 2 times daily), visual checks on the state of the instruments outside as well as appropriate adjustments to the measurement setup depending on the present synoptic/ local weather situation.

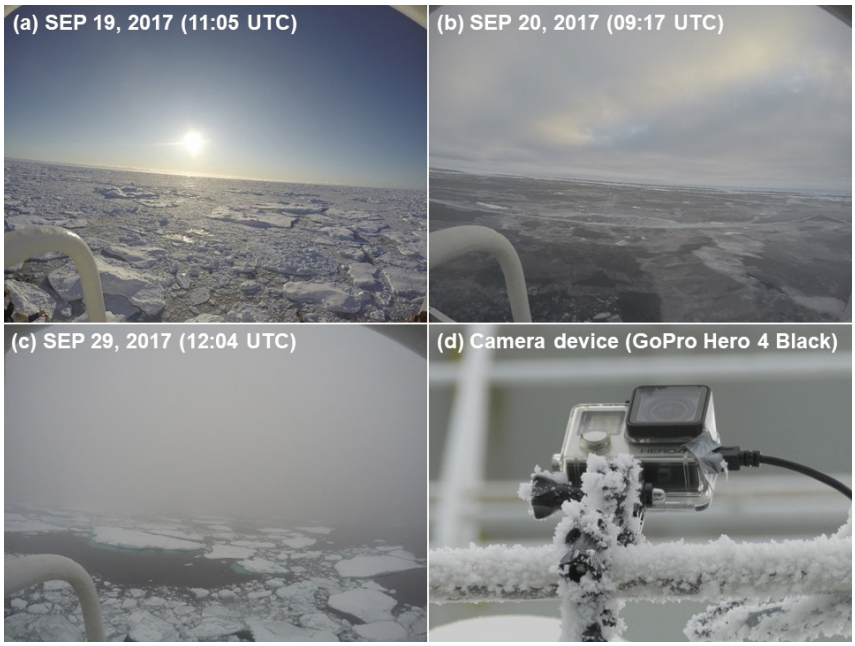

Fig. 12.2: Selected photographs from the installed camera devices, in (a) to (c) particularly from the camera on the portside of Polarstern. The device itself (GoPro Hero 4 Black) is depicted in panel (d).

Preliminary (expected) results

One of our main outcomes of the cruise PS109 are continuous measurements of vertical wind profiles that were derived from VAD-scans with varying temporal frequency (mostly 10-15 minutes) and multiple angular set-ups (with six and eight beams). A time series of those measurements is depicted in Fig. 12.3.

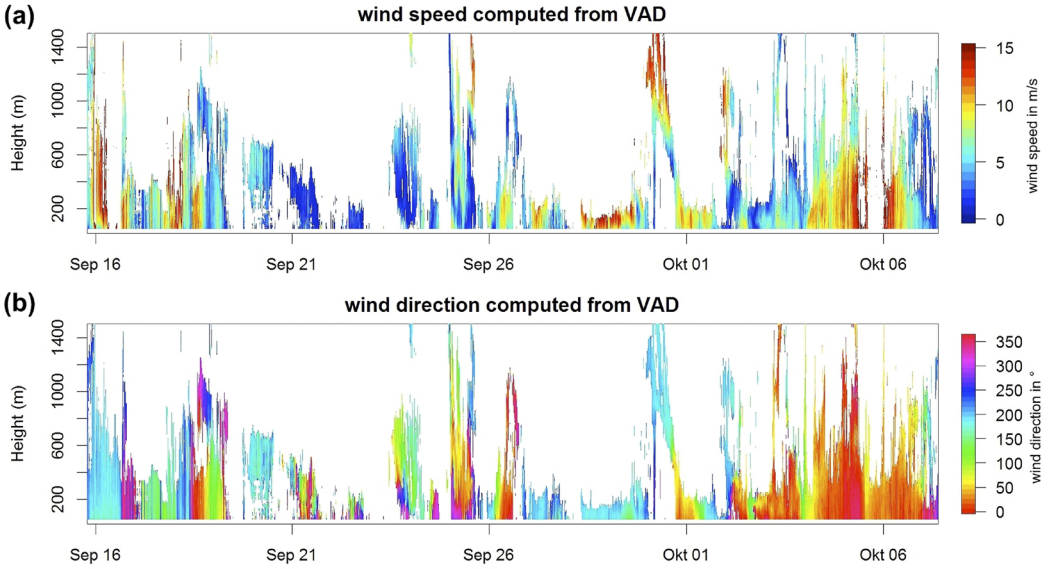

Fig. 12.3: Overview on the wind speed (a) and wind direction (b) profiles (computed from VAD) over the complete measurement period during PS109 (September 15 to October 07).

It features the complete measurement period of the LiDAR starting from September 15 (12.00 UTC) until October 07 (09.30 UTC) (x-axis), as well as wind speed (in m/s; top panel) and wind direction (in °; bottom panel) on the y-axis, respectively. This time series is able to capture most of the wind conditions during PS109, with varying vertical coverage depending on the available amount of scattering particles in the lower atmosphere. Especially during the period from 19-24 September there were frequent cloud-free conditions around the ship (Fig. 12.2a), which resulted in the coverage gaps of around 4-12 hours at some parts of the time series. On the other hand, low- and medium-level cloud cover (Fig. 12.2b) is more favourable for stronger signals up to a height of up to 1,200 m. However, thick low-level clouds and especially fog (Fig. 12.2c) again prohibit that the emitted light beam is able to traverse a long distance through the air column, as it gets fully attenuated once it reaches these thick layers where multiple scattering occurs.

Quite generally, the captured patterns of wind speed and direction fit well to the synoptic situation along the track of PS109 (compare Chapter 2). Approaching the sea-ice edge at the beginning of the cruise, we see that the recorded high wind speeds are fairly homogeneous with height, both in terms of magnitude and direction (south and north with quick veering in between). This probably stems from the more or less homogeneous surface topography in both directions and a strong atmospheric pressure gradient during the time of measurement. When approaching the coast of Northeast-Greenland and especially in direct proximity of Djimphna Sound or the 79NG, we notice the sheltering influence of the surrounding topography, as the lower 100-400 m frequently feature (north-) westerly winds coming downslope from the glacier as cold-air flows while the upper layers adjust more to the large-scale synoptic wind patterns. However, surface wind speeds were quite low during this period, so that wind directions appeared to be quite variable between September 21 and September 23. When leaving the sheltering proximity of the coast around September 26, wind speeds increased again and the directional flow again became more homogeneous with altitude.

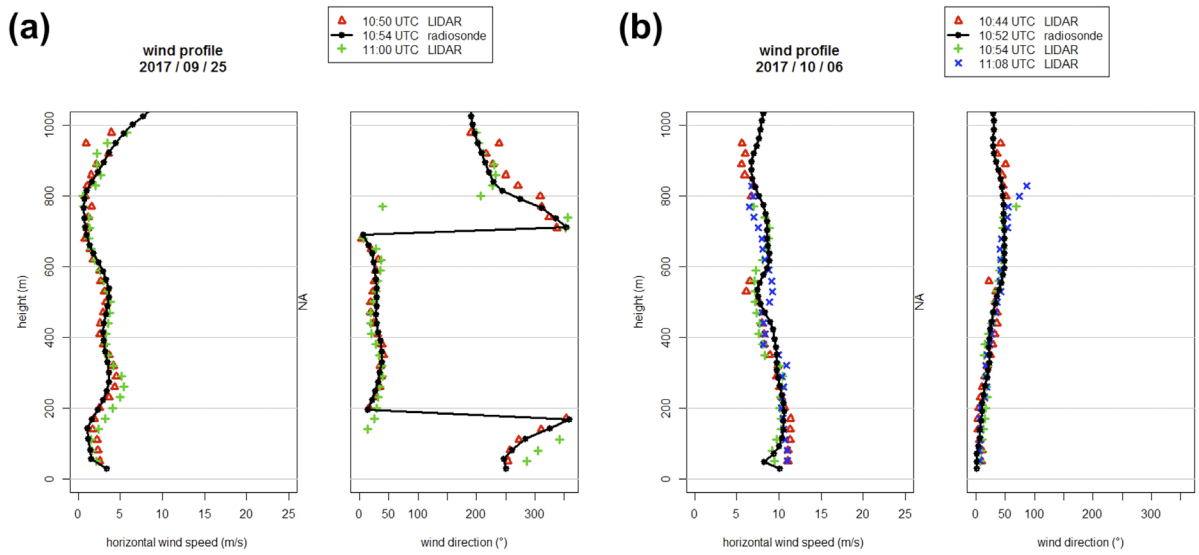

Fig. 12.4: Two examples for wind-profile comparisons between radiosonde launches on board Polarstern (black) and adjacent LiDAR measurements (red/green/blue), with the dates being (a) September 25, 11.00 UTC, and (b) October 06, 11.00 UTC.

For the whole cruise period, the meteorological office on-board *Polarstern* kindly provided us with up to twice daily radiosonde data (around 07.00 and 11.00 UTC), which are ideally suited to serve as a methodical comparison data set in order evaluate our recorded data directly on-site. It shows (examples in Fig. 12.4) that both data sets are matching quite well when the signal strength is high, but can also be quite off if this is not the case or if the time between adjacent measurements becomes too long. The RMSD (radiosondes vs. LiDAR) in wind speed from previous campaigns was estimated with ~1 m/s (PS85 & PS96), depending on the selected height. Fig. 12.4 first shows one case (September 25, 11.00 UTC) where the sheltering effect of the coastal topography becomes apparent with a change in wind direction from West to North at 200 m height (left side panels). The other case (October 06, 11.00 UTC) features a day towards the end of the scientific programme (east of the sea-ice edge; open water) with a more or less homogeneous wind direction with height and stronger winds around 10 m/s coming from northern directions. More in-depth comparisons between our LiDAR measurements and all available radiosonde profiles will be conducted in the near future. Other short-term utilizations of the acquired data set after the cruise include a more detailed investigation of single case studies (e.g., near the 79NG) as well as processing of the data for the verification of the regional climate model COSMO CLM (Gutjahr et al., 2016).

Data management

All LiDAR data will be stored on data servers at the University of Trier. After a detailed quality control, further processing and publication in a peer-reviewed journal, the LiDAR data will be stored in the PANGAEA data base. Acquired photographs from installed camera devices are available on request.

References

Gutjahr O, Heinemann G, Preußer A, Willmes S, Drüe C (2016) Quantification of ice production in Laptev Sea polynyas and its sensitivity to thin-ice parameterizations in a regional climate model. The Cryosphere 10, 2999-3019, doi:10.5194/tc-10-2999-2016.

Heinemann G, Zentek R (2016) Measurements of the atmospheric boundary layer using a wind lidar. In: The Expedition PS96 of the Research Vessel *POLARSTERN* to the southern Weddell Sea in 2015/2016 (ed. M. Schröder). Reports on Polar and Marine Research 700, Alfred-Wegener-Institute for Polar and Marine Research, Bremerhaven, Germany, 148pp. http://doi.pangaea.de/10013/epic.48157.d001.

Hirsikko A, O'Connor EJ, Komppula M, Korhonen K, Pfüller A, Giannakaki E, Wood CR, Bauer-Pfundstein M, Poikonen A, Karppinen T, Lonka H, Kurri M, Heinonen J, Moisseev D, Asmi E, Aaltonen V, Nordbo A, Rodriguez E, Lihavainen H, Laaksonen A, Lehtinen KEJ, Laurila T, Petäjä T, Kulmala M, and Viisanen Y (2014) Observing wind, aerosol particles, cloud and precipitation: Finland's new ground-based remote-sensing network. Atmos. Meas. Tech. 7:1351–1375, doi:10.5194/amt-7-1351-2014.g.

APPENDIX

A.1 PARTICIPATING INSTITUTIONS

A.2 CRUISE PARTICIPANTS

A.3 SHIP'S CREW

A.4 STATION LIST

A.1 TEILNEHMENDEINSTITUTE/PARTICIPATINGINSTITUTIONS

	Address
AWI	Alfred-Wegener-Institut Helmholtz-Zentrum für Polar- und Meeresforschung Postfach 120161 27515 Bremerhaven, Germany
DUR	Durham University Department of Geography Science Laboratories South Rd Durham, DH1 3LE, UK
DWD	Deutscher Wetterdienst Geschäftsbereich Wettervorhersage Seeschifffahrtsberatung Bernhard Nocht Str. 76 20359 Hamburg, Germany
GEOMAR	Helmholtz-Zentrum für Ozeanforschung (GEOMAR) Wischhofstr. 1-3 24148 Kiel, Germany
GEUS	Geological Survey of Denmark and Greenland Øster Voldgade 10 DK-1350 Copenhagen K, Denmark
HeliService	Heli Service International GmbH Gorch Fock Strasse 105 26721 Emden, Germany
KU Leuven	KU Leuve Catholic University of Leuven Laboratory of Biodiversity and Evolutionary Genomics Charles Deberiotstraat 32 bus 2439 B-3000 Leuven, Belgium
MPIMM	Max-Planck-Institut for Marine Microbiology Celsiusstr.1 28835 Bremen, Germany
TU Dresden	Technische Universität Dresden Institut für Planetare Geodäsie 01062 Dresden, Germany

	Address
TUB	Technische Universität Braunschweig Institute of Flight Guidance Hermann-Blenk-Str.27 38108 Braunschweig, Germany
UDEL	University of Delaware 111 Robinson Hall Newark, DE 19716, USA
UHB	Universität Bremen Marine Zoologie (FB 02) Postfach 330 440 28334 Bremen, Germany
UHB-IUP	University of Bremen Institute of Environmental Physics (IUP) – Oceanography Otto-Hahn-Allee 28359 Bremen, Germany
UIT	University of Tromsø Muninbakken 21 9019 Tromsø, Norway
Uni Ghent	Ghent University Campus Ufo, Rectorate Sint-Pietersnieuwstraat 25 B-9000 Ghent, Belgium
Uni Trier	University Trier Universitätsring 15 54296 Trier, Germany
WHOI	Woods Hole Oceanographic Institution 266 Woods Hole Road Woods Hole, MA 02543-1050, USA

A.2 FAHRTTEILNEHMER / CRUISE PARTICIPANTS

Name/ Last name	Vorname/ First name	Institut/ Institute	Beruf/ Profession	Fachrichtung/ Discipline
Albedyll, von	Luisa	UHB	Student	Oceanography
Asendorf	Volker	MPIMM	Technician	Biogeochemistry
Barz	Jakob	MPIMM	Technician	Biogeochemistry
Beaird	Nicolas L.	WHOI	Scientist	Oceanography
Behrendt	Axel	AWI	Scientist	Oceanography
Braeckmann	Ulrike	Uni Ghent	Scientist	Biogeochemistry
Breckenfelder	Tilia	UHB-IUP	Scientist	Tracer Oceanography
Brünjes	Jonas	UHB-IUP	Student	Tracer Oceanography
Busack	Michael	AWI	Scientist	Oceanography
Codling	Peter	DUR	Scientist	Geology
Dietrich	Ulrike	UIT	Scientist	Sea Ice Biology
Ehrlich	Julia	AWI	Scientist	Biology
Eis	Julia	UHB	Scientist	Glaciology
Engicht	Carina	AWI	Technician	Oceanography
Felden	Janine	UHB	Scientist	Biogeochemistry
Graupner	Rainer	AWI	Technician	Oceanography
Grübner	Lars	AWI	Media Designer	Communication & Media
Hempelt	Juliane	DWD	Technician	Meteorology
Hofmann	Zerlina	GEOMAR	Student	Oceanography
Huhn	Oliver	UHB-IUP	Scientist	Tracer Oceanography
Hutter	Nils	AWI	Student	Oceanography
Jones	Richard R.	DUR	Scientist	Geology
Kanzow	Torsten	AWI	Chief Scientist	Oceanography
Kappelsberger	Maria	TU Dresden	Student	Geodesy
Kendzia	Jan	HeliService	Pilot	
Knöfel	Christoph	TU Dresden	Scientist	Geodesy
Krüger	Thomas	TUB	Scientist Engineering	
Lehmenhecker	Sascha	AWI	Technician AUV/ UAV	
Lloyd	Jerry M.	DUR	Scientist Geology	
Lunz	Susanne	TU Dresden	Student Geodesy	
Lüttig	Christine	AWI	Scientist	Glaciology
Maes	Sarah	KU Leuven	Student	Biology
Meier	Michaela	AWI	Scientist	Seismology
Miller	Max	DWD	Meteorologist	
Münchow	Andreas	UDEL	Scientist	Oceanography
Ó Cofaigh	Colm	DUR	Scientist	Geology
Pätzold	Falk	TUB	Scientist	Engineering

Name/ Last name	**Vorname/ First name**	**Institut/ Institute**	**Beruf/ Profession**	**Fachrichtung/ Discipline**
Preusser	Andreas	Uni Trier	Scientist	Meteorology
Richter	Roland	HeliService	Technician	
Rohleder	Christian	DWD	Technician	Meteorology
Rothenburg	Mark	HeliService	Technician	
Schaffer	Janin	AWI	Scientist	Oceanography
Specht	Mia Sophie	AWI	Student	Oceanography
Streuff	Katharina	DUR	Scientist	Geology
Syring	Nicole	AWI	Scientist	Geology
Tippenhauer	Sandra	AWI	Scientist	AUV
Vaupel	Lars	HeliService	Chief pilot	
Verdugo	Maria Josefa	AWI	Scientist	Biology
Vermassen	Flor	GEUS	Scientist	Geology
Washam	Peter	UDEL	Scientist	Oceanography
Wulff	Thorben	AWI	Scientist	AUV

A.3 SCHIFFSBESATZUNG / SHIP‘S CREW

No.	Name	Rank
1	Wunderlich, Thomas	Master
2	Lauber, Felix	1. Offc.
3	Westphal, Henning	Ch. Eng.
4	Kentges, Felix	1. Offc.(Cargo)
5	Neumann, Ralph	2. Offc.
6	Peine, Lutz	2. Offc.
7	Scholl, Thomas	Doctor
8	Hofmann, Jörg	R. Offc.
9	Buch, Erik-Torsten	2. Eng.
10	Grafe, Jens	2. Eng.
11	Rusch, Torben	2. Eng.
12	Redmer, Jens	Elec. Eng.
13	Feiertag, Thomas	ELO
14	Ganter, Armin	ELO
15	Markert, Winfried	ELO
16	Winter, Andreas	Sys-man
17	Sedlak, Andreas	Boatsw.
18	Neisner, Winfried	Carpenter
19	Becker, Holger	A.B.
20	Brickmann, Peter	A.B.
21	Brück, Sebastian	A.B.
22	Burzan, Ekkehard	A.B.
23	Clasen, Nils	A.B.
24	Fölster, Michael	A.B.
25	Hartwig-Labahn, Andreas	A.B.
26	Müller, Steffen	A.B.
27	Schröder, Norbert	A.B.
28	Beth, Detlef	Storek.
29	Dinse, Horst	Mot-man
30	Klein, Gert	Mot-man
31	Krösche, Eckard	Mot-man
32	Plehn, Markus	Mot-man
33	Watzel, Bernhard	Mot-man
34	Redmer, Klaus-Peter	Cook
35	Möller, Wolfgang	Cooksmate
36	Tupy, Mario	Cooksmate
37	Wartenberg, Irina	1. Stwdess
38	Schwitzky, Carmen	2. Stwdess/N.
39	Duka, Maribel	2. Stwdess
40	Chen, Quan Lun	2. Steward

No.	Name	Rank
41	Hischke, Peggy	2. Stwdess
42	Krause, Tomasz	2. Steward
43	Shi, Wubo	2. Steward
44	Ruan, Hui Guang	Laundrym.

A.4 STATIONSLISTE / STATION LIST

Station	Date	Time	Latitude	Longitude	Depth [m]	Gear	Action	Comment
PS109_0_ Underway-1	2017-09-12	04:00	69,67955	18,99667		WST	profile start	
PS109_0_ Underway-1	2017-10-13	19:15	53,56683	8,55505		WST	profile end	
PS109_0_ Underway-2	2017-09-12	13:20	69,69783	19,07297	3	ADCP_150	profile start	
PS109_0_ Underway-2	2017-10-13	14:29	53,88735	7,74377	12,8	ADCP_150	profile end	
PS109_0_ Underway-3	2017-09-12	14:58	69,84692	19,7544	180	FBOX	profile start	
PS109_0_ Underway-3	2017-10-12	11:00	57,30167	5,08362	45	FBOX	profile end	
PS109_0_ Underway-4	2017-09-12	14:59	69,84833	19,75742	179	PCO2_GO	profile start	
PS109_0_ Underway-4	2017-10-12	11:00	57,30167	5,08362	45	PCO2_GO	profile end	
PS109_0_ Underway-5	2017-09-12	14:58	69,84752	19,75567	180	PCO2_SUB	profile start	
PS109_0_ Underway-5	2017-10-12	11:00	57,30167	5,08362	45	PCO2_SUB	profile end	
PS109_0_ Underway-6	2017-09-12	13:21	69,69783	19,07293	2,9	TSG_KEEL	profile start	
PS109_0_ Underway-6	2017-10-10	21:30	62,9249	2,12848	863	TSG_KEEL	profile end	
PS109_0_Under-way-7	2017-09-15	10:00	78,81683	0,00075	2614	LIDAR	profile start	
PS109_0_ Underway-7	2017-10-07	09:30	76,14715	-5,8905	2704	LIDAR	profile end	
PS109_1-1	2017-09-14	09:26	76,43775	6,76387	2725	OBS	station start	
PS109_2-1	2017-09-14	11:29	76,4416	7,50572	2692	OBS	station start	
PS109_3-1	2017-09-14	13:33	76,7235	7,71725	2499	OBS	station start	
PS109_4-1	2017-09-14	15:05	76,7294	7,00002	2359	OBS	station start	
PS109_5-1	2017-09-15	02:45	78,15228	0,0043	3062	CTDOZE	station start	
PS109_5-1	2017-09-15	03:08	78,15287	0,00803	3067	CTDOZE	at depth	
PS109_5-1	2017-09-15	03:48	78,15367	0,01118	3033	CTDOZE	station end	
PS109_5-2	2017-09-15	04:25	78,15075	0,03312	3112	BONGO	station start	
PS109_5-2	2017-09-15	04:25	78,15038	0,03468	3030	BONGO	profile start	
PS109_5-2	2017-09-15	04:39	78,14413	0,06413	3057	BONGO	at depth	
PS109_5-2	2017-09-15	04:54	78,13748	0,09258	3079	BONGO	profile end	
PS109_5-2	2017-09-15	05:00	78,13678	0,09757	3035	BONGO	station end	
PS109_6-1	2017-09-15	09:11	78,81783	-0,00188	2619	CTDOZE	station start	
PS109_6-1	2017-09-15	09:35	78,81683	0,00032	2612	CTDOZE	at depth	
PS109_6-1	2017-09-15	10:15	78,8163	0,0007	2612	CTDOZE	station end	
PS109_7-1	2017-09-15	14:43	79,48077	0,02433	2801	CTDOZE	station start	
PS109_7-1	2017-09-15	15:43	79,48023	0,01357	2835	CTDOZE	at depth	

Station	Date	Time	Latitude	Longitude	Depth [m]	Gear	Action	Comment
PS109_7-1	2017-09-15	17:21	79,48192	0,00973	2835	CTDOZE	station end	
PS109_7-2	2017-09-15	17:41	79,47977	0,00815	2836	BONGO	station start	
PS109_7-2	2017-09-15	17:42	79,47962	0,00837	2836	BONGO	profile start	
PS109_7-2	2017-09-15	17:55	79,47262	0,01833	2794	BONGO	at depth	
PS109_7-2	2017-09-15	18:09	79,46495	0,03178	2850	BONGO	profile end	
PS109_7-2	2017-09-15	18:15	79,46435	0,03252	2849	BONGO	station end	
PS109_8-1	2017-09-15	23:40	80,13082	-0,07348	2720	CTDOZE	station start	
PS109_8-1	2017-09-16	00:05	80,12693	-0,06248	2705	CTDOZE	at depth	
PS109_8-1	2017-09-16	00:35	80,12303	-0,04967	2679	CTDOZE	station end	
PS109_9-1	2017-09-16	07:31	80,82892	0,02823	3107	CTDOZE	station start	
PS109_9-1	2017-09-16	07:53	80,82945	0,03278	3105	CTDOZE	at depth	
PS109_9-1	2017-09-16	08:16	80,83065	0,03752	3102	CTDOZE	station end	
PS109_10-1	2017-09-16	12:24	80,59938	-1,48135	3339	CTDOZE	station start	
PS109_10-1	2017-09-16	12:49	80,59842	-1,45185	3363	CTDOZE	at depth	
PS109_10-1	2017-09-16	13:13	80,5985	-1,4238	3383	CTDOZE	station end	
PS109_11-1	2017-09-16	15:45	80,38445	-3,12157	3254	CTDOZE	station start	
PS109_11-1	2017-09-16	16:53	80,3812	-3,15013	3232	CTDOZE	at depth	
PS109_11-1	2017-09-16	18:38	80,37602	-3,21005	3212	CTDOZE	station end	
PS109_12-1	2017-09-16	19:54	80,33045	-4,00305	2595	CTDOZE	station start	
PS109_12-1	2017-09-16	20:23	80,33015	-4,0093	2570	CTDOZE	at depth	
PS109_12-1	2017-09-16	20:46	80,33045	-4,01562	2576	CTDOZE	station end	
PS109_13-1	2017-09-16	21:38	80,30727	-4,53652	2089	CTDOZE	station start	
PS109_13-1	2017-09-16	22:04	80,30828	-4,54053	2088	CTDOZE	at depth	
PS109_13-1	2017-09-16	22:27	80,30813	-4,5386	2089	CTDOZE	station end	
PS109_14-1	2017-09-16	23:18	80,28767	-4,99728	1550	CTDOZE	station start	
PS109_14-1	2017-09-16	23:57	80,29145	-4,9928	1546	CTDOZE	at depth	
PS109_14-1	2017-09-17	00:56	80,29535	-4,97545	1529	CTDOZE	station end	
PS109_15-1	2017-09-17	02:13	80,26572	-5,49553	917	CTDOZE	station start	
PS109_15-1	2017-09-17	02:37	80,26528	-5,49157	921	CTDOZE	at depth	
PS109_15-1	2017-09-17	03:20	80,26595	-5,48777	927	CTDOZE	station end	
PS109_16-1	2017-09-17	04:48	80,23653	-6,07628	359	CTDOZE	station start	
PS109_16-1	2017-09-17	05:03	80,23547	-6,0864	358	CTDOZE	at depth	
PS109_16-1	2017-09-17	05:31	80,23463	-6,09832	354	CTDOZE	station end	
PS109_17-1	2017-09-17	06:46	80,22272	-6,51772	302	CTDOZE	station start	
PS109_17-1	2017-09-17	06:59	80,22367	-6,5173	281	CTDOZE	at depth	
PS109_17-1	2017-09-17	07:25	80,2252	-6,52095	299	CTDOZE	station end	
PS109_18-1	2017-09-17	08:58	80,20283	-7,008	282	CTDOZE	station start	
PS109_18-1	2017-09-17	09:09	80,20405	-7,01305	287	CTDOZE	at depth	
PS109_18-1	2017-09-17	09:24	80,20532	-7,01708	282	CTDOZE	station end	
PS109_19-1	2017-09-17	11:26	80,14882	-7,951	321	CTDOZE	station start	
PS109_19-1	2017-09-17	11:37	80,14847	-7,94642	321	CTDOZE	at depth	
PS109_19-1	2017-09-17	11:45	80,14773	-7,9497	317	CTDOZE	station end	
PS109_19-2	2017-09-17	12:17	80,1477	-7,94908	317	TVMUC	station start	

Station	Date	Time	Latitude	Longitude	Depth [m]	Gear	Action	Comment
PS109_19-2	2017-09-17	12:24	80,14745	-7,94972	316	TVMUC	at depth	
PS109_19-2	2017-09-17	12:38	80,14732	-7,95032	313	TVMUC	at depth	
PS109_19-2	2017-09-17	12:53	80,14655	-7,94577	315	TVMUC	station end	
PS109_19-3	2017-09-17	14:02	80,1475	-7,95138	316	LAND	station start	
PS109_19-3	2017-09-17	14:14	80,14722	-7,94857	315	LAND	station start	
PS109_19-3	2017-09-17	14:27	80,14735	-7,9478	315	LAND	station start	
PS109_19-3	2017-09-17	14:29	80,14733	-7,94768	315	LAND	at depth	
PS109_19-4	2017-09-17	15:02	80,13573	-7,93195	310	TVMUC	station start	
PS109_19-4	2017-09-17	15:16	80,13415	-7,93173	315	TVMUC	at depth	
PS109_19-4	2017-09-17	15:30	80,133	-7,9306	316	TVMUC	station end	
PS109_20-1	2017-09-17	16:41	80,19012	-8,14663	317	MOOR	station end	
PS109_20-1	2017-09-17	16:43	80,19	-8,14552	317	MOOR	station end	
PS109_20-1	2017-09-17	16:44	80,18998	-8,14455	317	MOOR	station end	
PS109_20-1	2017-09-17	16:55	80,1891	-8,14522	302	MOOR	station end	
PS109_20-1	2017-09-17	16:59	80,18892	-8,14612	317	MOOR	station end	
PS109_20-1	2017-09-17	17:02	80,18893	-8,145	320	MOOR	station end	
PS109_21-1	2017-09-17	18:59	80,17165	-7,60927	299	GC	station start	
PS109_21-1	2017-09-17	19:06	80,17168	-7,60955	302	GC	at depth	
PS109_21-1	2017-09-17	19:16	80,17185	-7,60798	300	GC	station end	
PS109_22-1	2017-09-17	20:11	80,18338	-7,44365	317	GC	station start	
PS109_22-1	2017-09-17	20:20	80,18363	-7,44312	330	GC	at depth	
PS109_22-1	2017-09-17	20:32	80,18505	-7,44268	331	GC	station end	
PS109_23-1	2017-09-17	21:56	80,2126	-6,88427	283	GC	station start	
PS109_23-1	2017-09-17	22:01	80,21278	-6,88462	289	GC	at depth	
PS109_23-1	2017-09-17	22:15	80,21308	-6,8844	290	GC	station end	
PS109_24-1	2017-09-17	22:56	80,21102	-6,75393	266	GC	station start	
PS109_24-1	2017-09-17	23:01	80,21147	-6,75282	289	GC	at depth	
PS109_24-1	2017-09-17	23:11	80,21182	-6,75155	289	GC	station end	
PS109_25-1	2017-09-18	00:51	80,23907	-5,93157	395	GC	station start	
PS109_25-1	2017-09-18	01:01	80,23952	-5,93005	397	GC	at depth	
PS109_25-1	2017-09-18	01:14	80,24033	-5,92783	397	GC	station end	
PS109_26-1	2017-09-18	07:00	80,67073	-7,92112	76	CTDOZE	station start	
PS109_26-1	2017-09-18	07:06	80,67102	-7,92787	74	CTDOZE	at depth	
PS109_26-1	2017-09-18	07:15	80,67122	-7,93432	73	CTDOZE	station end	
PS109_27-1	2017-09-18	09:41	80,55178	-7,8626	258	CTDOZE	station start	
PS109_27-1	2017-09-18	09:53	80,55258	-7,86527	260	CTDOZE	at depth	
PS109_27-1	2017-09-18	10:00	80,55312	-7,8657	261	CTDOZE	station end	
PS109_28-1	2017-09-18	10:40	80,5337	-7,78403	259	GC	station start	
PS109_28-1	2017-09-18	10:47	80,53388	-7,77948	262	GC	at depth	
PS109_28-1	2017-09-18	10:59	80,53455	-7,7704	258	GC	station end	
PS109_29-1	2017-09-18	12:12	80,46162	-7,9069	236	CTDOZE	station start	
PS109_29-1	2017-09-18	12:23	80,46107	-7,89743	236	CTDOZE	at depth	
PS109_29-1	2017-09-18	12:40	80,45973	-7,88355	237	CTDOZE	station end	

Station	Date	Time	Latitude	Longitude	Depth [m]	Gear	Action	Comment
PS109_30-1	2017-09-18	13:53	80,38282	-7,94447	250	CTDOZE	station start	
PS109_30-1	2017-09-18	14:07	80,37958	-7,9328	248	CTDOZE	at depth	
PS109_30-1	2017-09-18	14:13	80,37817	-7,92805	248	CTDOZE	station end	
PS109_30-2	2017-09-18	14:45	80,35882	-7,77997	248	BONGO	station start	
PS109_30-2	2017-09-18	14:59	80,36398	-7,75592	250	BONGO	at depth	
PS109_30-2	2017-09-18	15:16	80,37197	-7,74315	251	BONGO	station end	
PS109_31-1	2017-09-18	16:08	80,305	-8,02088	264	CTDOZE	station start	
PS109_31-1	2017-09-18	16:25	80,30402	-8,02627	263	CTDOZE	at depth	
PS109_31-1	2017-09-18	16:48	80,30342	-8,03407	264	CTDOZE	station end	
PS109_32-1	2017-09-18	18:20	80,14577	-7,9658	339	LAND	at depth	
PS109_32-1	2017-09-18	19:02	80,14612	-7,95733	319	LAND	station end	
PS109_32-1	2017-09-18	19:06	80,14615	-7,95862	319	LAND	station end	
PS109_32-1	2017-09-18	19:25	80,1466	-7,97188	316	LAND	station end	
PS109_32-1	2017-09-18	19:36	80,14502	-7,98753	325	LAND	station end	
PS109_32-1	2017-09-18	19:49	80,14422	-8,00545	328	LAND	station end	
PS109_33-1	2017-09-18	20:54	80,22202	-8,17993	284	CTDOZE	station start	
PS109_33-1	2017-09-18	21:08	80,22203	-8,17867	273	CTDOZE	at depth	
PS109_33-1	2017-09-18	21:16	80,22207	-8,17727	259	CTDOZE	station end	
PS109_34-1	2017-09-18	23:01	80,14497	-8,31793	328	CTDOZE	station start	
PS109_34-1	2017-09-18	23:18	80,14838	-8,31242	332	CTDOZE	at depth	
PS109_34-1	2017-09-18	23:34	80,1529	-8,30535	330	CTDOZE	station end	
PS109_35-1	2017-09-19	00:50	80,06125	-8,34182	204	CTDOZE	station start	
PS109_35-1	2017-09-19	01:00	80,0624	-8,32982	211	CTDOZE	at depth	
PS109_35-1	2017-09-19	01:16	80,0639	-8,3093	458	CTDOZE	station end	
PS109_36-1	2017-09-19	04:57	80,32837	-9,96792	314	CTDOZE	station start	
PS109_36-1	2017-09-19	05:09	80,32663	-9,9733	314	CTDOZE	at depth	
PS109_36-1	2017-09-19	05:30	80,32445	-9,9872	315	CTDOZE	station end	
PS109_36-2	2017-09-19	05:55	80,31762	-10,02898	318	TVMUC	station start	
PS109_36-2	2017-09-19	06:09	80,31763	-10,03173	318	TVMUC	at depth	
PS109_36-2	2017-09-19	06:21	80,31718	-10,03887	305	TVMUC	station end	
PS109_36-3	2017-09-19	06:42	80,3127	-10,08342	310	TVMUC	station start	
PS109_36-3	2017-09-19	06:55	80,31298	-10,08642	310	TVMUC	at depth	
PS109_36-3	2017-09-19	07:07	80,3135	-10,09095	311	TVMUC	station end	
PS109_37-1	2017-09-19	13:23	80,36453	-10,5564	324	GC	station start	
PS109_37-1	2017-09-19	13:31	80,36455	-10,54477	326	GC	at depth	
PS109_37-1	2017-09-19	13:45	80,3649	-10,52605	324	GC	station end	
PS109_38-1	2017-09-19	14:14	80,36363	-10,58417	319	GC	station start	
PS109_38-1	2017-09-19	14:24	80,36398	-10,57217	320	GC	at depth	
PS109_38-1	2017-09-19	14:35	80,36467	-10,55687	323	GC	station end	
PS109_39-1	2017-09-19	15:06	80,35973	-10,58448	308	GC	station start	
PS109_39-1	2017-09-19	15:14	80,3598	-10,57712	310	GC	at depth	
PS109_39-1	2017-09-19	15:26	80,36	-10,56693	312	GC	station end	
PS109_40-1	2017-09-19	15:58	80,35178	-10,66103	291	GC	station start	

Station	Date	Time	Latitude	Longitude	Depth [m]	Gear	Action	Comment
PS109_40-1	2017-09-19	16:07	80,35187	-10,65652	291	GC	at depth	
PS109_40-1	2017-09-19	16:18	80,3515	-10,65325	292	GC	station end	
PS109_41-1	2017-09-20	03:21	79,99675	-14,79822	153	CTDOZE	station start	
PS109_41-1	2017-09-20	03:29	79,99608	-14,79615	148	CTDOZE	at depth	
PS109_41-1	2017-09-20	03:43	79,99368	-14,79298	145	CTDOZE	station end	
PS109_42-1	2017-09-20	05:10	80,0168	-15,12913	206	CTDOZE	station start	
PS109_42-1	2017-09-20	05:21	80,01555	-15,13172	214	CTDOZE	at depth	
PS109_42-1	2017-09-20	05:45	80,01242	-15,1356	206	CTDOZE	station end	
PS109_43-1	2017-09-20	08:19	80,09612	-15,6074	429	CTDOZE	station start	
PS109_43-1	2017-09-20	08:31	80,09537	-15,6083	431	CTDOZE	at depth	
PS109_43-1	2017-09-20	08:53	80,09405	-15,60968	430	CTDOZE	station end	
PS109_44-1	2017-09-20	15:11	80,14855	-17,40118	164	MOOR	station end	
PS109_44-2	2017-09-20	15:32	80,148	-17,39883	165	CTDOZE	station start	
PS109_44-2	2017-09-20	15:42	80,14795	-17,39882	165	CTDOZE	at depth	
PS109_44-2	2017-09-20	15:55	80,1478	-17,39647	164	CTDOZE	station end	
PS109_44-3	2017-09-20	16:19	80,14743	-17,39018	164	MSS	station start	
PS109_44-3	2017-09-20	16:25	80,1475	-17,39182	164	MSS	station end	
PS109_45-1	2017-09-20	17:31	80,13505	-17,69082	204	CTDOZE	station start	
PS109_45-1	2017-09-20	17:44	80,13488	-17,691	204	CTDOZE	at depth	
PS109_45-1	2017-09-20	18:09	80,13453	-17,69438	203	CTDOZE	station end	
PS109_45-2	2017-09-20	18:25	80,1344	-17,69782	204	TVMUC	station start	
PS109_45-2	2017-09-20	18:48	80,13423	-17,70227	210	TVMUC	at depth	
PS109_45-2	2017-09-20	19:00	80,13417	-17,70323	205	TVMUC	station end	
PS109_45-3	2017-09-20	19:14	80,13423	-17,70305	205	TVMUC	station start	
PS109_45-3	2017-09-20	19:25	80,13428	-17,70297	160	TVMUC	at depth	
PS109_45-3	2017-09-20	19:36	80,13438	-17,70183	178	TVMUC	station end	
PS109_45-4	2017-09-20	19:52	80,1343	-17,7087	218	TVMUC	station start	
PS109_45-4	2017-09-20	20:05	80,13437	-17,7105	219	TVMUC	at depth	
PS109_45-4	2017-09-20	20:17	80,13457	-17,70687	220	TVMUC	station end	
PS109_46-1	2017-09-20	21:23	80,1543	-17,35923	179	CTDOZE	station start	
PS109_46-1	2017-09-20	21:32	80,15435	-17,36053	176	CTDOZE	at depth	
PS109_46-1	2017-09-20	21:45	80,15433	-17,36257	175	CTDOZE	station end	
PS109_47-1	2017-09-20	22:22	80,13158	-17,42477	152	CTDOZE	station start	
PS109_47-1	2017-09-20	22:30	80,13147	-17,4261	152	CTDOZE	at depth	
PS109_47-1	2017-09-20	22:40	80,13148	-17,42787	152	CTDOZE	station end	
PS109_48-1	2017-09-21	00:01	80,1037	-17,4138	92	CTDOZE	station start	
PS109_48-1	2017-09-21	00:11	80,10317	-17,41503	92	CTDOZE	at depth	
PS109_48-1	2017-09-21	00:18	80,10328	-17,41638	92	CTDOZE	station end	
PS109_49-1	2017-09-21	01:23	80,13748	-17,09553	195	CTDOZE	station start	
PS109_49-1	2017-09-21	01:33	80,13735	-17,09505	196	CTDOZE	at depth	
PS109_49-1	2017-09-21	01:49	80,13745	-17,09325	196	CTDOZE	station end	
PS109_50-1	2017-09-21	13:49	79,58355	-19,3401	380	MOOR	station end	
PS109_50-1	2017-09-21	13:53	79,58352	-19,3403	377	MOOR	station end	

Station	Date	Time	Latitude	Longitude	Depth [m]	Gear	Action	Comment
PS109_50-1	2017-09-21	13:58	79,58343	-19,34107	379	MOOR	station end	
PS109_50-1	2017-09-21	14:02	79,5834	-19,3408	377	MOOR	station end	
PS109_50-1	2017-09-21	14:04	79,58337	-19,34062	378	MOOR	station end	
PS109_50-1	2017-09-21	14:06	79,58335	-19,34048	378	MOOR	station end	
PS109_50-1	2017-09-21	14:09	79,58333	-19,34027	379	MOOR	station end	
PS109_51-1	2017-09-21	15:05	79,56865	-19,45883	501	MOOR	station end	
PS109_51-1	2017-09-21	15:09	79,56872	-19,45813	309	MOOR	station end	
PS109_51-1	2017-09-21	15:11	79,56882	-19,45782	311	MOOR	station end	
PS109_51-1	2017-09-21	15:13	79,5689	-19,45752	397	MOOR	station end	
PS109_51-1	2017-09-21	15:14	79,56897	-19,45718	349	MOOR	station end	
PS109_51-1	2017-09-21	15:16	79,56903	-19,45673	396	MOOR	station end	
PS109_51-1	2017-09-21	15:18	79,56905	-19,45658	145	MOOR	station end	
PS109_51-1	2017-09-21	15:29	79,5691	-19,45607	319	MOOR	station end	
PS109_51-1	2017-09-21	15:37	79,56908	-19,45595	310	MOOR	station end	
PS109_51-1	2017-09-21	15:37	79,56908	-19,45597	389	MOOR	station end	
PS109_51-1	2017-09-21	15:39	79,56907	-19,45592	447	MOOR	station end	
PS109_52-1	2017-09-21	17:24	79,43863	-19,77543	46	MOOR	at depth	
PS109_52-1	2017-09-21	17:44	79,44002	-19,77592	322	MOOR	station end	
PS109_52-1	2017-09-21	17:52	79,44005	-19,7775	321	MOOR	station end	
PS109_52-1	2017-09-21	17:54	79,44	-19,77787	321	MOOR	station end	
PS109_52-1	2017-09-21	17:59	79,43982	-19,77947	321	MOOR	station end	
PS109_52-1	2017-09-21	18:03	79,4396	-19,7807	322	MOOR	station end	
PS109_52-2	2017-09-21	18:43	79,43932	-19,77908	321	CTDOZE	station start	
PS109_52-2	2017-09-21	18:57	79,43973	-19,77698	321	CTDOZE	at depth	
PS109_52-2	2017-09-21	19:27	79,4407	-19,77583	321	CTDOZE	station end	
PS109_53-1	2017-09-21	22:10	79,56878	-19,45843	898	TVMUC	station start	
PS109_53-1	2017-09-21	22:30	79,5688	-19,4589	556	TVMUC	at depth	
PS109_53-1	2017-09-21	22:46	79,5688	-19,45868	1075	TVMUC	station end	
PS109_54-1	2017-09-22	00:09	79,64032	-19,13053	420	CTDOZE	station start	
PS109_54-1	2017-09-22	00:24	79,64045	-19,1294	421	CTDOZE	at depth	
PS109_54-1	2017-09-22	00:39	79,64048	-19,13015	421	CTDOZE	station end	
PS109_55-1	2017-09-22	01:21	79,63185	-19,23293	404	CTDOZE	station start	
PS109_55-1	2017-09-22	01:39	79,63172	-19,23282	402	CTDOZE	at depth	
PS109_55-1	2017-09-22	02:13	79,63167	-19,23247	404	CTDOZE	station end	
PS109_56-1	2017-09-22	03:25	79,61745	-19,28862	352	CTDOZE	station start	
PS109_56-1	2017-09-22	03:36	79,61737	-19,28758	352	CTDOZE	at depth	
PS109_56-1	2017-09-22	03:45	79,61743	-19,2861	354	CTDOZE	station end	
PS109_57-1	2017-09-22	04:42	79,60193	-19,3247	330	CTDOZE	station start	
PS109_57-1	2017-09-22	04:56	79,60172	-19,3224	331	CTDOZE	at depth	
PS109_57-1	2017-09-22	05:31	79,60295	-19,3212	333	CTDOZE	station end	
PS109_58-1	2017-09-22	06:39	79,59327	-19,33803	317	CTDOZE	station start	
PS109_58-1	2017-09-22	06:52	79,59347	-19,3395	319	CTDOZE	at depth	
PS109_58-1	2017-09-22	07:01	79,5938	-19,34142	324	CTDOZE	station end	

Station	Date	Time	Latitude	Longitude	Depth [m]	Gear	Action	Comment
PS109_59-1	2017-09-22	09:07	79,51672	-19,43182	291	MOOR	station start	
PS109_59-1	2017-09-22	09:15	79,51662	-19,43035	291	MOOR	station end	
PS109_59-1	2017-09-22	09:24	79,51645	-19,4303	291	MOOR	station start	
PS109_59-1	2017-09-22	09:33	79,51648	-19,43303	291	MOOR	station end	
PS109_60-1	2017-09-22	13:37	79,56943	-19,30055	318	AUV	station start	
PS109_60-1	2017-09-22	13:41	79,56972	-19,29985	308	AUV	station end	
PS109_60-1	2017-09-22	13:44	79,56992	-19,29913	295	AUV	station start	
PS109_60-1	2017-09-22	13:54	79,57017	-19,2976	273	AUV	station start	
PS109_60-1	2017-09-22	14:25	79,5693	-19,29758	279	AUV	station start	
PS109_60-1	2017-09-22	14:41	79,5695	-19,29888	294	AUV	station end	
PS109_60-1	2017-09-22	14:46	79,56958	-19,29922	299	AUV	profile start	
PS109_60-1	2017-09-22	14:48	79,56958	-19,29925	299	AUV	station start	
PS109_60-1	2017-09-22	15:02	79,56917	-19,30018	315	AUV	station end	
PS109_60-1	2017-09-22	15:25	79,56838	-19,29778	290	AUV	station end	
PS109_60-1	2017-09-22	17:28	79,568	-19,29042	223	AUV	station start	
PS109_60-1	2017-09-22	17:35	79,568	-19,29042	222	AUV	station start	
PS109_60-1	2017-09-22	17:38	79,56797	-19,29028	222	AUV	station end	
PS109_60-1	2017-09-22	17:40	79,56797	-19,29027	222	AUV	station start	
PS109_60-1	2017-09-22	17:42	79,56797	-19,29027	222	AUV	station end	
PS109_60-1	2017-09-22	18:15	79,56812	-19,29282	256	AUV	station start	
PS109_60-1	2017-09-22	18:23	79,56805	-19,29183	248	AUV	station end	
PS109_60-1	2017-09-22	18:41	79,56802	-19,28995	224	AUV	station start	
PS109_60-1	2017-09-22	18:46	79,56805	-19,28898	216	AUV	station end	
PS109_60-1	2017-09-22	19:03	79,56458	-19,29937	306	AUV	station start	
PS109_60-1	2017-09-22	19:23	79,56442	-19,29855	301	AUV	station end	
PS109_60-1	2017-09-22	19:36	79,56432	-19,29908	304	AUV	station start	
PS109_60-1	2017-09-22	20:42	79,56723	-19,29798	295	AUV	station end	
PS109_61-1	2017-09-22	21:42	79,55663	-19,22058	162	TVMUC	station start	
PS109_61-1	2017-09-22	22:17	79,55655	-19,22082	162	TVMUC	at depth	
PS109_61-1	2017-09-22	22:27	79,55653	-19,22162	161	TVMUC	station end	
PS109_62-1	2017-09-22	23:17	79,50677	-19,32157	302	TVMUC	station start	
PS109_62-1	2017-09-22	23:37	79,50667	-19,32192	301	TVMUC	at depth	
PS109_62-1	2017-09-22	23:50	79,50677	-19,3219	301	TVMUC	station end	
PS109_63-1	2017-09-23	01:09	79,58255	-19,33123	376	CTDOZE	at depth	
PS109_63-1	2017-09-23	01:23	79,58243	-19,33575	377	CTDOZE	station end	
PS109_64-1	2017-09-23	02:30	79,57577	-19,35982	444	CTDOZE	at depth	
PS109_64-1	2017-09-23	02:42	79,57577	-19,35985	444	CTDOZE	station end	
PS109_65-1	2017-09-23	03:05	79,57023	-19,4126	466	CTDOZE	station start	
PS109_65-1	2017-09-23	03:21	79,57022	-19,4126	466	CTDOZE	at depth	
PS109_65-1	2017-09-23	03:55	79,57022	-19,41257	466	CTDOZE	station end	
PS109_66-1	2017-09-23	04:56	79,56837	-19,46745	474	CTDOZE	station start	
PS109_66-1	2017-09-23	05:13	79,56838	-19,4675	474	CTDOZE	at depth	
PS109_66-1	2017-09-23	05:26	79,56837	-19,4674	474	CTDOZE	station end	

Station	Date	Time	Latitude	Longitude	Depth [m]	Gear	Action	Comment
PS109_67-1	2017-09-23	05:54	79,56727	-19,51008	470	CTDOZE	station start	
PS109_67-1	2017-09-23	06:10	79,56727	-19,51003	470	CTDOZE	at depth	
PS109_67-1	2017-09-23	06:37	79,56727	-19,51007	470	CTDOZE	station end	
PS109_68-1	2017-09-23	09:02	79,55618	-19,2198	168	LAND	station start	
PS109_68-1	2017-09-23	09:13	79,55618	-19,21975	169	LAND	station start	
PS109_68-1	2017-09-23	09:31	79,55618	-19,21975	169	LAND	station start	
PS109_68-1	2017-09-23	09:34	79,55618	-19,21977	169	LAND	station start	
PS109_68-1	2017-09-23	09:37	79,55618	-19,21977	165	LAND	station end	
PS109_69-1	2017-09-23	11:01	79,50578	-19,31907	301	LAND	station start	
PS109_69-1	2017-09-23	11:08	79,50568	-19,31843	301	LAND	station start	
PS109_69-1	2017-09-23	11:26	79,5053	-19,31712	301	LAND	station start	
PS109_69-1	2017-09-23	11:29	79,5053	-19,31715	301	LAND	station start	
PS109_69-1	2017-09-23	11:31	79,50523	-19,31687	301	LAND	station end	
PS109_70-1	2017-09-23	12:26	79,51925	-19,43085	288	MOOR	station end	
PS109_71-1	2017-09-23	13:43	79,56723	-19,46335	475	MOOR	station start	
PS109_71-1	2017-09-23	13:51	79,56723	-19,46337	476	MOOR	station start	
PS109_71-1	2017-09-23	13:59	79,56723	-19,46337	475	MOOR	station start	
PS109_71-1	2017-09-23	14:01	79,56722	-19,46337	475	MOOR	station start	
PS109_71-1	2017-09-23	14:06	79,56722	-19,46332	475	MOOR	station start	
PS109_71-1	2017-09-23	14:14	79,56722	-19,46335	475	MOOR	station start	
PS109_71-1	2017-09-23	14:27	79,56722	-19,46338	475	MOOR	station start	
PS109_71-1	2017-09-23	14:57	79,56722	-19,46337	475	MOOR	station start	
PS109_71-2	2017-09-23	16:14	79,56435	-19,45278	470	MSS	station start	
PS109_71-2	2017-09-23	16:20	79,56408	-19,45047	469	MSS	at depth	
PS109_71-2	2017-09-23	16:22	79,56388	-19,44932	467	MSS	station end	
PS109_71-2	2017-09-23	16:31	79,56318	-19,44518	383	MSS	station start	
PS109_71-2	2017-09-23	16:43	79,5623	-19,43932	315	MSS	station end	
PS109_71-2	2017-09-23	16:45	79,56225	-19,43882	310	MSS	station start	
PS109_71-2	2017-09-23	17:00	79,56123	-19,43158	247	MSS	station end	
PS109_72-1	2017-09-23	19:43	79,47688	-19,23308	438	GC	station start	
PS109_72-1	2017-09-23	19:52	79,47683	-19,23287	438	GC	at depth	
PS109_72-1	2017-09-23	20:07	79,47678	-19,23237	439	GC	station end	
PS109_73-1	2017-09-23	20:56	79,4416	-19,24753	185	GC	station start	
PS109_73-1	2017-09-23	21:02	79,44155	-19,2475	184	GC	at depth	
PS109_73-1	2017-09-23	21:12	79,44148	-19,2476	184	GC	station end	
PS109_74-1	2017-09-23	22:27	79,50818	-18,90083	481	GC	station start	
PS109_74-1	2017-09-23	22:37	79,50817	-18,90198	480	GC	at depth	
PS109_74-1	2017-09-23	22:53	79,50815	-18,90372	480	GC	station end	
PS109_75-1	2017-09-24	00:13	79,59097	-19,10487	168	GC	station start	
PS109_75-1	2017-09-24	00:17	79,59115	-19,10447	179	GC	at depth	
PS109_75-1	2017-09-24	00:24	79,59135	-19,10507	180	GC	station end	
PS109_76-1	2017-09-24	01:09	79,62012	-19,29162	365	TVMUC	station start	
PS109_76-1	2017-09-24	01:23	79,62	-19,29147	365	TVMUC	at depth	

Station	Date	Time	Latitude	Longitude	Depth [m]	Gear	Action	Comment
PS109_76-1	2017-09-24	01:51	79,62	-19,2907	362	TVMUC	station end	
PS109_76-2	2017-09-24	02:22	79,62018	-19,28933	365	TVMUC	station start	
PS109_76-2	2017-09-24	02:41	79,62022	-19,28872	367	TVMUC	at depth	
PS109_76-2	2017-09-24	03:13	79,62037	-19,28808	367	TVMUC	station end	
PS109_77-1	2017-09-24	04:09	79,5666	-19,3223	415	CTDOZE	station start	
PS109_77-1	2017-09-24	04:23	79,56663	-19,3235	415	CTDOZE	at depth	
PS109_77-1	2017-09-24	04:50	79,56693	-19,32443	415	CTDOZE	station end	
PS109_78-1	2017-09-24	05:55	79,54988	-19,33902	362	CTDOZE	station start	
PS109_78-1	2017-09-24	06:08	79,55043	-19,3408	360	CTDOZE	at depth	
PS109_78-1	2017-09-24	06:25	79,55113	-19,34382	360	CTDOZE	station end	
PS109_79-1	2017-09-24	07:11	79,53223	-19,36388	339	CTDOZE	at depth	
PS109_79-1	2017-09-24	07:36	79,53273	-19,36547	340	CTDOZE	station end	
PS109_80-1	2017-09-24	08:36	79,51572	-19,33447	307	CTDOZE	station start	
PS109_80-1	2017-09-24	08:49	79,51575	-19,33488	307	CTDOZE	at depth	
PS109_80-1	2017-09-24	09:07	79,5158	-19,33527	309	CTDOZE	station end	
PS109_81-1	2017-09-24	10:14	79,43763	-19,79643	328	ADCP_150	profile start	
PS109_81-1	2017-09-24	13:12	79,6636	-19,26445	258	ADCP_150	profile end	
PS109_82-1	2017-09-24	15:08	79,50188	-19,27787	329	CTDOZE	station start	
PS109_82-1	2017-09-24	15:27	79,50207	-19,27577	333	CTDOZE	at depth	
PS109_82-1	2017-09-24	15:41	79,50185	-19,27258	341	CTDOZE	station end	
PS109_83-1	2017-09-24	18:00	79,55642	-19,22397	173	LAND	at depth	
PS109_83-1	2017-09-24	18:28	79,55578	-19,21733	182	LAND	station end	
PS109_83-1	2017-09-24	18:36	79,55552	-19,21592	189	LAND	station end	
PS109_83-1	2017-09-24	18:45	79,55557	-19,2165	185	LAND	station end	
PS109_83-1	2017-09-24	18:58	79,55548	-19,22057	179	LAND	station end	
PS109_84-1	2017-09-24	20:14	79,50505	-19,30892	313	LAND	at depth	
PS109_84-1	2017-09-24	21:02	79,50468	-19,31535	308	LAND	station end	
PS109_84-1	2017-09-24	21:16	79,5044	-19,31565	307	LAND	station end	
PS109_84-1	2017-09-24	21:23	79,50458	-19,3118	311	LAND	station end	
PS109_84-1	2017-09-24	21:33	79,50425	-19,31132	309	LAND	station end	
PS109_84-2	2017-09-24	22:11	79,50638	-19,31673	311	TVMUC	station start	
PS109_84-2	2017-09-24	23:03	79,50627	-19,31827	309	TVMUC	at depth	
PS109_84-2	2017-09-24	23:17	79,50615	-19,319	308	TVMUC	station end	
PS109_85-1	2017-09-24	23:32	79,5285	-19,28157	146	TVMUC	station start	
PS109_85-1	2017-09-25	00:25	79,5568	-19,22725	156	TVMUC	at depth	
PS109_85-1	2017-09-25	00:35	79,55692	-19,22955	155	TVMUC	station end	
PS109_87-1	2017-09-25	03:20	79,51693	-18,65883	491	CTDOZE	station start	
PS109_87-1	2017-09-25	03:37	79,51688	-18,659	491	CTDOZE	at depth	
PS109_87-1	2017-09-25	03:58	79,51685	-18,6594	491	CTDOZE	station end	
PS109_88-1	2017-09-25	04:14	79,52883	-18,62342	492	HS	profile start	
PS109_88-1	2017-09-25	08:15	79,70675	-17,63523	392	HS	profile end	
PS109_89-1	2017-09-25	22:13	79,20312	-17,30445	305	CTDOZE	station start	
PS109_89-1	2017-09-25	22:27	79,20305	-17,30553	307	CTDOZE	at depth	

Station	Date	Time	Latitude	Longitude	Depth [m]	Gear	Action	Comment
PS109_89-1	2017-09-25	22:40	79,20287	-17,30698	306	CTDOZE	station end	
PS109_90-1	2017-09-26	01:46	79,2383	-16,78908	399	CTDOZE	station start	
PS109_90-1	2017-09-26	01:52	79,23842	-16,78963	390	CTDOZE	station start	
PS109_90-1	2017-09-26	02:03	79,23808	-16,78942	389	CTDOZE	at depth	
PS109_90-1	2017-09-26	02:33	79,23712	-16,78802	390	CTDOZE	station end	
PS109_91-1	2017-09-26	05:33	79,22902	-16,03983	273	CTDOZE	station start	
PS109_91-1	2017-09-26	05:44	79,22842	-16,0367	273	CTDOZE	at depth	
PS109_91-1	2017-09-26	06:06	79,22742	-16,03205	273	CTDOZE	station end	
PS109_92-1	2017-09-26	07:34	79,24583	-16,39177	337	CTDOZE	station start	
PS109_92-1	2017-09-26	07:48	79,2442	-16,39448	337	CTDOZE	at depth	
PS109_92-1	2017-09-26	08:03	79,24227	-16,39892	339	CTDOZE	station end	
PS109_93-1	2017-09-26	11:14	79,19593	-17,08585	390	CTDOZE	station start	
PS109_93-1	2017-09-26	11:27	79,1946	-17,09293	390	CTDOZE	at depth	
PS109_93-1	2017-09-26	11:49	79,19165	-17,10315	389	CTDOZE	station end	
PS109_93-2	2017-09-26	12:09	79,19077	-17,11335	387	TVMUC	station start	
PS109_93-2	2017-09-26	12:27	79,18915	-17,11998	386	TVMUC	at depth	
PS109_93-2	2017-09-26	12:43	79,18777	-17,12657	159	TVMUC	station end	
PS109_93-3	2017-09-26	13:21	79,18443	-17,14063	189	TVMUC	station start	
PS109_93-3	2017-09-26	13:37	79,18408	-17,14652	69	TVMUC	at depth	
PS109_93-3	2017-09-26	14:01	79,18317	-17,15382	182	TVMUC	station end	
PS109_94-1	2017-09-26	14:53	79,19495	-17,48523	96	CTDOZE	station start	
PS109_94-1	2017-09-26	15:02	79,19497	-17,48457	97	CTDOZE	at depth	
PS109_94-1	2017-09-26	15:13	79,19493	-17,483	104	CTDOZE	station end	
PS109_95-1	2017-09-27	14:47	78,45613	-18,31442	267	HS	profile start	
PS109_95-1	2017-09-27	21:29	78,45983	-18,62618	265	HS	profile end	
PS109_95-2	2017-09-27	15:52	78,42125	-18,71365	80	BOAT	station start	
PS109_95-2	2017-09-27	18:10	78,39785	-18,40817	401	BOAT	station end	
PS109_96-1	2017-09-27	22:51	78,4654	-18,53843	417	MSS	station start	
PS109_96-1	2017-09-27	23:00	78,46445	-18,53888	401	MSS	at depth	
PS109_96-1	2017-09-27	23:20	78,46345	-18,53945	394	MSS	at depth	
PS109_96-1	2017-09-27	23:39	78,46198	-18,54015	373	MSS	at depth	
PS109_96-1	2017-09-27	23:46	78,46178	-18,54013	372	MSS	station end	
PS109_97-1	2017-09-28	00:35	78,42283	-18,61953	487	GC	station start	
PS109_97-1	2017-09-28	00:42	78,42335	-18,61915	211	GC	at depth	
PS109_97-1	2017-09-28	00:53	78,4246	-18,61677	212	GC	station end	
PS109_98-1	2017-09-28	01:15	78,4231	-18,62278	206	GC	station start	
PS109_98-1	2017-09-28	01:23	78,42327	-18,6232	207	GC	at depth	
PS109_98-1	2017-09-28	01:34	78,42322	-18,62473	205	GC	station end	
PS109_99-1	2017-09-28	02:21	78,41038	-18,42873	412	GC	station start	
PS109_99-1	2017-09-28	02:30	78,41023	-18,42787	412	GC	at depth	
PS109_99-1	2017-09-28	02:46	78,40998	-18,42663	413	GC	station end	
PS109_100-1	2017-09-28	04:40	78,44595	-18,55832	319	CTDOZE	station start	
PS109_100-1	2017-09-28	04:53	78,44598	-18,5583	319	CTDOZE	at depth	

Station	Date	Time	Latitude	Longitude	Depth [m]	Gear	Action	Comment
PS109_100-1	2017-09-28	05:14	78,44605	-18,55778	320	CTDOZE	station end	
PS109_101-1	2017-09-28	06:07	78,47963	-18,55568	439	CTDOZE	station start	
PS109_101-1	2017-09-28	06:21	78,47967	-18,55597	439	CTDOZE	at depth	
PS109_101-1	2017-09-28	06:51	78,47968	-18,55615	439	CTDOZE	station end	
PS109_102-1	2017-09-28	07:50	78,47153	-18,4985	425	CTDOZE	station start	
PS109_102-1	2017-09-28	08:03	78,4715	-18,4985	426	CTDOZE	at depth	
PS109_102-1	2017-09-28	08:22	78,47147	-18,49865	444	CTDOZE	station end	
PS109_103-1	2017-09-28	08:58	78,45135	-18,42833	467	CTDOZE	station start	
PS109_103-1	2017-09-28	09:11	78,45158	-18,428	454	CTDOZE	at depth	
PS109_103-1	2017-09-28	09:36	78,45177	-18,42775	442	CTDOZE	station end	
PS109_104-1	2017-09-28	10:38	78,42743	-18,34158	509	CTDOZE	station start	
PS109_104-1	2017-09-28	10:52	78,42805	-18,34028	508	CTDOZE	at depth	
PS109_104-1	2017-09-28	11:12	78,42892	-18,3384	506	CTDOZE	station end	
PS109_105-1	2017-09-28	12:06	78,4816	-18,55728	440	TVMUC	station start	
PS109_105-1	2017-09-28	12:26	78,48133	-18,55618	440	TVMUC	at depth	
PS109_105-1	2017-09-28	13:14	78,48108	-18,55518	440	TVMUC	station end	
PS109_105-2	2017-09-28	13:15	78,48108	-18,55518	440	TVMUC	station start	
PS109_105-2	2017-09-28	13:29	78,48108	-18,5552	441	TVMUC	at depth	
PS109_105-2	2017-09-28	13:44	78,48108	-18,55517	442	TVMUC	station end	
PS109_106-1	2017-09-28	15:57	78,45222	-18,03057	635	HS	profile end	
PS109_107-1	2017-09-28	17:21	78,456	-17,92193	659	LAND	station start	
PS109_107-1	2017-09-28	17:32	78,45675	-17,92018	657	LAND	station start	
PS109_107-1	2017-09-28	17:57	78,45857	-17,91587	646	LAND	station start	
PS109_107-1	2017-09-28	17:58	78,45862	-17,91568	646	LAND	station start	
PS109_107-1	2017-09-28	17:59	78,45867	-17,91553	645	LAND	at depth	
PS109_107-1	2017-09-28	17:59	78,45872	-17,91542	645	LAND	station end	
PS109_108-1	2017-09-28	19:38	78,41718	-17,57725	561	GC	station start	
PS109_108-1	2017-09-28	20:09	78,41785	-17,57092	564	GC	station end	
PS109_109-1	2017-09-29	00:21	78,32753	-17,19533	1128	GC	station start	
PS109_109-1	2017-09-29	00:32	78,32825	-17,19152	512	GC	at depth	
PS109_109-1	2017-09-29	00:49	78,3288	-17,18803	514	GC	station end	
PS109_110-1	2017-09-29	05:43	78,19877	-15,80352	354	MSS	station start	
PS109_110-1	2017-09-29	05:53	78,19783	-15,8044	355	MSS	at depth	
PS109_110-1	2017-09-29	06:05	78,19627	-15,80552	355	MSS	at depth	
PS109_110-1	2017-09-29	06:19	78,19443	-15,80647	355	MSS	at depth	
PS109_110-1	2017-09-29	06:34	78,19258	-15,80868	359	MSS	at depth	
PS109_110-1	2017-09-29	06:43	78,19148	-15,81037	360	MSS	station end	
PS109_111-1	2017-09-29	07:36	78,20877	-15,5612		MOOR	at depth	
PS109_111-1	2017-09-29	07:41	78,20893	-15,56047		MOOR	station start	
PS109_111-1	2017-09-29	07:49	78,20967	-15,5596		MOOR	station end	
PS109_111-1	2017-09-29	07:52	78,20982	-15,55863		MOOR	station start	
PS109_111-1	2017-09-29	07:55	78,20998	-15,5579		MOOR	station end	
PS109_111-1	2017-09-29	08:05	78,21232	-15,55953		MOOR	station start	

Station	Date	Time	Latitude	Longitude	Depth [m]	Gear	Action	Comment
PS109_111-1	2017-09-29	08:06	78,21277	-15,56025		MOOR	station end	
PS109_111-1	2017-09-29	08:07	78,21308	-15,56073		MOOR	station start	
PS109_111-1	2017-09-29	08:27	78,2151	-15,55832		MOOR	station end	
PS109_111-1	2017-09-29	09:26	78,20473	-15,56575		MOOR	station start	
PS109_111-1	2017-09-29	09:32	78,20538	-15,567		MOOR	station end	
PS109_111-1	2017-09-29	10:08	78,21078	-15,56373	265	MOOR	station end	
PS109_112-1	2017-09-29	11:15	78,17695	-15,72247	356	MOOR	station end	
PS109_112-1	2017-09-29	11:18	78,17718	-15,72215	357	MOOR	station end	
PS109_112-1	2017-09-29	11:29	78,1777	-15,7221	358	MOOR	station end	
PS109_112-1	2017-09-29	11:29	78,17775	-15,72212	358	MOOR	station end	
PS109_113-1	2017-09-29	12:15	78,1515	-15,89345	413	MOOR	station start	
PS109_113-1	2017-09-29	12:51	78,15037	-15,89797	413	MOOR	station end	
PS109_114-1	2017-09-29	16:11	77,9305	-17,0894	365	MOOR	at depth	
PS109_114-1	2017-09-29	16:48	77,927	-17,08997	362	MOOR	station end	
PS109_114-1	2017-09-29	16:52	77,92693	-17,09023	362	MOOR	station end	
PS109_114-1	2017-09-29	16:57	77,92707	-17,08998	362	MOOR	station end	
PS109_114-1	2017-09-29	16:59	77,92702	-17,09003	362	MOOR	station end	
PS109_114-1	2017-09-29	17:00	77,92702	-17,08993	362	MOOR	station end	
PS109_114-1	2017-09-29	17:10	77,92695	-17,08997	362	MOOR	station end	
PS109_114-2	2017-09-29	17:31	77,92882	-17,08808	361	CTDOZE	station start	
PS109_114-2	2017-09-29	18:12	77,92695	-17,08075	361	CTDOZE	station end	
PS109_115-1	2017-09-29	21:53	78,03113	-16,57412	508	CTDOZE	station start	
PS109_115-1	2017-09-29	22:07	78,03122	-16,57135	509	CTDOZE	at depth	
PS109_115-1	2017-09-29	22:31	78,03235	-16,55408	505	CTDOZE	station end	
PS109_115-2	2017-09-29	22:44	78,03245	-16,54935	504	TVMUC	station start	
PS109_115-2	2017-09-29	23:02	78,03282	-16,5406	503	TVMUC	at depth	
PS109_115-2	2017-09-29	23:17	78,03252	-16,53678	504	TVMUC	station end	
PS109_115-3	2017-09-29	23:33	78,03325	-16,52022	502	TVMUC	station start	
PS109_115-3	2017-09-30	00:04	78,03313	-16,51653	502	TVMUC	station end	
PS109_116-1	2017-09-30	07:42	78,42975	-17,93502	670	CTDOZE	station start	
PS109_116-1	2017-09-30	08:01	78,42953	-17,93517	671	CTDOZE	at depth	
PS109_116-1	2017-09-30	08:31	78,42893	-17,93588	672	CTDOZE	station end	
PS109_116-2	2017-09-30	08:39	78,42872	-17,93595	671	TVMUC	station start	
PS109_116-2	2017-09-30	09:03	78,42777	-17,93685	669	TVMUC	at depth	
PS109_116-2	2017-09-30	09:23	78,42672	-17,93425	671	TVMUC	station end	
PS109_117-1	2017-09-30	10:57	78,45818	-17,9111	640	LAND	station end	
PS109_117-1	2017-09-30	11:37	78,45595	-17,9024	642	LAND	station end	
PS109_117-1	2017-09-30	11:42	78,45525	-17,90048	643	LAND	station end	
PS109_117-1	2017-09-30	11:58	78,45268	-17,89812	654	LAND	station end	
PS109_118-1	2017-09-30	14:59	78,57552	-17,86028	603	ICE	station end	
PS109_119-1	2017-09-30	19:41	78,91958	-17,77927	199	HS	profile start	
PS109_119-1	2017-10-01	12:00	78,9032	-17,98623	470	HS	profile end	
PS109_119-3	2017-10-01	10:46	78,9069	-17,96697	468	CTDOZE	station start	

Station	Date	Time	Latitude	Longitude	Depth [m]	Gear	Action	Comment
PS109_119-3	2017-10-01	11:00	78,90625	-17,97497	472	CTDOZE	at depth	
PS109_119-3	2017-10-01	11:29	78,90545	-17,9773	471	CTDOZE	station end	
PS109_120-1	2017-10-01	15:41	78,88177	-17,22658	436	ICE	station start	
PS109_120-1	2017-10-01	19:48	78,85928	-17,19677	117	ICE	station end	
PS109_121-1	2017-10-02	06:33	78,3366	-16,71897	481	GC	station start	
PS109_121-1	2017-10-02	06:42	78,33563	-16,72002	480	GC	at depth	
PS109_121-1	2017-10-02	06:59	78,33415	-16,7301	485	GC	station end	
PS109_122-1	2017-10-02	15:22	77,91008	-13,17883	142	TVMUC	station start	
PS109_122-1	2017-10-02	15:42	77,91147	-13,17427	140	TVMUC	at depth	
PS109_122-1	2017-10-02	15:53	77,91208	-13,17302	138	TVMUC	station end	
PS109_122-2	2017-10-02	15:53	77,91205	-13,17308	140	AUV	station start	
PS109_122-2	2017-10-02	15:56	77,91193	-13,17325	139	AUV	station end	
PS109_122-2	2017-10-02	16:53	77,89948	-13,3454	144	AUV	station start	
PS109_122-2	2017-10-02	17:07	77,89918	-13,35077	145	AUV	station start	
PS109_122-2	2017-10-02	17:40	77,90037	-13,35497	142	AUV	profile start	
PS109_122-2	2017-10-02	17:46	77,90125	-13,35302	141	AUV	station end	
PS109_122-2	2017-10-02	22:13	77,7992	-13,64302	389	AUV	station start	
PS109_122-2	2017-10-02	22:27	77,80082	-13,6367	390	AUV	station end	
PS109_122-2	2017-10-02	22:42	77,79928	-13,6256	392	AUV	station start	
PS109_122-2	2017-10-02	23:20	77,80222	-13,61438	397	AUV	station end	
PS109_122-2	2017-10-02	23:28	77,80317	-13,61412	397	AUV	station end	
PS109_123-1	2017-10-02	18:23	77,88807	-13,34627	169	CTDOZE	station start	
PS109_123-1	2017-10-02	18:33	77,88833	-13,34572	171	CTDOZE	at depth	
PS109_123-1	2017-10-02	18:38	77,88853	-13,3445	170	CTDOZE	station end	
PS109_123-2	2017-10-02	19:02	77,89185	-13,33503	162	MSS	station start	
PS109_123-2	2017-10-02	19:06	77,8923	-13,3337	161	MSS	at depth	
PS109_123-2	2017-10-02	19:09	77,89277	-13,33212	162	MSS	at depth	
PS109_123-2	2017-10-02	19:15	77,8938	-13,32903	158	MSS	at depth	
PS109_123-2	2017-10-02	19:22	77,89493	-13,32565	158	MSS	at depth	
PS109_123-2	2017-10-02	19:29	77,89607	-13,3219	150	MSS	at depth	
PS109_123-2	2017-10-02	19:35	77,89697	-13,31872	149	MSS	station end	
PS109_124-1	2017-10-02	20:26	77,86683	-13,41375	12	CTDOZE	station start	
PS109_124-1	2017-10-02	20:37	77,86677	-13,4116	160	CTDOZE	at depth	
PS109_124-1	2017-10-02	20:58	77,86697	-13,40748	187	CTDOZE	station end	
PS109_125-1	2017-10-02	23:41	77,7996	-13,63402	390	TVMUC	station start	
PS109_125-1	2017-10-03	00:30	77,79927	-13,63192	388	TVMUC	at depth	
PS109_125-1	2017-10-03	00:39	77,79967	-13,63245	392	TVMUC	station end	
PS109_125-2	2017-10-03	00:55	77,79935	-13,63312	391	TVMUC	station start	
PS109_125-2	2017-10-03	01:10	77,79863	-13,62778	391	TVMUC	at depth	
PS109_125-2	2017-10-03	01:26	77,7974	-13,62155	390	TVMUC	station end	
PS109_125-3	2017-10-03	01:50	77,7959	-13,62148	393	TVMUC	station start	
PS109_125-3	2017-10-03	02:09	77,79578	-13,6255	392	TVMUC	at depth	
PS109_125-3	2017-10-03	02:21	77,79553	-13,62918	392	TVMUC	station end	

Station	Date	Time	Latitude	Longitude	Depth [m]	Gear	Action	Comment
PS109_125-4	2017-10-03	02:42	77,79522	-13,63577	385	CTDOZE	station start	
PS109_125-4	2017-10-03	02:55	77,7958	-13,63743	389	CTDOZE	at depth	
PS109_125-4	2017-10-03	03:20	77,79687	-13,64173	389	CTDOZE	station end	
PS109_125-5	2017-10-03	03:42	77,7982	-13,64693	388	MSS	station start	
PS109_125-5	2017-10-03	03:51	77,79895	-13,6489	388	MSS	at depth	
PS109_125-5	2017-10-03	04:23	77,8016	-13,65822	384	MSS	at depth	
PS109_125-5	2017-10-03	04:31	77,8024	-13,6606	385	MSS	station end	
PS109_126-1	2017-10-03	05:23	77,83262	-13,52113	402	CTDOZE	station start	
PS109_126-1	2017-10-03	05:36	77,8333	-13,52247	402	CTDOZE	at depth	
PS109_126-1	2017-10-03	05:58	77,83437	-13,52448	402	CTDOZE	station end	
PS109_127-1	2017-10-03	06:35	77,86757	-13,41088	300	MSS	station start	
PS109_127-1	2017-10-03	06:41	77,8685	-13,41157	290	MSS	at depth	
PS109_127-1	2017-10-03	06:54	77,87078	-13,41342	264	MSS	at depth	
PS109_127-1	2017-10-03	07:05	77,87273	-13,41512	246	MSS	at depth	
PS109_127-1	2017-10-03	07:11	77,8737	-13,41613	238	MSS	station end	
PS109_128-1	2017-10-03	07:43	77,90742	-13,26887	143	CTDOZE	station start	
PS109_128-1	2017-10-03	07:51	77,90752	-13,27265	142	CTDOZE	at depth	
PS109_128-1	2017-10-03	08:10	77,9085	-13,28092	145	CTDOZE	station end	
PS109_129-1	2017-10-03	08:40	77,91283	-13,17372	138	TVMUC	station start	
PS109_129-1	2017-10-03	09:01	77,91255	-13,17717	139	TVMUC	at depth	
PS109_129-1	2017-10-03	09:10	77,91272	-13,17793	138	TVMUC	station end	
PS109_129-2	2017-10-03	09:48	77,9137	-13,17858	135	BONGO	station start	
PS109_129-2	2017-10-03	09:58	77,92525	-13,17052	122	BONGO	at depth	
PS109_129-2	2017-10-03	10:10	77,93897	-13,15858	117	BONGO	station end	
PS109_130-1	2017-10-03	11:44	77,90632	-12,00088	154	CTDOZE	station start	
PS109_130-1	2017-10-03	11:52	77,90672	-12,00115	155	CTDOZE	at depth	
PS109_130-1	2017-10-03	12:07	77,9068	-12,00445	154	CTDOZE	station end	
PS109_131-1	2017-10-03	13:25	77,9047	-11,00587	214	CTDOZE	station start	
PS109_131-1	2017-10-03	13:37	77,90622	-11,00755	214	CTDOZE	at depth	
PS109_131-1	2017-10-03	13:50	77,90687	-11,0094	214	CTDOZE	station end	
PS109_132-1	2017-10-03	15:09	77,90602	-10,00045	230	CTDOZE	station start	
PS109_132-1	2017-10-03	15:20	77,90703	-10,00483	230	CTDOZE	at depth	
PS109_132-1	2017-10-03	15:32	77,90827	-10,0073	227	CTDOZE	station end	
PS109_132-2	2017-10-03	15:59	77,90603	-9,98848	228	MOOR	station start	
PS109_132-2	2017-10-03	16:02	77,90622	-9,99	225	MOOR	station start	
PS109_132-2	2017-10-03	16:05	77,90637	-9,991	227	MOOR	station start	
PS109_132-2	2017-10-03	16:08	77,90653	-9,99212	229	MOOR	station start	
PS109_132-2	2017-10-03	16:17	77,90658	-9,99478	227	MOOR	station start	
PS109_132-2	2017-10-03	16:23	77,90705	-9,99643	229	MOOR	station start	
PS109_132-2	2017-10-03	16:25	77,90695	-9,99695	229	MOOR	station start	
PS109_132-2	2017-10-03	16:26	77,90685	-9,99735	230	MOOR	station end	
PS109_132-2	2017-10-03	16:27	77,9068	-9,9977	230	MOOR	station end	
PS109_133-1	2017-10-03	19:00	77,48288	-10,0018	262	MOOR	station start	

Station	Date	Time	Latitude	Longitude	Depth [m]	Gear	Action	Comment
PS109_133-1	2017-10-03	19:06	77,48322	-10,00105	261	MOOR	station start	
PS109_133-1	2017-10-03	19:09	77,48328	-10,00128	262	MOOR	station start	
PS109_133-1	2017-10-03	19:13	77,48328	-10,0018	262	MOOR	station start	
PS109_133-1	2017-10-03	19:17	77,48337	-10,00197	262	MOOR	station start	
PS109_133-1	2017-10-03	19:23	77,48335	-10,0021	262	MOOR	station start	
PS109_133-1	2017-10-03	19:24	77,48335	-10,0021	262	MOOR	station start	
PS109_133-1	2017-10-03	19:25	77,48337	-10,0021	260	MOOR	station end	
PS109_133-2	2017-10-03	19:48	77,49498	-9,95927	254	CTDOZE	station start	
PS109_133-2	2017-10-03	19:59	77,495	-9,96017	254	CTDOZE	at depth	
PS109_133-2	2017-10-03	20:07	77,49397	-9,9632	253	CTDOZE	station end	
PS109_133-3	2017-10-03	20:41	77,50448	-9,96497	260	BONGO	station start	
PS109_133-3	2017-10-03	20:55	77,5135	-9,96382	255	BONGO	at depth	
PS109_133-3	2017-10-03	21:15	77,52457	-9,96155	252	BONGO	station end	
PS109_133-4	2017-10-03	21:22	77,52797	-9,96013	254	BONGO	station start	
PS109_133-4	2017-10-03	21:37	77,53727	-9,95593	251	BONGO	at depth	
PS109_133-4	2017-10-03	22:00	77,54737	-9,94898	242	BONGO	station end	
PS109_134-1	2017-10-04	01:07	77,90637	-7,9961	219	CTDOZE	station start	
PS109_134-1	2017-10-04	01:19	77,90743	-7,99133	224	CTDOZE	at depth	
PS109_134-1	2017-10-04	01:36	77,90835	-7,98668	225	CTDOZE	station end	
PS109_134-2	2017-10-04	01:56	77,90965	-7,97742	227	BONGO	station start	
PS109_134-2	2017-10-04	02:10	77,91493	-7,93845	227	BONGO	at depth	
PS109_134-2	2017-10-04	02:28	77,92082	-7,89642	224	BONGO	station end	
PS109_134-3	2017-10-04	02:37	77,92227	-7,88563	222	BONGO	station start	
PS109_134-3	2017-10-04	02:51	77,92682	-7,8552	224	BONGO	at depth	
PS109_134-3	2017-10-04	03:08	77,93283	-7,81352	232	BONGO	station end	
PS109_135-1	2017-10-04	04:41	77,90605	-9,00542	236	CTDOZE	station start	
PS109_135-1	2017-10-04	04:52	77,90652	-9,0053	235	CTDOZE	at depth	
PS109_135-1	2017-10-04	05:09	77,90707	-9,00473	235	CTDOZE	station end	
PS109_135-2	2017-10-04	05:26	77,90833	-9,00085	235	BONGO	station start	
PS109_135-2	2017-10-04	05:40	77,91308	-8,9776	231	BONGO	at depth	
PS109_135-2	2017-10-04	06:00	77,91907	-8,9501	231	BONGO	station end	
PS109_136-1	2017-10-04	08:00	77,69943	-10,0039	234	CTDOZE	station start	
PS109_136-1	2017-10-04	08:11	77,7002	-10,00668	234	CTDOZE	at depth	
PS109_136-1	2017-10-04	08:17	77,70082	-10,00702	232	CTDOZE	station end	
PS109_137-1	2017-10-04	10:52	77,27428	-10,00522	342	CTDOZE	station start	
PS109_137-1	2017-10-04	11:04	77,2749	-10,00628	345	CTDOZE	at depth	
PS109_137-1	2017-10-04	11:27	77,27755	-10,02805	345	CTDOZE	station end	
PS109_138-1	2017-10-04	12:48	77,06627	-9,99143	426	CTDOZE	station start	
PS109_138-1	2017-10-04	13:07	77,06793	-9,99487	427	CTDOZE	at depth	
PS109_138-1	2017-10-04	13:32	77,06713	-9,99715	426	CTDOZE	station end	
PS109_138-2	2017-10-04	13:50	77,06595	-10,00125	424	MOOR	station start	
PS109_138-2	2017-10-04	14:02	77,0661	-10,00167	424	MOOR	station start	
PS109_138-2	2017-10-04	14:19	77,06642	-10,00208	424	MOOR	station start	

Station	Date	Time	Latitude	Longitude	Depth [m]	Gear	Action	Comment
PS109_138-2	2017-10-04	14:24	77,06635	-10,00192	424	MOOR	station start	
PS109_138-2	2017-10-04	14:33	77,06642	-10,00188	424	MOOR	station start	
PS109_138-2	2017-10-04	14:35	77,06645	-10,00187	424	MOOR	at depth	
PS109_139-1	2017-10-04	17:06	76,79797	-8,6216	356	MOOR	at depth	
PS109_139-1	2017-10-04	18:08	76,80015	-8,64018	355	MOOR	station end	
PS109_139-1	2017-10-04	18:13	76,79987	-8,64227	356	MOOR	station end	
PS109_139-1	2017-10-04	18:16	76,79965	-8,64357	356	MOOR	station end	
PS109_139-1	2017-10-04	18:20	76,79933	-8,64555	356	MOOR	station end	
PS109_139-1	2017-10-04	18:21	76,79927	-8,64618	356	MOOR	station end	
PS109_139-1	2017-10-04	18:23	76,79917	-8,64708	356	MOOR	station end	
PS109_139-1	2017-10-04	18:24	76,79908	-8,64785	356	MOOR	station end	
PS109_139-1	2017-10-04	18:27	76,7989	-8,64927	355	MOOR	station end	
PS109_139-1	2017-10-04	18:33	76,7985	-8,65182	355	MOOR	station end	
PS109_139-1	2017-10-04	18:37	76,79823	-8,6531	356	MOOR	station end	
PS109_139-1	2017-10-04	18:37	76,7982	-8,65322	356	MOOR	station end	
PS109_139-2	2017-10-04	18:55	76,79842	-8,65753	356	TVMUC	station start	
PS109_139-2	2017-10-04	19:13	76,79963	-8,6604	354	TVMUC	at depth	
PS109_139-2	2017-10-04	19:26	76,80017	-8,6613	353	TVMUC	station end	
PS109_139-3	2017-10-04	20:56	76,79993	-8,65848	356	LAND	station start	
PS109_139-3	2017-10-04	21:09	76,80012	-8,64853	356	LAND	station start	
PS109_139-3	2017-10-04	21:20	76,80003	-8,64357	357	LAND	station start	
PS109_139-3	2017-10-04	21:35	76,80073	-8,63738	358	LAND	station start	
PS109_139-3	2017-10-04	21:37	76,80077	-8,63715	357	LAND	station end	
PS109_139-4	2017-10-04	21:49	76,8004	-8,63435	357	TVMUC	station start	
PS109_139-4	2017-10-04	22:10	76,80178	-8,6252	357	TVMUC	at depth	
PS109_139-4	2017-10-04	22:25	76,80218	-8,62102	357	TVMUC	station end	
PS109_139-5	2017-10-04	22:48	76,80233	-8,63178	357	BONGO	station start	
PS109_139-5	2017-10-04	23:03	76,80798	-8,65122	354	BONGO	at depth	
PS109_139-5	2017-10-04	23:20	76,81612	-8,65292	353	BONGO	station end	
PS109_139-6	2017-10-04	23:26	76,81783	-8,6532	354	BONGO	station start	
PS109_139-6	2017-10-04	23:38	76,82502	-8,65458	360	BONGO	at depth	
PS109_139-6	2017-10-04	23:54	76,83263	-8,656	362	BONGO	station end	
PS109_140-1	2017-10-05	00:36	76,84408	-8,86915	352	CTDOZE	station start	
PS109_140-1	2017-10-05	00:49	76,8429	-8,8754	355	CTDOZE	at depth	
PS109_140-1	2017-10-05	01:18	76,84183	-8,88835	357	CTDOZE	station end	
PS109_141-1	2017-10-05	02:31	76,73793	-8,32052	343	CTDOZE	station start	
PS109_141-1	2017-10-05	02:49	76,7374	-8,32912	346	CTDOZE	at depth	
PS109_141-1	2017-10-05	03:16	76,73658	-8,34268	341	CTDOZE	station end	
PS109_142-1	2017-10-05	05:38	76,4865	-7,1208	1182	TVMUC	station start	
PS109_142-1	2017-10-05	06:02	76,48678	-7,12538	1177	TVMUC	station end	
PS109_142-2	2017-10-05	06:43	76,48673	-7,1335	1170	CTDOZE	station start	
PS109_142-2	2017-10-05	07:11	76,48775	-7,13807	1163	CTDOZE	at depth	
PS109_142-2	2017-10-05	07:57	76,48633	-7,14773	1158	CTDOZE	station end	

Station	Date	Time	Latitude	Longitude	Depth [m]	Gear	Action	Comment
PS109_142-3	2017-10-05	08:17	76,49007	-7,1902	1105	BONGO	station start	
PS109_142-3	2017-10-05	08:31	76,4952	-7,22095	1064	BONGO	at depth	
PS109_142-3	2017-10-05	08:49	76,49982	-7,2534	1018	BONGO	station end	
PS109_143-1	2017-10-05	09:28	76,54452	-7,37413	773	CTDOZE	station start	
PS109_143-1	2017-10-05	09:48	76,54355	-7,38438	768	CTDOZE	at depth	
PS109_143-1	2017-10-05	10:29	76,54045	-7,4167	741	CTDOZE	station end	
PS109_144-1	2017-10-05	11:38	76,5714	-7,5017	539	CTDOZE	station start	
PS109_144-1	2017-10-05	11:51	76,56765	-7,50877	545	CTDOZE	station end	
PS109_145-1	2017-10-05	15:53	76,31713	-6,36208	2244	GC	station start	
PS109_145-1	2017-10-05	16:31	76,31788	-6,36623	2240	GC	at depth	
PS109_145-1	2017-10-05	17:24	76,31867	-6,3732	2233	GC	station end	
PS109_146-1	2017-10-06	06:23	76,4711	-7,05562	1279	GC	station start	
PS109_146-1	2017-10-06	06:54	76,47083	-7,0584	1279	GC	at depth	
PS109_146-1	2017-10-06	07:28	76,4711	-7,06003	1277	GC	station end	
PS109_147-1	2017-10-06	08:49	76,54985	-7,4754	644	GC	station start	
PS109_147-1	2017-10-06	09:02	76,5504	-7,48768	629	GC	at depth	
PS109_147-1	2017-10-06	09:21	76,54988	-7,50613	606	GC	station end	
PS109_148-1	2017-10-06	10:15	76,5464	-7,37435	766	MOOR	station start	
PS109_148-1	2017-10-06	10:31	76,54652	-7,374	767	MOOR	station start	
PS109_148-1	2017-10-06	10:35	76,54625	-7,3748	763	MOOR	station start	
PS109_148-1	2017-10-06	10:47	76,54628	-7,37512	761	MOOR	station start	
PS109_148-1	2017-10-06	10:48	76,54628	-7,37515	766	MOOR	station start	
PS109_148-1	2017-10-06	10:59	76,54653	-7,37422	766	MOOR	station start	
PS109_148-1	2017-10-06	11:04	76,5462	-7,37555	766	MOOR	station start	
PS109_148-1	2017-10-06	11:07	76,54623	-7,37555	766	MOOR	station start	
PS109_148-1	2017-10-06	11:09	76,54632	-7,37525	766	MOOR	station end	
PS109_149-1	2017-10-06	14:40	76,95577	-9,42355	372	CTDOZE	station start	
PS109_149-1	2017-10-06	14:53	76,95682	-9,4227	371	CTDOZE	at depth	
PS109_149-1	2017-10-06	15:11	76,95895	-9,42	372	CTDOZE	station end	
PS109_150-1	2017-10-06	16:44	76,79792	-8,63805	358	LAND	at depth	
PS109_150-1	2017-10-06	17:29	76,79937	-8,64352	357	LAND	station end	
PS109_150-1	2017-10-06	17:41	76,80123	-8,6413	357	LAND	station end	
PS109_150-1	2017-10-06	17:50	76,80225	-8,64053	357	LAND	station end	
PS109_150-1	2017-10-06	18:02	76,80348	-8,64153	357	LAND	station end	
PS109_151-1	2017-10-06	20:16	76,63163	-7,75698	327	CTDOZE	station start	
PS109_151-1	2017-10-06	20:28	76,6317	-7,75738	327	CTDOZE	at depth	
PS109_151-1	2017-10-06	20:50	76,63183	-7,75745	327	CTDOZE	station end	
PS109_152-1	2017-10-06	21:27	76,60385	-7,63238	330	CTDOZE	station start	
PS109_152-1	2017-10-06	21:41	76,60407	-7,63287	330	CTDOZE	at depth	
PS109_152-1	2017-10-06	22:00	76,60522	-7,6419	328	CTDOZE	station end	
PS109_152-2	2017-10-06	22:15	76,6112	-7,64692	330	BONGO	station start	
PS109_152-2	2017-10-06	22:29	76,61955	-7,64895	327	BONGO	at depth	
PS109_152-2	2017-10-06	22:58	76,62815	-7,66212	326	BONGO	station end	

Station	Date	Time	Latitude	Longitude	Depth [m]	Gear	Action	Comment
PS109_153-1	2017-10-06	23:37	76,5734	-7,49467	533	CTDOZE	station start	
PS109_153-1	2017-10-06	23:38	76,5734	-7,49465	533	CTDOZE	at depth	
PS109_153-1	2017-10-07	00:31	76,57422	-7,49632	527	CTDOZE	station end	
PS109_154-1	2017-10-07	01:32	76,48782	-7,10945	1195	TVMUC	station start	
PS109_154-1	2017-10-07	02:06	76,4869	-7,13202	1176	TVMUC	at depth	
PS109_154-1	2017-10-07	02:36	76,48752	-7,13822	1169	TVMUC	station end	
PS109_154-2	2017-10-07	02:56	76,48593	-7,10513	1205	TVMUC	station start	
PS109_154-2	2017-10-07	03:28	76,48637	-7,10935	1200	TVMUC	at depth	
PS109_154-2	2017-10-07	03:56	76,48678	-7,1086	1200	TVMUC	station end	
PS109_155-1	2017-10-07	05:20	76,35633	-6,57412	2031	GC	station start	
PS109_155-1	2017-10-07	05:57	76,3567	-6,57335	2030	GC	at depth	
PS109_155-1	2017-10-07	06:42	76,35737	-6,56973	2030	GC	station end	
PS109_155-2	2017-10-07	07:19	76,35793	-6,51537	2053	BONGO	station start	
PS109_155-2	2017-10-07	07:34	76,35855	-6,47463	2080	BONGO	at depth	
PS109_155-2	2017-10-07	07:58	76,35867	-6,42145	2115	BONGO	station end	
PS109_156-1	2017-10-07	11:54	75,82212	-4,85172	3339	CTDOZE	station start	
PS109_156-1	2017-10-07	13:05	75,8186	-4,85977	3339	CTDOZE	at depth	
PS109_156-1	2017-10-07	14:41	75,81357	-4,8839	3340	CTDOZE	station end	
PS109_157-1	2017-10-07	20:03	75,00085	-2,99903	3630	CTDOZE	station start	
PS109_157-1	2017-10-07	21:18	75,00003	-2,9998	3630	CTDOZE	at depth	
PS109_157-1	2017-10-07	22:53	75,00025	-3,00003	3631	CTDOZE	station end	

Gear abbreviations	Gear
ADCP_150	ADCP 150kHz
AUV	Autonomous Underwater Vehicle
BOAT	Boat
BONGO	Bongo Net
CTDOZE	CTD AWI-OZE
FBOX	FerryBox
GC	Gravity Corer
HCTD	Hand CTD
HS	Hydrosweep
ICE	Ice Station
LAND	Lander
LIDAR	Doppler-Wind LIDAR
MOOR	Mooring
MSS	Mikrostruktur Sonde
OBS	Ocean Bottom Seismograph
PCO2_GO	pCO2 GO
PCO2_SUB	pCO2 Subctech
TSG_KEEL	Thermosalinograph Keel
TVMUC	Video Multi Corer
WST	Weatherstation

Die **Berichte zur Polar- und Meeresforschung** (ISSN 1866-3192) werden beginnend mit dem Band 569 (2008) als Open-Access-Publikation herausgegeben. Ein Verzeichnis aller Bände einschließlich der Druckausgaben (ISSN 1618-3193, Band 377-568, von 2000 bis 2008) sowie der früheren **Berichte zur Polarforschung** (ISSN 0176-5027, Band 1-376, von 1981 bis 2000) befindet sich im electronic Publication Information Center **(ePIC)** des Alfred-Wegener-Instituts, Helmholtz-Zentrum für Polar- und Meeresforschung (AWI); see http://epic.awi.de. Durch Auswahl “Reports on Polar- and Marine Research“ (via “browse”/”type”) wird eine Liste der Publikationen, sortiert nach Bandnummer, innerhalb der absteigenden chronologischen Reihenfolge der Jahrgänge mit Verweis auf das jeweilige pdf-Symbol zum Herunterladen angezeigt.

The **Reports on Polar and Marine Research** (ISSN 1866-3192) are available as open access publications since 2008. A table of all volumes including the printed issues (ISSN 1618-3193, Vol. 377-568, from 2000 until 2008), as well as the earlier **Reports on Polar Research** (ISSN 0176-5027, Vol. 1-376, from 1981 until 2000) is provided by the electronic Publication Information Center **(ePIC)** of the Alfred Wegener Institute, Helmholtz Centre for Polar and Marine Research (AWI); see URL http://epic.awi.de. To generate a list of all Reports, use the URL http://epic.awi.de and select “browse”/ ”type” to browse ”Reports on Polar and Marine Research”. A chronological list in declining order will be presented, and pdf-icons displayed for downloading.

Zuletzt erschienene Ausgaben:

Recently published issues:

715 (2018) The Expedition PS109 of the Research Vessel POLARSTERN to the Nordic Seas in 2017, edited by Torsten Kanzow

714 (2017) The Expedition SO258/2 of the Research Vessel SONNE to the central Indian Ocean in 2017, edited by Wolfram Geissler

713 (2017) The Expedition PS102 of the Research Vessel POLARSTERN to the Atlantic Ocean in 2016, edited by Karen Wiltshire, Eva-Maria Brodte, Annette Wilson and Peter Lemke

712 (2017) The Expedition PS104 of the Research Vessel POLARSTERN to the Amundsen Sea in 2017, edited by Karsten Gohl

711 (2017) Mid-Range forecasting of the German Waterways streamflow based on hydrologic, atmospheric and oceanic data by Monica Ionita

710 (2017) The Expedition PS103 of the Research Vessel POLARSTERN to the Weddell Sea in 2016/2017, edited by Olaf Boebel

709 (2017) Russian-German Cooperation: Expeditions to Siberia in 2016, edited by Pier Paul Overduin, Franziska Blender, Dmitry Y. Bolshiyanov, Mikhail N. Grigoriev, Anne Morgenstern, Hanno Meyer

708 (2017) The role of atmospheric circulation patterns on the variability of ice core constitutents in coastal Dronning Maud Land, Antarctica by Kerstin Schmidt

707 (2017) Distribution patterns and migratory behavior of Antarctic blue whales by Karolin Thomisch

706 (2017) The Expedition PS101 of the Research Vessel POLARSTERN to the Arctic Ocean in 2016, edited by Antje Boetius and Autun Purser

705 (2017) The Expedition PS100 of the Research Vessel POLARSTERN to the Fram Strait in 2016, edited by Torsten Kanzow

704 (2016) The Expeditions PS99.1 and PS99.2 of the Research Vessel POLARSTERN to the Fram Strait in 2016, edited by Thomas Soltwedel

ALFRED-WEGENER-INSTITUT
HELMHOLTZ-ZENTRUM FÜR POLAR-
UND MEERESFORSCHUNG

BREMERHAVEN

Am Handelshafen 12
27570 Bremerhaven
Telefon 0471 4831-0
Telefax 0471 4831-1149
www.awi.de

HELMHOLTZ
GEMEINSCHAFT